

NASA X-Hab Challenge 2017/18 Spring Semester Final Report

Hybrid Dehumidification and Reclamation Apparatus (HYDRA) Project

University of Colorado – Boulder

Ann & H.J. Smead Aerospace Engineering Sciences Department

Authors:

*Jonathan Eble, Zachary Fester, Lee Huynh, Mario Maggio,
Thomas Pearson, Grant Vincent, Mitchell Woolever*



Purpose

This report documents the progress of the HYDRA Team during the 2018 Spring Semester and presents final project outcomes.

Project Description

The design, predicted performance modeling, manufacturing, assembly, laboratory integration, performance characterization, and model validation of two cabin air dehumidifier concepts.

Contents

Contents.....	2
1. Team Overview.....	6
1.1. Team Organization	6
1.2. Roles and Responsibilities.....	6
1.3. Project Significance	7
2. Project Scope	8
3. Systems Engineering Overview	9
3.1. Project Objectives	9
3.2. Ground Rules and Assumptions.....	9
3.3. Mission Level Concept of Operations.....	10
3.4. Project Concept of Operations	11
3.5. Functional Block Diagram	11
3.6. Project Requirements.....	12
3.6.1. System Requirement Definition and Verification	12
3.6.2. Safety Requirements	14
3.6.3. Controls Requirements	15
3.6.4. Mechanical Requirements.....	16
3.6.5. Modeling Requirements.....	16
3.6.6. Manufacturing Requirements.....	17
3.7. System Interfaces	17
3.8. Systems Engineering Lessons Learned.....	17
4. Modeling.....	19
4.1. Water Cryocooler System (WCS) Modeling.....	19
4.1.1. Model Assumptions	19
4.1.2. Model Implementation.....	19
4.1.3. Model Inputs.....	22
4.1.4. Lab-Scale Design	23
4.1.5. Monte-Carlo Uncertainty Analysis.....	23
4.1.6. Model Performance Summary.....	24
4.2. Ionic Liquid System (ILS) Modeling	24
4.2.1. Introduction.....	24
4.2.2. Ionic Liquid Selection.....	25

HYDRA Project Spring 2018 Final Report

4.2.3.	Dimensional Analysis.....	25
4.2.4.	Improved Mass Transfer Model Theory.....	27
4.2.5.	Distribution Coefficient.....	28
4.2.6.	Model Limitations.....	28
4.2.7.	Model Outputs.....	29
5.	Manufacturing.....	32
5.1.	Water Cryocooler System (WCS) Design and Manufacturing.....	32
5.2.	Ionic Liquid System (ILS) Article Design & Manufacturing:.....	34
5.2.1.	ILS Mechanical Considerations.....	38
6.	Testing.....	42
6.1.	AETHER.....	42
6.2.	Test Integration.....	44
6.2.1.	Sensor and Instrumentation Integration.....	44
6.2.2.	Test Article Integration.....	46
6.2.3.	Integration Difficulties.....	49
6.2.4.	Recommended Improvements.....	49
6.3.	Experimental Design and Testing Configuration.....	50
6.3.1.	Overview.....	50
6.3.2.	WCS.....	50
6.3.3.	ILS.....	51
6.3.4.	Auxiliary Tests.....	52
7.	Experimental Results and Model Validation.....	52
7.1.	Water Cryocooler System (WCS) Model Validation.....	52
7.1.1.	Data Analysis Procedures.....	52
7.1.2.	Error Analysis Procedures.....	53
7.1.3.	Results Summary.....	53
7.1.4.	Flight Scale Design.....	55
7.2.	Ionic Liquid System (ILS) Model Validation.....	56
7.2.1.	Water Accumulation in the Ionic Liquid.....	56
7.2.2.	Ionic Liquid Bake Out.....	59
7.2.3.	ILS Performance.....	59
7.2.4.	Interaction of Carbon Dioxide in the ILS.....	60
7.2.5.	Results Summary.....	61
7.2.6.	ILS Scaling Analysis.....	61

8. Recommended Future Work..... 62

9. Works Cited..... 63

Appendix A: Budget..... 63

Appendix B: ILS Model Output Sensitivities..... 64

Appendix B: WCS Detailed Manufacturing and Assembly..... 67

Appendix C: ILS Detailed Manufacturing and Assembly..... 69

Appendix D: Sensor Specifications..... 88

Appendix E: WCS Modeling Scripts..... 93

Appendix G: ILS Modeling Scripts..... 107

Figures

Figure 1. HYDRA team organization. 6

Figure 2. Mission level ConOps. 10

Figure 3. Project level ConOps. 11

Figure 4. Functional block diagram. 12

Figure 5. Overview of geometry in the WCS model. 21

Figure 6. Overall structure of WCS model. 22

Figure 7. Initial output dew point and dew point change after 5 hours vs inner diameter. Wall temperature is -30 °C. Tube length is 0.61 m. flowrate is 9 L/min, and input humidity is 70%RH. Design point is marked with dashed lines..... 23

Figure 8. Histogram of results of the Monte-Carlo simulation. The dashed line indicates the nominal output. 23

Figure 9: HFMC dimensional performance analysis. 26

Figure 10: HFMC dimensional performance with improved model..... 26

Figure 11: Visualization of mass transfer in the ILS..... 28

Figure 12: Geometry used in model. 29

Figure 13: Actual geometry and flow pattern of ILS. 29

Figure 14: Dew Point of Air Passing Through the Contactor..... 30

Figure 15: Output dew point sensitivity to IL flow rate..... 31

Figure 16: Output Dew Point Sensitivity to Water Content in the Ionic Liquid 31

Figure 17. WCS final design with dimensions..... 32

Figure 18. WCS exploded assembly. 32

Figure 19. WCS cross section with O-rings..... 33

Figure 20. Ionic Liquid System overview. 34

Figure 21. Ionic Liquid System exploded view..... 35

Figure 22. Fiber assembly after fiber potting. 36

Figure 23. Screw Lock Ring with screws. 37

Figure 24. Full ILS assembly..... 37

Figure 25. Ionic liquid manifold..... 38

Figure 26. Initial fiber housing design..... 39

Figure 27. End cap with radial O-ring groove added..... 40

Figure 28. Fiber Guide 3 with radial O-ring groove added. 41

Figure 29. Fiber Guide 1 with axial O-ring groove added. 42

HYDRA Project Spring 2018 Final Report

Figure 30. The AETHER Test Rig with Key Components Highlighted.43

Figure 31. CAD drawing of the dew point sensor block.46

Figure 32. CAD drawing of the relative humidity sensor block.47

Figure 33. CAD drawing of the thermocouple integration to measure the downstream air temperature of the WCS.48

Figure 34. CAD drawing of the thermocouple integrating into the manifold of the ILS.49

Figure 35. Experimental data and best fit power series of output dew point vs air flowrate. Input humidity was 70%RH.53

Figure 36. Experimental data and model prediction of output dew point minus wall temperature vs air flowrate.54

Figure 37. Experimental data and model prediction of dew point vs time at 9 L/min. Input humidity was 70%RH.55

Figure 38. Ice accumulation after approximately 1 hour of testing at flow rates below 3 L/min. 55

Figure 39. Scaling analysis for the WCS. Air flowrate is 30 cfm, wall temperature is -70°C and input humidity is 70 %RH.56

Figure 40: Inlet and Outlet Water Concentration during ILS Testing.....57

Figure 41: Estimated Accumulation of Water in the ILS during Testing58

Figure 42: Electrical Conductivity Measurements during ILS Testing58

Figure 43: Water Accumulation in the ILS During Testing59

Figure 44: Outlet Dew Point during ILS Testing.....60

Figure 45: Carbon Dioxide Concentration Upstream and Downstream of the ILS61

Figure 46: Contactor Performance at the End of a Cycle given the Cycle Time.....62

Figure 47. Project budget breakdown.....64

Figure 48. Manufacturing and supplies budget breakdown.....64

Figure 49. Custom flange stock.....67

Figure 50. One end of WCS outer pipe assembly.68

Figure 51. Outer pipe assembly.68

Figure 52. Completed WCS.69

Figure 53. Fiber guide 1.70

Figure 54. Fiber guide 2.71

Figure 55. Pin supporting piece.....72

Figure 56. Fiber guide 3.73

Figure 57. Screw lock ring.....74

Figure 58. Spacer.75

Figure 59. End caps.....76

Figure 60. Fiber housing.76

Figure 61. Compression plate and assembly.77

Figure 62. Structure of the fiber assembly.....79

Figure 63. Threading fibers through the fiber guides.80

Figure 64. Fiber Assembly fully threaded.81

Figure 65. Cup used to mix adhesive.82

Figure 66. Adding fishing weights to fibers.83

Figure 67. Fiber Assembly inserted into one end cap.....84

Figure 68. Fiber Guide 3 fitting snugly into the fiber housing.85

Figure 69. ILS assembly without compression assembly.86

Figure 70. ILS contactor with compression assembly installed.....86

Figure 71. ILS final assembly.87

1. Team Overview

1.1. Team Organization

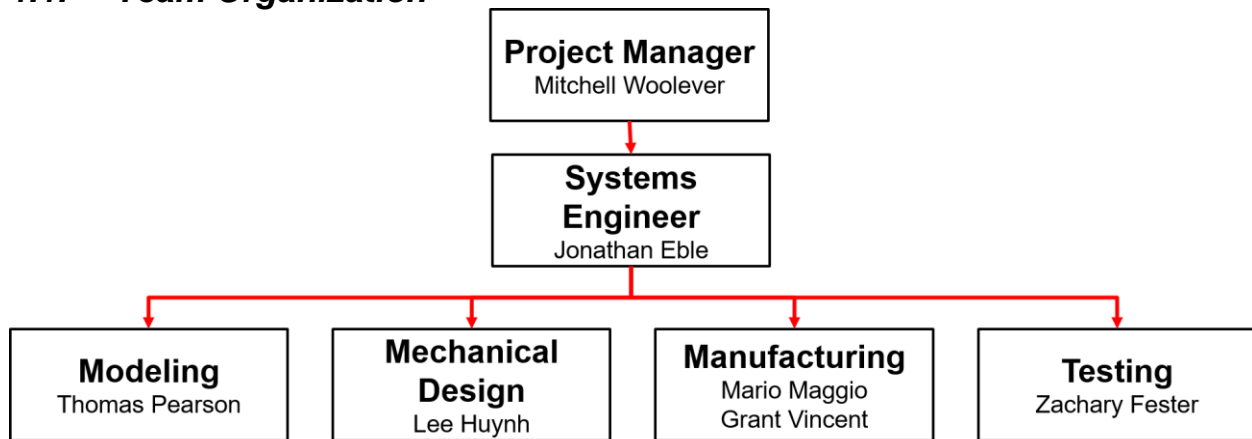


Figure 1. HYDRA team organization.

1.2. Roles and Responsibilities

Table 1. Team Roles and Responsibilities

Members	Role/Description
Prof. James Naby	Principal Investigator and Primary Advisor
Mitchell Woolever	Project Manager: Primary project leadership. Control documentation and schedule and oversee group meetings and team progress. Also, in charge of maintaining detailed finances and expense records. Main point of contact for advisors and sponsors.
Jonathan Eble	Systems Engineer: Technical leader of the team. Ensures technical progress is being made on all fronts and that all teams/subsystems are meshing appropriately. Ensures that requirements are appropriate and are being met in the overall team's progress. Assists the Project Manager as necessary.
Thomas Pearson	Modeling Lead: Develops mathematical models and simulations to analyze and optimize the humidifier/dehumidifier and heat exchanger geometry. Works closely with the Testing Lead to develop experimental procedures to quantitatively analyze the prototype system.

Lee Huynh	Mechanical Design Lead: In charge of materials selection, managing mechanical requirements, and solid modeling. Works with the Modeling Lead to provide solid models for analysis and to inform the prototype design.
Mario Maggio Grant Vincent	Manufacturing Leads: In charge of procuring materials and developing procedures to build test articles. Works with the Mechanical Design Lead to design and build test articles which satisfy the mechanical requirements.
Zachary Fester	Testing Lead: In charge of developing, testing, and integrating instrumentation, sensors, wiring, power systems, and software. Develops software and instrumentation solutions early in the design process in collaboration with the Modeling Lead.

1.3. *Project Significance*

The significance of this project arises directly from NASA's technology roadmap, which deals with human health, life support, and habitation systems. An air revitalization objective, 6.1.1, within this document states: "[There exists a need to] reliably and efficiently condition and revitalize spacecraft and habitat atmospheres to provide safe and comfortable environments within which crewmembers may live and work." Two listed challenges of this objective are to simplify and increase robustness of current carbon dioxide scrubbing technology while reducing dedicated crew maintenance time. As the practicality of resupply decreases with increased distance from Earth, the application of regenerable technologies becomes increasingly important. Specifically, NASA needs reduced-volume, low-power technologies that can maintain cabin CO₂ levels below 2 mmHg. NASA Ames is investigating cabin atmosphere cryogenic cooling to freeze out and accumulate CO₂ as dry ice, as this concept has great promise in reliability, self-sufficiency, and sustainability (Belancik, 2017). However, the CO₂-laden air must be dried to avoid freezing water in the cryogenic CO₂ removal system, since the presence of water will reduce the purity of the CO₂ stream and the expansion characteristic of liquid water freezing could damage process plumbing.

2. Project Scope

This project encompassed the design, predictive performance modeling, manufacturing, assembly, laboratory integration, performance characterization, and model validation of an atmosphere humidity control system using a cryogenic H₂O removal system dubbed the Water Cryocooler System (WCS) and a closed circulating loop of hygroscopic ionic liquid dubbed the Ionic Liquid System (ILS) to remove water vapor from the cabin air. The high-level objectives of the project were as follows: Computational models shall be developed to anticipate Relative Humidity (RH) depression performance, mass and heat transfer, and fluid flow properties in each selected dehumidification system. Additionally, the project team shall design and manufacture (or assemble from COTS components) test articles and support equipment such as laboratory sensors and controls, for the chosen dehumidifier system configurations. A quantitative characterization shall be performed for each test article configuration. These numerical models will be validated with data collected during test article characterization and performance tests. Lastly, a final report shall be prepared that describes the quantitative analysis of the chosen dehumidifier system configuration, recommendations for improvement, and recommendations on future work.

3. Systems Engineering Overview

3.1. Project Objectives

The primary project objective was to design, build, and test a prototype dehumidification system. Secondary objectives included reporting any changes in flow composition cause by the test article and estimating full scale performance of the dehumidification system. The full list of project objectives is given in Table 2. Project Objectives.

Table 2. Project Objectives.

Main Project Objectives:	
PO1	Design, build and test a dehumidification system for cabin air revitalization
PO2	Characterize H₂O uptake and desorption rates
PO3	Report any change in flow composition including CO₂ and contaminants
PO4	Justify chosen flow rate to be scalable to 30 scfm
PO5	Estimate power required to operate a full scale dehumidification system

To assess PO1, the most important project objective, three different levels of technical success were established. Success level 3 success is derived from NASA project performance targets, while the other two quotas stem from order of magnitude decrements on the challenging NASA performance target. The project levels of success are as follows:

- Level 1: ≤ 0°C Dew point (90+% of H₂O removed from the gas stream)
- Level 2: ≤ -43°C Dew point (99+% of H₂O removed from the gas stream)
- Level 3: ≤ -90°C Dew point (Virtually all of the H₂O removed from the gas stream)

3.2. Ground Rules and Assumptions

The NASA customer as well as the course organizer set a number of ground rules for the project. The ground rules helped to shape the project objectives and narrow the scope of the project. Some of the ground rules were also derived from the project objectives, which were discussed previously. They define a general timeline of the project, and state the expected deliverables.

The HYDRA team made some key assumptions to support and guide the design and testing of the dehumidification systems. Many of the assumptions were aimed at informing the test setup. The assumptions also outline available resources and define what is meant by spacecraft atmosphere. A summary of the ground rules and assumptions can be seen in Table 3. HYDRA Ground Rules and Assumptions.. The combination of the project objectives, ground rules, and assumptions allowed for a requirement breakdown to take place.

Table 3. HYDRA Ground Rules and Assumptions.

Ground Rules	
GR1	The designed system will be capable of dehumidifying the gas stream
GR2	The contactor(s) will be capable of being produced "in house"
GR3	Fall semester work will include modeling, conceptual design and preliminary experiments

GR4	Spring semester work will include manufacture of test article(s) and characterization experiments
GR5	A final report will be prepared upon concluding experimentation which describes the quantitative characterization of the configuration
GR6	The system will rid itself of H ₂ O after the dehumidification process
Assumptions	
ASM1	Extensive data is available to aid in the selection of the working fluid
ASM2	Contactor characterization from CARIL will help aid in design and engineering decisions
ASM3	Primarily the CU Bioastronautics laboratory will be used for experimentation and system storage
ASM4	The AETHER test rig is available for HYDRA's use in experimentation
ASM5	Human and system safety are considered to be of very high importance
ASM6	The nominal input spacecraft environment is defined by: 101 kPa total pressure, 23 °C, 40% RH, and 4 crew members
ASM7	Working fluid preservation is considered high importance

3.3. Mission Level Concept of Operations

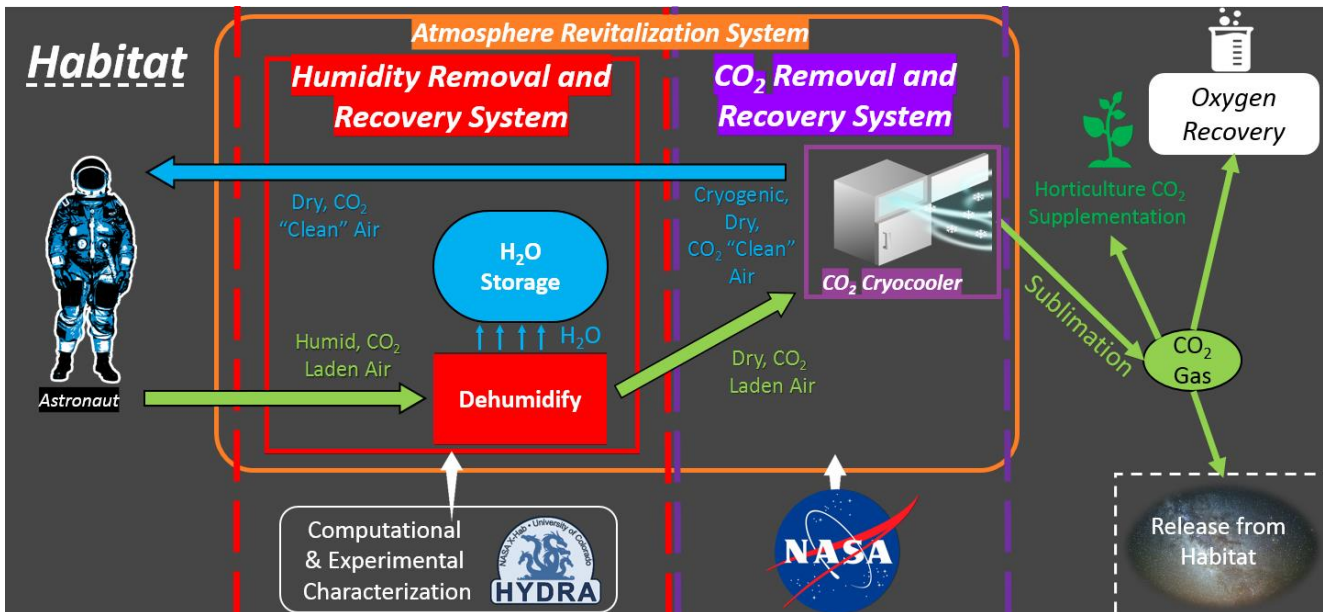


Figure 2. Mission level ConOps.

Figure 2. Mission level ConOps. shows the mission level Concept of Operations (ConOps) for the HYDRA project. In a practical implementation of cryogenic CO₂ removal system onboard a spacecraft, a dehumidification process must condition air for the cryogenic process. In the cabin astronauts produce humid CO₂ laden air. The CO₂ needs to be removed from the air with the potential for a number of potential reclamation processes including oxygen recovery and horticulture support. HYDRA will offer insight into the dehumidification process by providing computational and experimental characterization of a dehumidification system.

3.4. Project Concept of Operations

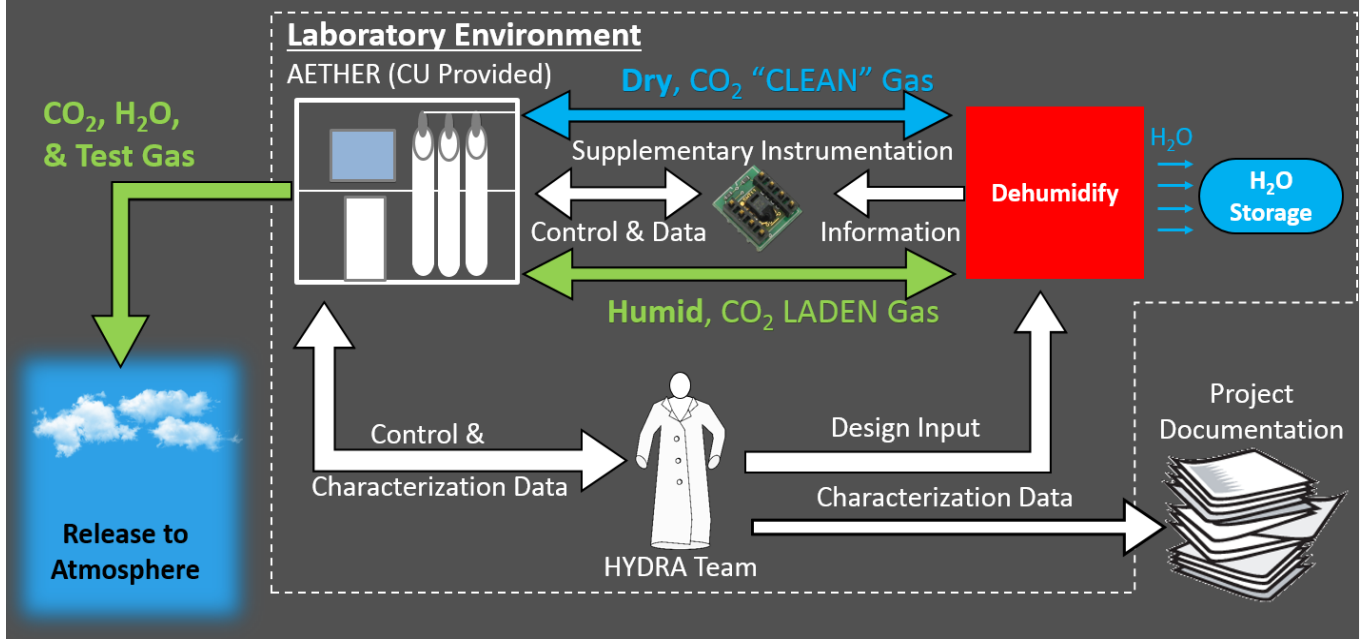


Figure 3. Project level ConOps.

The project level concept of operations, which is shown in Figure 3. Project level ConOps., outlines how the dehumidification system operates on a lab scale. The AETHER atmospheric revitalization test rig is used to run gas through the dehumidification system and collect data during the tests. The CU provided test rig is controlled by an operator with the ability to control the gas composition and flow rate of the gas being sent through the system. Data is collected by a number of sensors on the upstream and downstream side of the test article and sent back to AETHER. That data is then recorded for analysis.

3.5. Functional Block Diagram

Figure 4. Functional block diagram. shows the functional block diagram for the dehumidification systems. AETHER provides H₂O rich gas to the test article, which removes the humidity and sends the gas back to the AETHER system and then out to the atmosphere. Supplementing the AETHER sensors are an upstream humidity sensor and a downstream dew point sensor. The combination of sensors allows the system to be fully characterized. The working fluid source

provides the working fluid to the dehumidification system to remove the humidity. Data and controls are provided from AETHER using the user computer interface.

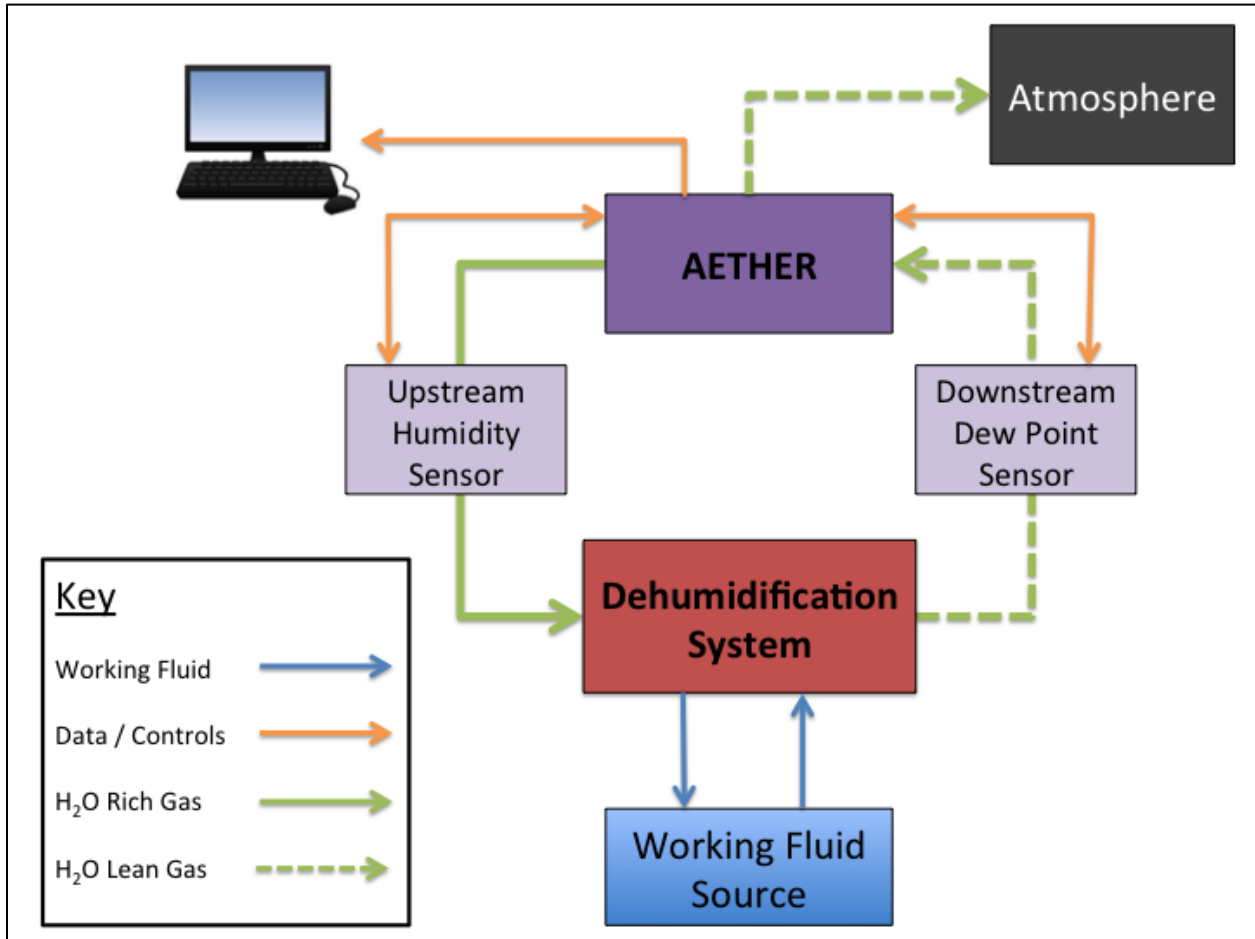


Figure 4. Functional block diagram.

3.6. Project Requirements

3.6.1. System Requirement Definition and Verification

The HYDRA team derived system requirements from the stated project objectives, ground rules, assumptions, and safety requirements. These requirements ensured that the design and manufactured system was safe and provided the data necessary to characterize the system.

Table 4. HYDRA Top-Level System Requirements. outlines the high-level system requirements.

Reference Number	Requirement
SR1	System shall dehumidify the supplied atmosphere
SR2	System shall facilitate the recovery of the water collected
SR3	System shall measure and record all parameters necessary to characterize system performance and validate models
SR4	System shall prevent contaminants from coming into contact with the working fluid and test gas
SR5	System shall operate within the CU Bioastronautics Laboratory environment

It should be noted that each of these top-level system requirements contains sub-requirements that provide further specifications and constraints. Each top-level requirement is also mapped to a parent specification from the Project Objectives, Ground Rules, or Assumptions. Every requirement for the HYDRA project is detailed and tracked in the HYDRA Master Requirements document.

Table 4. HYDRA Top-Level System Requirements.

Reference Number	Requirement
SR1	System shall dehumidify the supplied atmosphere
SR2	System shall facilitate the recovery of the water collected
SR3	System shall measure and record all parameters necessary to characterize system performance and validate models
SR4	System shall prevent contaminants from coming into contact with the working fluid and test gas
SR5	System shall operate within the CU Bioastronautics Laboratory environment

SR1 and SR2 stem directly from the objectives of the project. The system, which is the lab scale version in the context of the requirements, must be able to dehumidify the gas stream to previously defined levels of success. SR3 is traced back to the project objectives. The dehumidification system needs to be able to be characterized, which will allow for the validation of models. SR4 stems from previous experience with the AETHER test rig and ionic liquids. SR5 accounts for the physical constraints of the laboratory in which the testing will occur.

Requirement verification methods were determined for each system requirement. Table 4 shows the requirement verification matrix for the top-level system requirements. In the Master Requirement document, there is an additional column for the test ID that will be used to verify the requirement.

3.6.2. Safety Requirements

Reference Number	Verification Method	Requirement Verification Criterion
SFTY1	Inspection	Requirements SFTY1.1 - SFTY1.2 have been met
SFTY1.1	Inspection	The lab protocol has been taught and followed
SFTY1.2	Inspection	Chemical safety quiz has been passed and instructions followed
SFTY2	Inspection	Requirements SFTY2.1 - SFTY2.5 have been met
SFTY2.1	Test	Inspection of the system reveals a user display showing live health parameters
SFTY2.2	Test	Testing demonstrates the systems capability to monitor all relevant temperatures
SFTY2.3	Test	Testing demonstrates the system's capability to monitor all relevant pressures
SFTY2.4	Test	Testing demonstrates the system's capability to monitor humidity
SFTY2.5	Test	Testing demonstrates the system's capability to monitor CO2 concentration

HYDRA Project Spring 2018 Final Report

SFTY3	Inspection	Inspection of conceptual design reveals that working fluid will remain internal to the system even if it leaks out of the contactor/membrane. Inspection of the physical system reveals no working fluid leaks.
SFTY4	Test	Tests show that surface temperatures remain below 40 °C during experimentation.
SFTY5	Test	Tests show that exhaust temperatures remain below 40 °C during experimentation.
SFTY6	Analysis	Basic thermal analysis reveals that COTS components remain in the desired range.
SFTY7	Inspection, Test	Bare wires and wire terminals are covered. Tests reveal that no unintended voltage potentials are present.
SFTY8	Inspection	A design is implemented which mitigates contamination of the lab atmosphere with test gasses.
SFTY9	Inspection	System displays signage for all appropriate hazards.
SFTY9.1	Inspection	System displays signage for toxicity hazard.
SFTY9.2	Inspection	System displays signage for high CO2 concentration hazard.
SFTY9.3	Inspection	System displays signage for electrical shock hazard.

3.6.3. Controls Requirements

Reference Number	Verification Method	Requirement Verification Criterion
CTRL1	Analysis, Inspection	Analysis provides information regarding which parameters are important to system health. Both requirements CTRL1.1 and CTRL 1.2 are met.
CTRL1.1	Inspection, Test	Inspection of conceptual design and physical system shows that all required sensors for characterization are accounted for. Tests reveal that all of the aforementioned sensors are operating nominally.
CTRL1.2	Inspection	Inspection shows that data collected from system health sensors is being displayed in a readable format.
CTRL2	Test	Tests reveal that the system halts safety critical operations if any health parameter strays beyond the established limits.
CTRL3	Analysis, Inspection	Analysis provides information regarding the parameters needed to characterize the 3PSC. Inspection of conceptual design and of system reveal that all sensors required for this purpose are accounted for.

HYDRA Project Spring 2018 Final Report

CTRL3.1	Inspection	Manufacture data sheets show that sensor is capable of meeting performance requirements. Inspection reveals that sensors are installed properly.
CTRL3.2	Inspection	Manufacture data sheets show that sensor is capable of meeting performance requirements. Inspection reveals that sensors are installed properly.
CTRL3.3	Inspection	Manufacture data sheets show that sensor is capable of meeting performance requirements. Inspection reveals that sensors are installed properly.
CTRL3.4	Inspection	Manufacture data sheets show that sensor is capable of meeting performance requirements. Inspection reveals that sensors are installed properly.
CTRL3.5	Inspection	Manufacture data sheets show that sensor is capable of meeting performance requirements. Inspection reveals that sensors are installed properly.

3.6.4. Mechanical Requirements

Reference Number	Verification Method	Requirement Verification Criterion
MECH1	Inspection	Confirmation that MER1.1 and MER1.2 are met
MECH1.1	Inspection	System design incorporates methods for particulate mitigation that perform as desired. Inspection of system reveals that no visible particulate contaminates are introduced during operation
MECH1.1	Testing, Analysis	System design incorporates method(s) for unwanted gas mitigation that perform as desired. Testing and analysis show no trace amounts of any unwanted gas.
MECH2	Inspection	Inspection of system reveal no working fluid can escape the Test Article.
MECH3	Inspection, Test	Pressure tests and inspection reveal no gas escapes from the Test Article.

3.6.5. Modeling Requirements

Reference Number	Verification Method	Requirement Verification Criterion
MOD1	Inspection	Inspection of documentation shows that assumptions are listed along with the rationale for each.
MOD2	Analysis	A model is developed from first principles that predicts H2O uptake for each prospective working fluid
MOD2.1	Analysis	Data from model provides information on the absorption performance for each prospective working fluid.
MOD2.2	Analysis	Data from model provides information on working fluid performance in different geometries and quantities.

3.6.6. *Manufacturing Requirements*

Reference Number	Verification Method	Requirement Verification Criterion
MR1	Inspection	Components shall be manufactured in house or be available COTS
MR2	Inspection	Components manufactured within +/- 0.005"
MR3	Inspection, Test	Assembled systems shall be capable of integration with AETHER and/or chiller system
MR4	Inspection, Analysis, Test	System shall have material that is compatible with the working fluid and test gas
MR4.1	Analysis, Test	All materials in contact with cryogenic coolant or gas shall be able to withstand temperatures of -40°C
MR4.2	Test, Inspection	All materials in contact with the IL shall not react significantly with the IL

3.7. *System Interfaces*

There are three key interfaces that have been identified for the HYDRA project which includes both physical and data interfaces. The three key interfaces identified are:

1. The interface between the test article and the AETHER test rig
2. The interface between the test article and the environment.
3. The interface between the analytical models and the data collected

The physical interface between the test rig and the test article allows test article characterization data to be gathered from the AETHER system. It also allows for the control of the gas stream that passes through the test article. The interface with the environment governs the potential of leaks both of the air stream and the working fluid. It also accounts for any heat transfer taking place between the system and the environment. The data interface between the characterization data and the models allows for the validation of the models. The models were used to predict performance of the design, and must now be validated with the collected data.

3.8. *Systems Engineering Lessons Learned*

The rate of heat transfer between the test article (WCS) and the environment was not properly investigated during the systems design phase and as a result the chiller was not able to perform as well as expected and the downstream thermocouple readings were of no use in model validation. If this problem were more properly addressed in the months leading up to testing it may have been possible to mitigate or eliminate these undesired effects entirely. Similarly, the time, effort, and budget put into ensuring that the dew point sensor did not come into contact with

HYDRA Project Spring 2018 Final Report

freezing temperatures was entirely unnecessary as 1 foot of tubing with ambient heating was more than enough to raise the output air stream to room temperature. A simple calculation could (and should) have been done to estimate environmental heat transfer on all parts of the system experiencing cryogenic temperatures. This also may have caught the inlet freezing problem in the design phase.

Another lesson learned was to only make requirements as specific as they need to be. When things started going wrong it was necessary to set aside or relax certain requirements in order to get anything done. More thought put into the actual necessity of the requirements before testing and manufacturing started could have saved the team a lot of time.

4. Modeling

Table 5. Requirement Verification Matrix for the Top-Level System Requirements.

Reference Number	Verification Method	Requirement Verification Criteria
SR1	Analysis, Test	Working fluid demonstrates its capability to absorb H ₂ O. Experimentation and data acquisition paired with analysis shows that the H ₂ O is being removed from the supplied gas stream
SR2	Inspection, Test	Inspection and testing of the system reveals that H ₂ O content after expelling is zero
SR3	Analysis, Test	Analysis of the system design reveals that the system can be characterized with the design choices selected. Experimentation and proper data acquisition show that the system is measuring and recording all necessary values
SR4	Inspection	System design incorporates method(s) for particulate mitigation, which has historically proven to be effective at the desired performance and efficiency. Inspection of system reveals that no visible particulate contaminants are introduced during operation.
SR5	Inspection	No dimension in conceptual or physical system has a dimension larger than the desired maximum. Analysis of system design reveals that the total mass will be under OSHA lifting limits. Inspection of conceptual and physical system reveals that only resources available within the CU Bioastronautics Laboratory are needed for the system to be functional. No permanent modifications are made to said laboratory.

4.1. Water Cryocooler System (WCS) Modeling

4.1.1. Model Assumptions

- Air obeys ideal gas law.
- The plug flow model simplifies the system to 1-D.
- The system is in a quasi-steady state, meaning all derivatives with respect to time are set to zero apart from the ice deposition rate.
- The wall temperature is constant in time and uniform in space.
- The liquid phase of water is neglected, meaning any water that condenses out of the air is assumed to immediately freeze.

4.1.2. Model Implementation

The WCS model was adapted from Chambliss et al. (2012) which details a model for a CO₂ cryocooler system. From a design standpoint, the most important outputs of the model are pressure drop, output dew point, and time rate of ice deposition, as these values will determine the size of the WCS and its cycle time. Equation 1 gives the pressure gradient along the tube.

$$\frac{dP}{dx} = \frac{-f\rho v^2}{2D} \quad (1)$$

Where P is the total pressure in Pa, x is the length coordinate of the model in meters, f is the non-dimensional friction factor, ρ is the air density in kg/m^3 , v is the air velocity in m/s , and D is the diameter of the tube in meters. All of these values are functions of x . The friction factor is given by Equation 2.

$$f = \begin{cases} \frac{64/Re}{0.25} & \text{if } Re < 2300 \\ \frac{1}{\left[\log\left(\frac{\epsilon}{2D} + \frac{5.74}{Re^{0.9}}\right)\right]^2} & \text{if } Re \geq 2300 \end{cases} \quad (2)$$

Where Re is the local Reynolds number of the air flow, and ϵ is the average pipe roughness in mm (0.045 mm typical for stainless steel). Equations 3 and 4 are used to determine the velocity and density gradients in the tube and are based on the 1-dimensional continuity equation and the ideal gas equation respectively.

$$\frac{dv}{dx} = -v \left(\frac{1}{\rho} \frac{d\rho}{dx} + \frac{1}{A} \frac{dA}{dx} \right) \quad (3)$$

$$\frac{d\rho}{dx} = \frac{1}{RT^2} \left(T \frac{dP}{dx} - P \frac{dT}{dx} \right) \quad (4)$$

Where A is the cross-sectional area of the tube in m^2 , T is the temperature of the air in K, and R is the universal gas constant in J/K/mol . The temperature gradient is given by Equation 5.

$$\frac{dT}{dx} = \frac{1}{v\rho} \left(h(T_w - T) - \frac{dq}{dt} \Delta H \right) \quad (5)$$

Where T_w is the temperature of the tube wall in K, dq/dt is the time rate of ice deposition in $\text{mol/m}^2/\text{s}$, and ΔH is the latent heat of sublimation in J/mol (for water $\Delta H = 50.97 \text{ kJ/mol}$). The quantity h is the convective heat transfer coefficient in $\text{W/m}^2/\text{K}$ and is given by Equation 6.

$$h = \begin{cases} \frac{k_{air}}{D} \left(\frac{3.66 + \left(0.065 Re Pr \frac{D}{L}\right)}{1 + 0.04 \left(Re Pr * \frac{D}{L}\right)^{\frac{2}{3}}} \right) & \text{if } Re < 3000 \\ \frac{k_{air}}{D} \left(\frac{\frac{f}{8} (Re - 1000) Pr}{1 + 12.7 \sqrt{\frac{f}{8} (Pr^{\frac{2}{3}} - 1)}} \right) & \text{if } Re \geq 3000 \end{cases} \quad (6)$$

Where k_{air} is the conductive heat transfer coefficient of air in W/m/K , Pr is the Prandtl number, L is the total length of the tube in meters, and f is the same friction coefficient calculated in Equation 2. Equation 7 defines the concentration gradient and Equation 8 gives the time rate of ice deposition in the system assuming a linear driving force.

$$\frac{dC}{dx} = \frac{-1}{v} \left(\frac{dq}{dt} + C \frac{dv}{dx} \right) \quad (7)$$

$$\frac{dq}{dt} = k(C - C_e) \quad (8)$$

Where k is the mass transfer coefficient in m/s . C is the concentration of water in the air in mol/m^3 , and C_e is the saturated vapor concentration of water at the current temperature in mol/m^3 . The mass transfer coefficient is calculated based on a combination of the heat transfer analogies described in Muntahe et al. (2016) and Xanthopoulos et al (2012) for frost growth and is given in equations 9-13:

$$k = Sh \frac{D_f}{D} \quad (9)$$

$$Sh = NuLe^{2/3} \quad (10)$$

$$Nu = 1.86(RePr)^{1/3} \left(\frac{D}{L}\right)^{1/3} \left(\frac{\mu}{\mu_{wall}}\right)^{0.14} \quad (11)$$

$$Le = \frac{Sc}{Pr} \quad (12)$$

$$Sc = \frac{\mu}{\rho D_f} \quad (13)$$

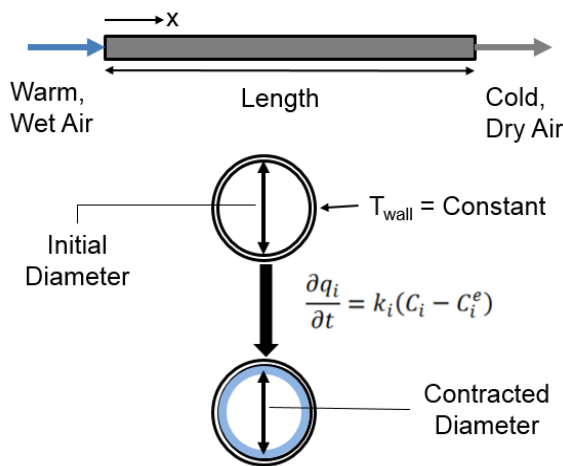


Figure 5. Overview of geometry in the WCS model.

Where Sh is the dimensionless Sherwood number, D_f is the mass diffusivity in m^2/s , Nu is the dimensionless Nusselt number, Le is the dimensionless Lewis number, μ and μ_{wall} are the dynamic viscosities in the bulk flow and at the wall respectively in m^2/s , Pr is the dimensionless Prandtl number, Sc is the dimensionless Schmidt number, and ρ is the air density in kg/m^3 .

A summary of the model geometry is given in Figure 5. Overview of geometry in the WCS model.

The model numerically integrates these equations in x and obtains a profile of dq/dt along the operator specified length of the tube. It then integrates this profile over a finite time step to determine how much ice has accumulated. The ice buildup is converted into a contraction of the tube diameter and the new diameter profile is fed

back into the length integration. This process is looped until the operator-defined time limit is reached or the pressure drop exceeds acceptable levels ($\Delta P > 2740$ Pa) [Weiland, 1998]. A flow chart of the overall model structure is given in Figure 6.

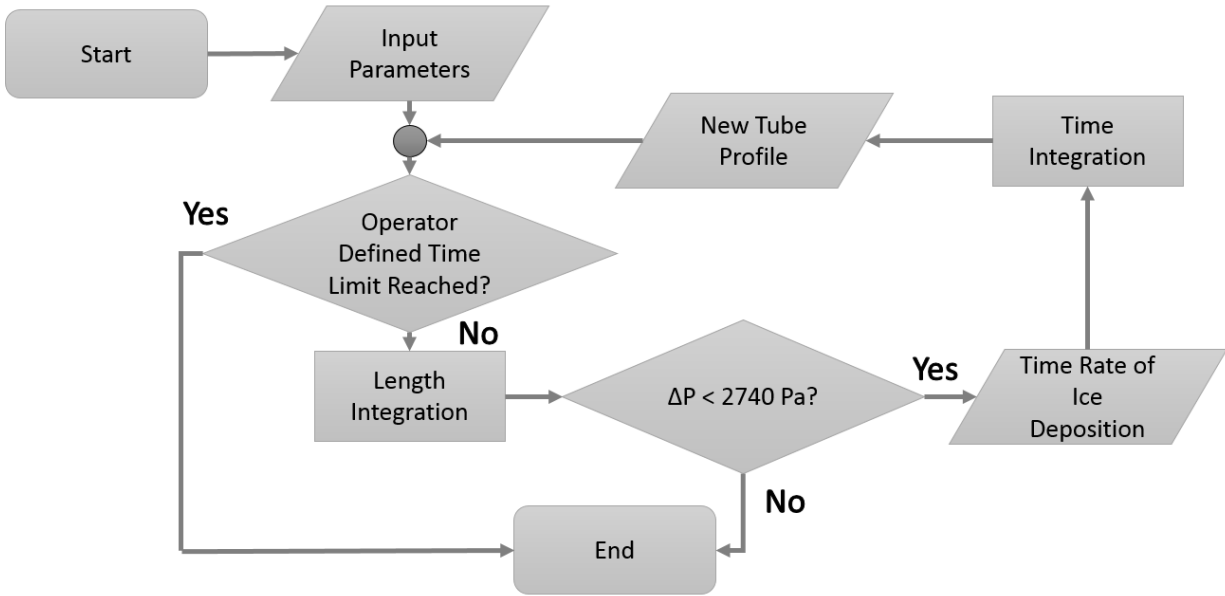


Figure 6. Overall structure of WCS model.

4.1.3. Model Inputs

The model takes as input the tube dimensions (length and inner diameter), the inlet air flow parameters (volumetric flowrate, temperature, pressure, vapor pressure of water), and some miscellaneous constants (ice density, wall temperature, mass transfer coefficient, total simulation time, and simulation time step).

4.1.4. Lab-Scale Design

The model insight most instrumental in the determination of the lab-scale WCS dimensions is summarized by Figure 7, which shows the initial output dew point vs tube diameter as well as the dew point change over a period of 5 hours. To ensure that the system fit easily in the CU Boulder lab space and to eliminate a design variable, the model length of the WCS was fixed at 0.61 m. AETHER has a design requirement of 70% Relative Humidity (RH) since this is the upper bound for spacecraft and the ISS. The upper limit on RH stems from the desire to maintain crew comfort and mitigate risk of condensation that could cause electrical problems [Weiland, 1998]. The maximum expected humidity is chosen to increase the rate of ice deposition and cause the system performance to deteriorate more quickly in order to shorten testing time. The flowrate of 9 L/min is the maximum flowrate that can be achieved in the low-flow mode on the AETHER system and was chosen in order to reduce the testing time. The system model is constrained to the low-flow mode because the higher flow modes have larger uncertainties on the measured flows that would lower confidence in model validation.

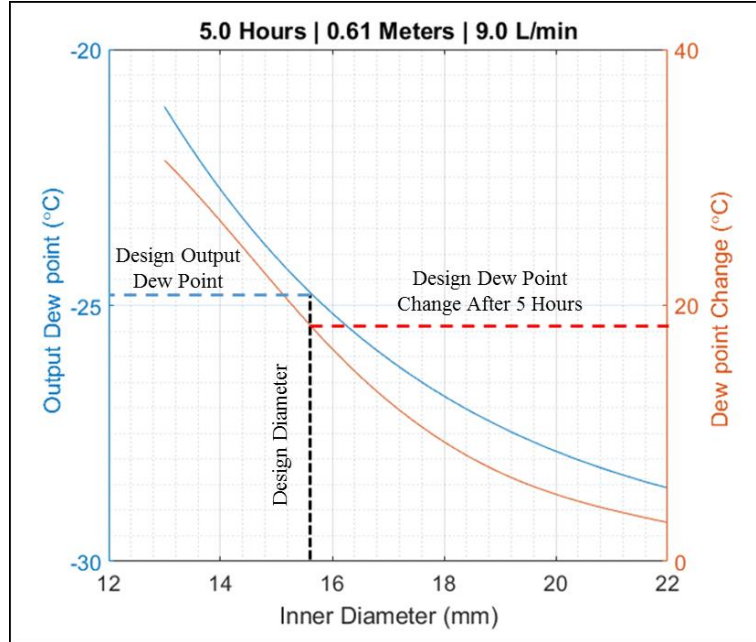


Figure 7. Initial output dew point and dew point change after 5 hours vs inner diameter. Wall temperature is -30 °C. Tube length is 0.61 m. flowrate is 9 L/min, and input humidity is 70%RH. Design point is marked with dashed lines.

Figure 7 highlights the air tube inner diameter chosen as the design point for the lab-scale WCS with dashed lines. This design point of 15.56 mm inner diameter is selected as a trade-off between a small diameter tube (shorter testing time) and a larger diameter (better performance and less sensitivity to input uncertainties). The selected diameter also allows for the use of standard (¾ in) tubing when manufacturing the WCS. All of the design work on the WCS was done assuming a constant mass transfer coefficient of 32 m/s as the heat transfer analogy method had not yet been developed.

4.1.5. Monte-Carlo Uncertainty Analysis

Figure 8 illustrates the results of Monte Carlo simulations that examined the effects of varying certain input quantities and model coefficients.

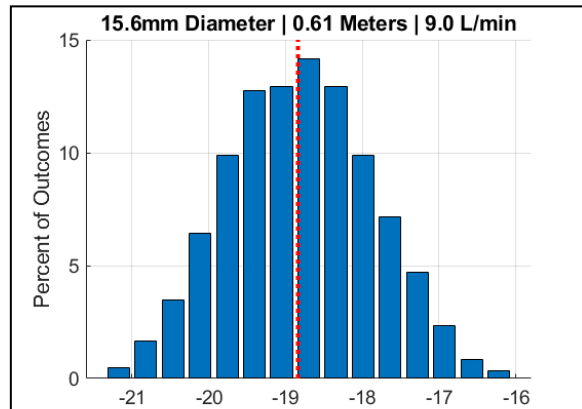


Figure 8. Histogram of results of the Monte-Carlo simulation. The dashed line indicates the nominal output.

The nominal model output dew point (-18.8 °C) is denoted by the dashed red line. The mean value is -18.8 °C and the standard deviation is 0.9 °C.

Table 6 shows the nominal input values and the range of inputs considered in the simulation. Note that the mass transfer coefficient is calculated here using the heat transfer analogy rather than assuming a constant value. These results show that the uncertainties in the gas input stream are not likely to affect the output dew point by more than 2 °C. The dew point sensor used for testing has an accuracy of ± 2 °C, so it was concluded that any input deviations should not pose a problem

Input Parameter	Nominal	Minimum	Maximum
Air Pressure	.84 atm	.79 atm	0.89 atm
Volumetric Flowrate	9 L/min	8.5 L/min	9.5 L/min
Air Temperature	296 K	293 K	300 K
Humidity	70 %RH	65 %RH	75 %RH
Length	0.61 m	0.58 m	0.64 m
Inner Diameter	15.56 mm	15.43 mm	15.69 mm

regarding model validation.

Table 6. Range of input values used in the Monte-Carlo simulation.

4.1.6. *Model Performance Summary*

The WCS model achieves the criteria of a good model in that:

- a) The WCS model is based on first principles, specifically the conservation of mass and energy.
- b) The WCS model can run 1000 iterations in 30 seconds, satisfying the reasonable execution time criterion.
- c) The WCS model is fundamentally a system of ordinary differential equations that are readily solved. Its operation should be clear to anyone with a technical background.
- d) Model performance will be assessed in the model validation phase of lab-scale WCS testing.

The WCS model has proven to inform design and predict performance.

4.2. *Ionic Liquid System (ILS) Modeling*

4.2.1. *Introduction*

Cross flow hollow fiber membrane contactors using ionic liquids have not yet been thoroughly characterized, making modelling efforts challenging. The initial model for the ILS relied on a heat transfer analogy based on the work by Dindore et al. (2005). This preliminary model was used to characterize the performance variations with hollow fiber membrane contactors with different dimensions. Once the contactor size was finalized, further refinements to the model were made based on fundamental mass transfer theory (Cussler, 1997). This increased the fidelity and reliability of the model, however one key parameter, the distribution coefficient, kept uncertainty in the model output higher than desirable. This parameter was initially measured experimentally, but the results of the test campaign discredited the initial measurement, while suggesting a new value. After ILS testing was complete, another experiment was run to remeasure the distribution coefficient properly and this value matched very well with the expected value predicted from ILS test results.

4.2.2. *Ionic Liquid Selection*

The ionic liquid selected for use in the ILS is 1 Ethyl-3-Methylimidazolium Ethyl sulfate [EMIM] [EtSO₄]. This ionic liquid was chosen due to its highly hygroscopic nature, its relative non-selectivity for carbon dioxide, and its non-toxicity. In fact, [EMIM] [EtSO₄] is only seriously dangerous if ingested, and contact with skin or eyes will only cause irritation. Our group chose to proceed with this ionic liquid because of the aforementioned reasons, along with the fact that this choice was suggested by Dr. Nabity who has much more ionic liquid expertise than any member in our group. Some useful properties of [EMIM] [EtSO₄] are given in the Table 7.

Table 7. Properties of [EMIM] [EtSO₄].

Product Name	Molar Mass	Melting Point [°C]	Viscosity at RT [mPas]	Electric Conductivity [μS/cm]	Distribution Coefficient at RT	Cost [\$/kg]
[EMIM] [EtSO ₄]	236.29	< -20	122	4 - 40	11000	\$369.50

4.2.3. *Dimensional Analysis*

The early iteration of the ILS model was used to inform the final size of the ILS. The primary take away from this model was that the test article would perform best with a high residence time of air in the fibers. This could be accomplished by increasing the number of fibers while keeping the total air flow rate constant, or by elongating the fibers. Ultimately, manufacturing constraints dictated the size of the contactor, opting for 484 fibers that were 0.508 m long. The results of this analysis and the dimensions of the final contactor design can be seen in Figure 9. Further analysis of the contactor using the test results and the new model indicate that our final design was larger than necessary. The water in the air and the ionic liquid reached equilibrium prior to the air reaching the end of the contactor. This is shown in Figure 10, which indicates that a much smaller contactor would have performed as well as the final design.

x = Selected contactor:
484 fibers, 508mm long

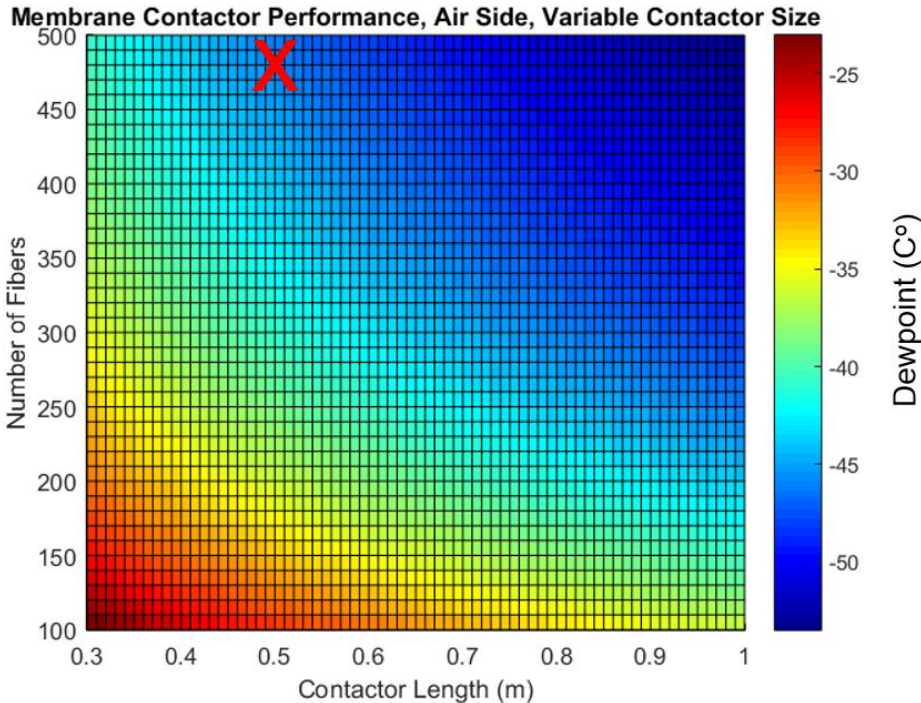


Figure 9: HFMC dimensional performance analysis.

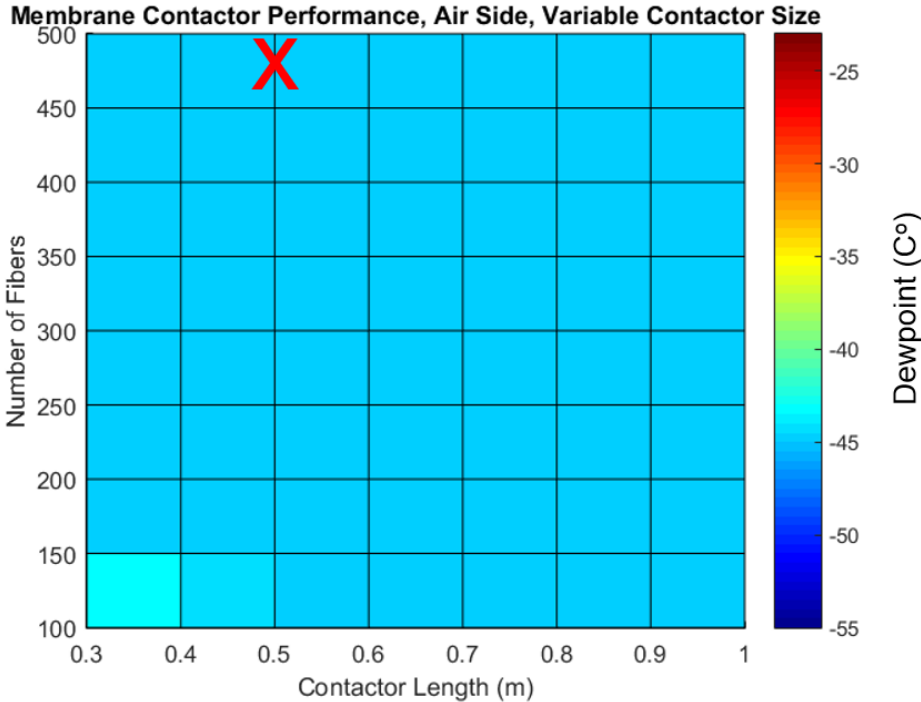


Figure 10: HFMC dimensional performance with improved model.

4.2.4. *Improved Mass Transfer Model Theory*

The transfer of water molecules from the air in the fibers to the ionic liquid in the shell can be separated into three distinct stages as shown in Figure 11. The first stage is the transfer of water through the air. Since the mass transfer of water vapor happens more than one hundred times faster in air than in fluids, this stage was neglected in the model and the concentration of water in the air was assumed to be constant. The fibers are made from hydrophobic material, thus the pores of the fiber were assumed to be filled with air (Dindore, 2005). The second stage of mass transfer occurs at the boundary between the air and the ionic liquid. This boundary is assumed to be in equilibrium, however due to the chemical affinity of the ionic liquid and water, the concentration of water on the ionic liquid side is much higher than the on the air side. This equilibrium ratio is known as the distribution coefficient (sometimes called the partition coefficient). This coefficient dictates the minimum dew point that the air can achieve for a given concentration of water in the ionic liquid, once the air and ionic liquid have reached equilibrium. The third stage of mass transfer is in the boundary layer of the ionic liquid. This is the mass transfer limiting step and the most challenging step to model. This was modelled as if the fibers were a solid block of material releasing water into the IL, allowing for the usage of the following mass transfer coefficient from the literature (Cussler, 1997):

$$\text{Flow outside and perpendicular to a capillary bed} \quad \frac{kd}{D} = 0.80 \left(\frac{dv^0}{\nu} \right)^{0.47} \left(\frac{\nu}{D} \right)^{1/3} \quad (14)$$

Where k is the mass transfer coefficient, d is the diameter of the capillaries (fibers), D is the diffusion coefficient, v^0 is the velocity of the fluid approaching the bed, and ν is the kinematic viscosity.

The diffusion coefficient is a function of the water concentration in the ionic liquid and is described by Rausch et al. (2011). Similarly, the viscosity also varies with the composition of the ionic liquid and is described by Rodriguez and Brennecke (2006). In order to take into account these variations of the ionic liquid properties, the model was discretized into a grid with 100 sections in the lengthwise direction.

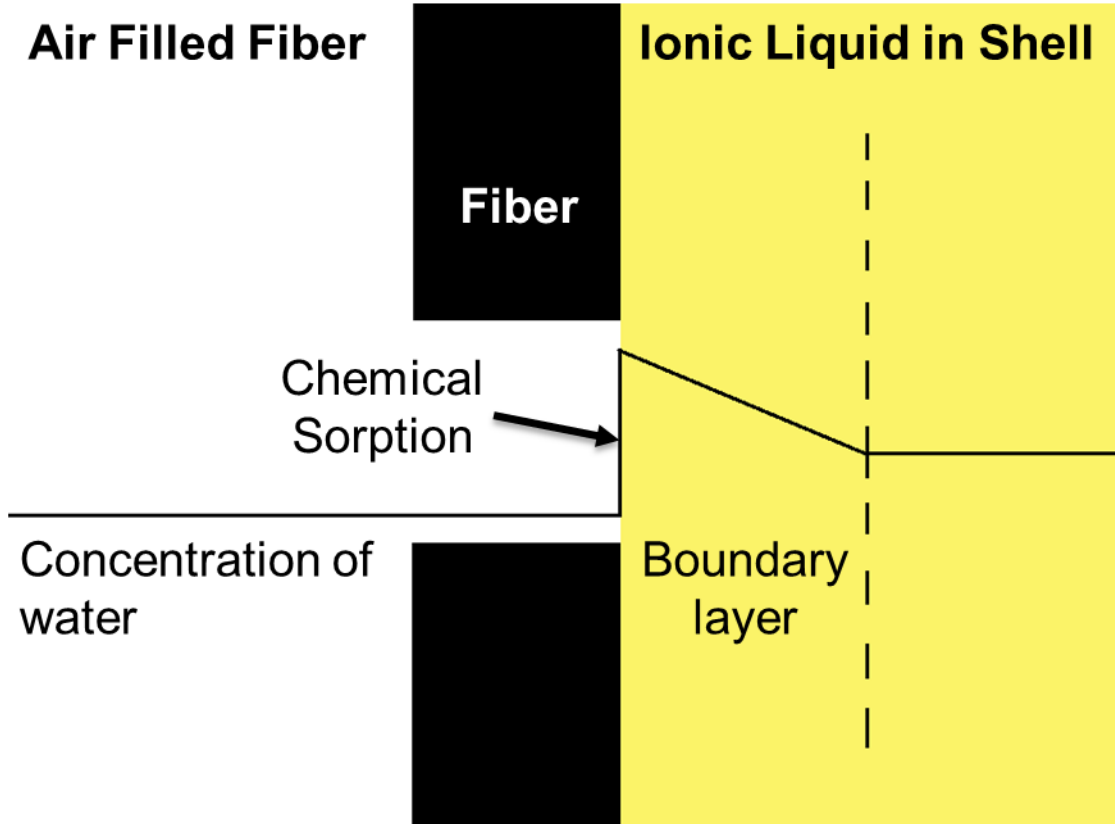


Figure 11: Visualization of mass transfer in the ILS.

4.2.5. *Distribution Coefficient*

The distribution coefficient is an equilibrium ratio of the concentration of water in the ionic liquid to the concentration of water in the air. An initial experiment was run to measure this value and was found to be 1200. During later testing of the ILS it was discovered that the water content in the ionic liquid exceeded the predicted saturation level and continued to extract water from the air, thus invalidating the original measurement. It was also discovered that 24 hours in a vacuum chamber was insufficient to reach equilibrium, indicating that the original experiment, which was run for ~2 hours, had not run long enough to reach equilibrium either. Tuning the model resulted in a distribution coefficient of 11000 that matched the actual ILS test data quite well. A second distribution coefficient test was deemed necessary, this time run for 3 days in a shallow container. This test found a value of 10500 for the distribution coefficient, thereby providing strong experimental justification for the tuned value used in the model.

4.2.6. *Model Limitations*

The primary limitations of the model are due to the complex geometry of the contactor. The model assumes that the contactor is a square prism with a uniform grid of fibers as shown in Figure 12, however the actual contactor is a cylinder with fibers laid out in concentric rings. As shown in Figure 13 the contactor has a complex flow pattern, which was not captured by the model. In between the inlets and the outlet, the flow is parallel to the fibers. Simulations show that this configuration results in significant reductions in mass transfer since the IL forms channels around the fibers that become saturated with water. Conversely, the IL near the inlets and outlet is flowing

faster than in the model, which would increase performance. It was not determined which of these two effects was greater since the air reached equilibrium for all ILS test cases.

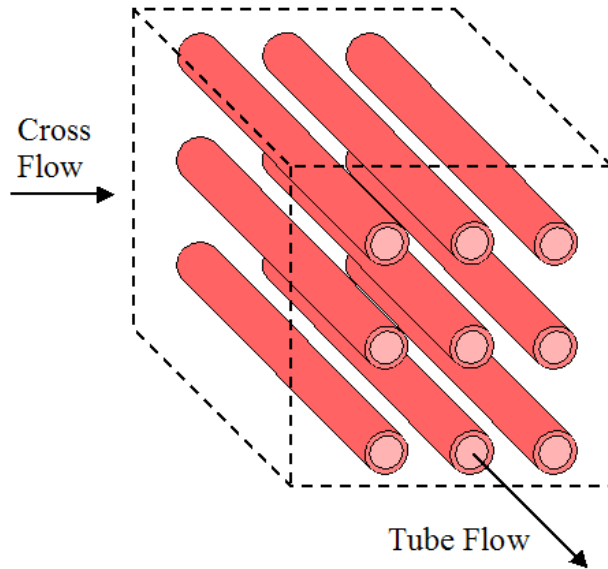


Figure 12: Geometry used in model.

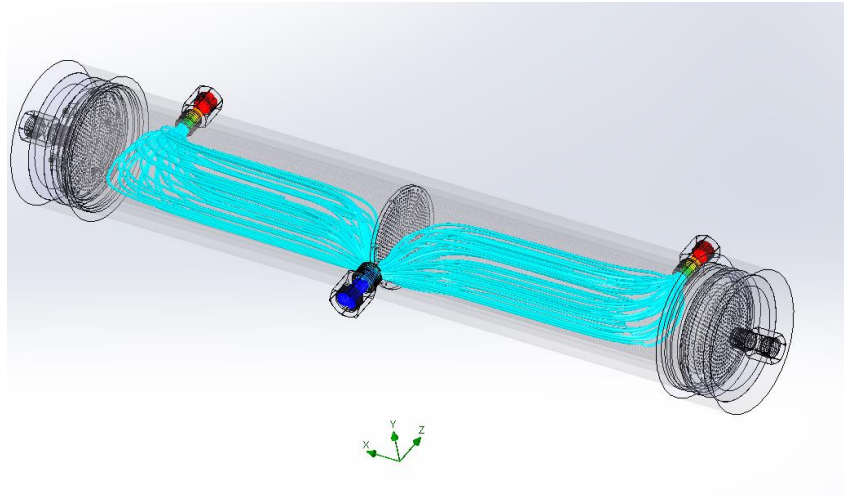


Figure 13: Actual geometry and flow pattern of ILS.

4.2.7. Model Outputs

As a result of the discretization, the model is able to produce a plot of the dew point in the air at every location in the virtual contactor as shown in Figure 14. This plot shows the performance of the contactor at the maximum water flux rate tested. Even in this worst case scenario, the contactor is able to reach equilibrium less than 20% of the way through the contactor. This indicates that the output dew point of the system should only be dictated by the initial concentration of water in the ionic liquid and the distribution coefficient. Reducing the relative humidity or flow rate of air will only cause equilibrium to be reached sooner in the contactor. Reducing the flow rate of the ionic liquid will reduce the rate of mass transfer, however it will only prevent the air from reaching equilibrium at a flow rate less than 0.1 LPM as shown in Figure 15,

well below the nominal test conditions. This indicates that within the test regime, it is only the concentration of water in the ionic liquid that has a significant impact on the output dew point. This sensitivity is shown in Figure 16.

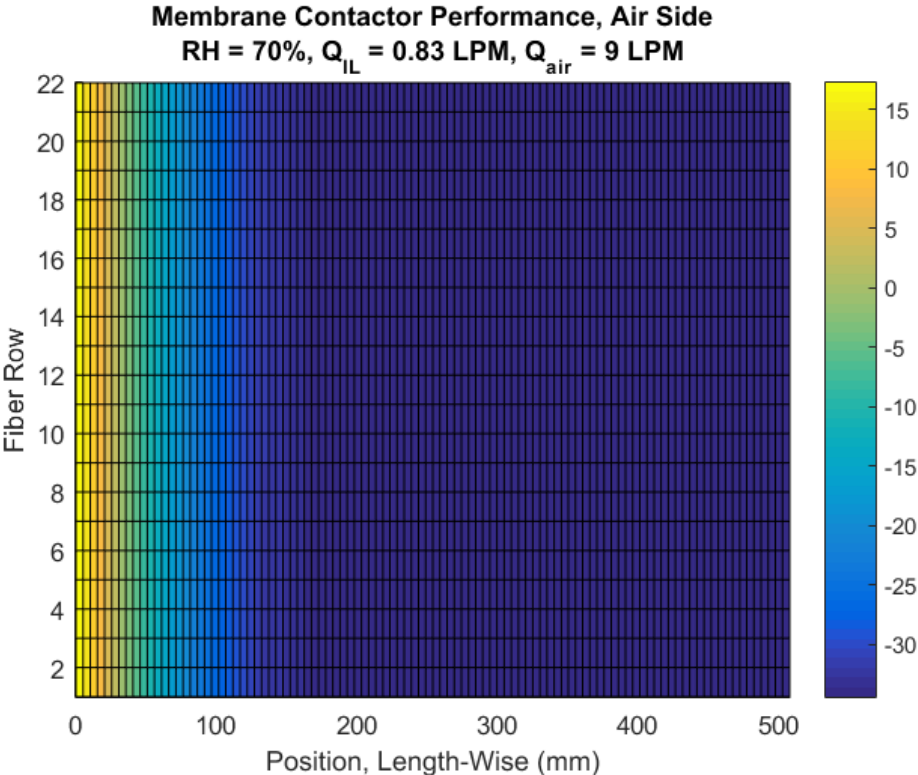


Figure 14: Dew Point of Air Passing Through the Contactor

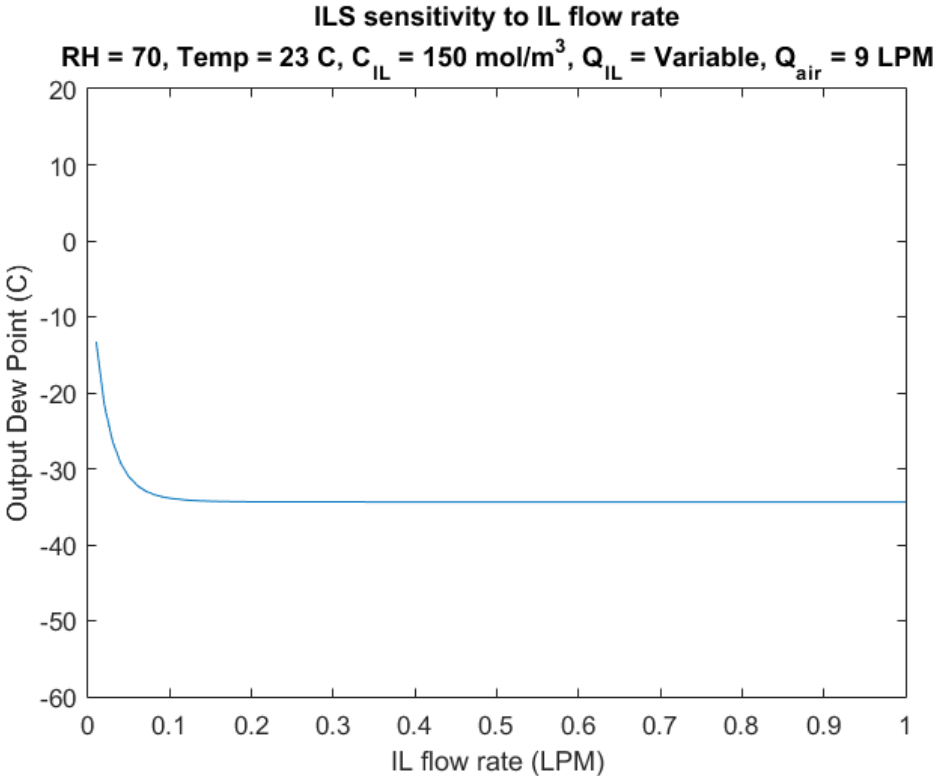


Figure 15: Output dew point sensitivity to IL flow rate.

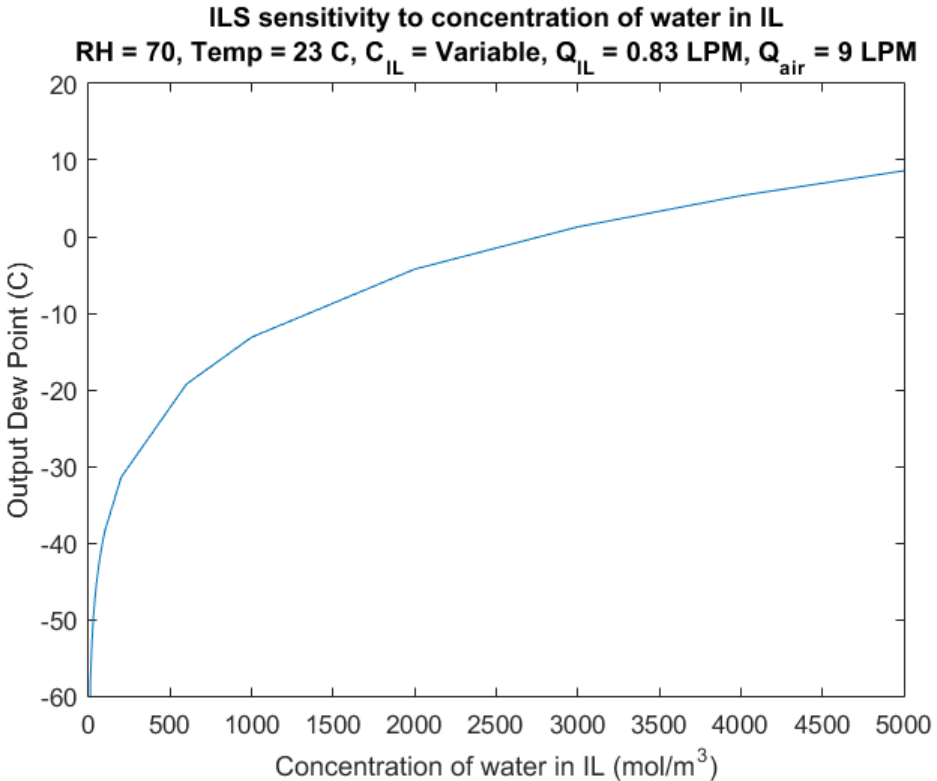


Figure 16: Output Dew Point Sensitivity to Water Content in the Ionic Liquid

5. Manufacturing

5.1. Water Cryocooler System (WCS) Design and Manufacturing

The mechanical design of the Water Cryocooler System (WCS) was designed to be as simple and robust as possible. The WCS was designed for laboratory scale and, as such, was 26 in. long and 4.25 in. in diameter. HYDRA's final WCS design used two concentric stainless-steel tubes, two off-the-shelf flanges, two custom built flanges, two bosses, four O-rings, and two gaskets. The final design connected the WCS to AETHER via two $\frac{1}{4}$ inch NPT compression fittings placed one either end of the cylindrical shaped system. There was one inlet and one outlet for the coolant as well. These $\frac{1}{2}$ inch NPT hose fittings were located about $\frac{1}{2}$ inch from the inside flanges and are attached on opposite ends of the outer pipe, both axially and radially, via bosses. The final design can be seen in **Error! Reference source not found.** and Figure 18 seen below.

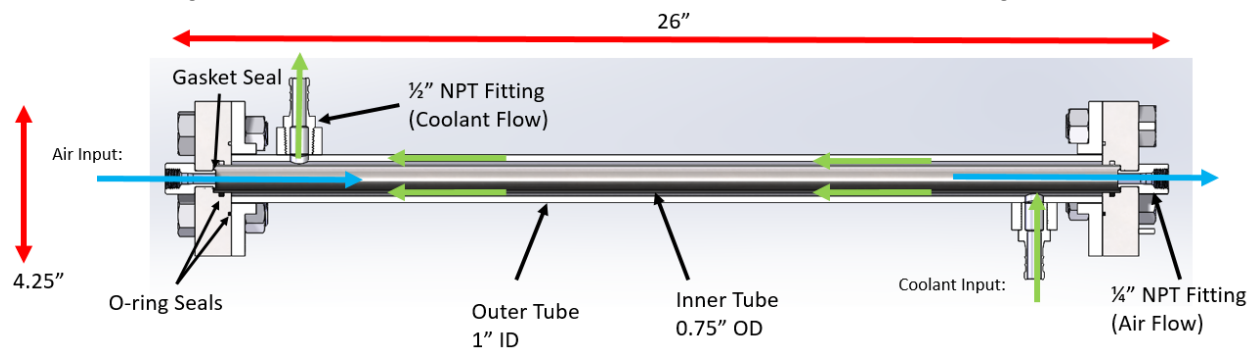


Figure 17. WCS final design with dimensions.

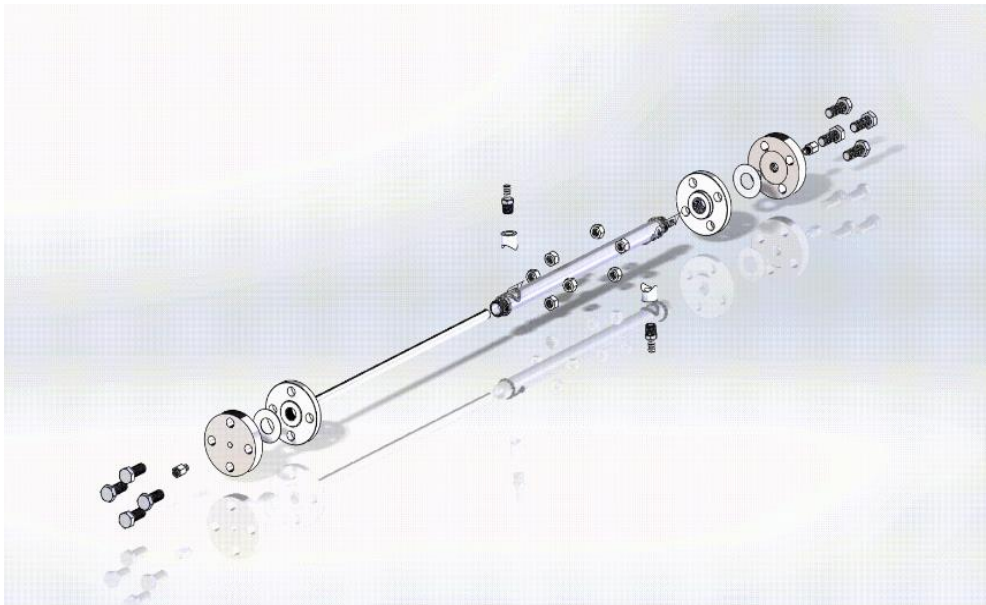


Figure 18. WCS exploded assembly.

All materials were bought off the shelf, except the custom flanges which were machined in-house. All the materials were designed to be made from stainless-steel, with the exceptions of the

gaskets and O-rings. Stainless-steel was chosen due to its heat transfer properties and its ability to be non-reactive with most materials. The O-rings and gaskets were made of Ethylene Propylene Diene Monomer Rubber (EPDM). EPDM was chosen as the material due to its ability to withstand cold temperatures and is chemically non-reactive with Propylene Glycol (the coolant chosen for this experiment). The system works by freezing water out of the air as it flows through the system. The propylene glycol was in a separate loop that was fed and cooled down to a consistent -30°C via a ThermoHaake Phoenix II CT90L.

The area inside the inner pipe was used to direct the air flow through the system. The inner pipe, seen between the green arrows in Figure 17, was chosen as the better location to flow the air because it provides more area to volume to hold frozen ice and is easier to remove and de-ice. The inner pipe was made of 304 stainless steel and was .083 in. with an outer diameter of $\frac{3}{4}$ in. Its original length of 4 ft. was cut down to 25 inches to fit between the two outer flanges securely. The outer pipe had an inner diameter 0.957 inches and outer diameter of 1.315 inches and was cut from its original length of 36 inches to 24 inches. Both pipes were cut using a horizontal band saw and left unthreaded. It can be seen in Figure 17 as labeled.

The largest amount of machining came from the outer flange. It was designed with a radial O-ring groove for one of the seals to separate the air and propylene glycol. An O-ring groove was also cut into the flat face of the flange to allow an O-ring to prevent any propylene glycol from leaking between the flanges. This piece was also made from 303 stainless steel stock and machined using a 3 degree of freedom CNC Lathe. The stock was 5 inches long and had a diameter of 5 inches. When finished, each flange was 4.25 inches in diameter and 1 inch thick. The inner flange was purchased at 4.25 in. in diameter and was 0.6875 inches thick. The inner flange was 304 stainless steel with an unthreaded hole diameter of 1.316 inches in the center.

The O-rings and gaskets chosen were all made from EPDM because of its ability to withstand cold temperatures without becoming brittle. The

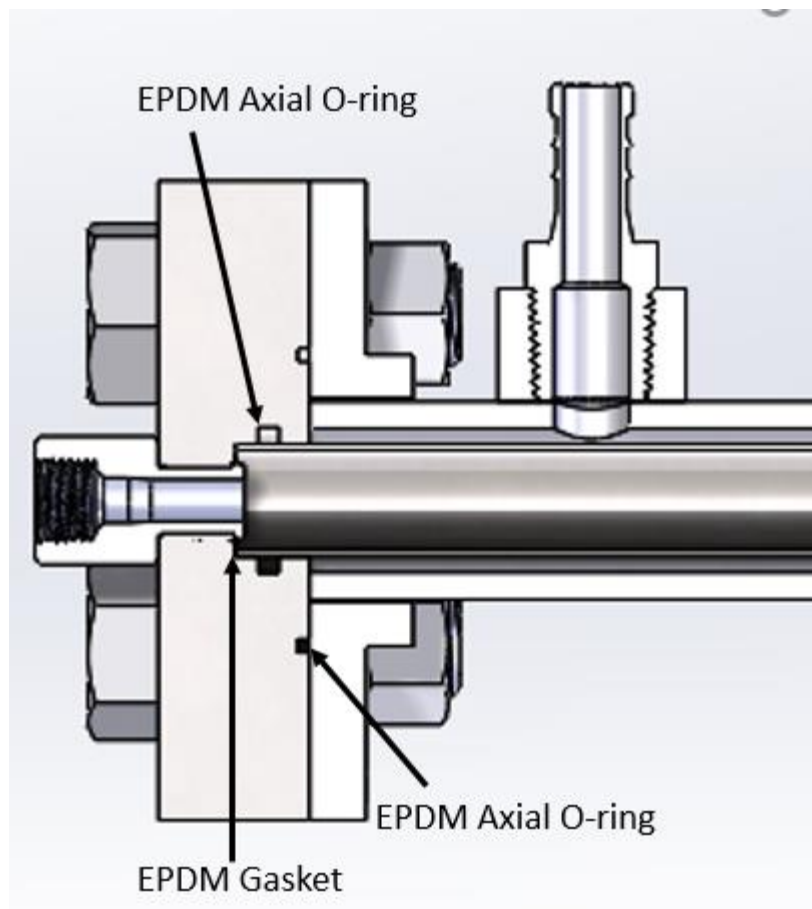


Figure 19. WCS cross section with O-rings.

gasket was cut to fit at the bottom of the custom flanges hole for the inner tube. The gasket was cut from a 6 in. x 6 in. sheet of 1/32 in. thick EPDM rubber. This piece was designed to compress and seal when the two pipes were attached together. This design was to protect the propylene glycol from mixing with the water. An O-ring was placed radially in the custom flange to create a second seal between propylene glycol and the water. The radial O-ring was a -210 EPDM O-ring. The propylene glycol was prevented from leaking from the system by an O-ring put between the custom and inner flange. This O-ring was a -032 EPDM O-ring with an inner diameter of 1.25 inches and an outer diameter of 2.625 inches. The O-rings are shown and labeled in Figure 19. The ¼ in. NPT compression fitting used for Air intake is seen in the left of Figure 19. The ½ in. NPT to hose fitting used for Coolant outflow is seen on the top of the outer pipe in Figure 19 as well. The bolts used to provide the compression between the two flanges are 3 inch-long 18-8 stainless steel hex head screws and 18-8 stainless steel bolts. The assembly of the WCS is explained in greater detail in Appendix C.

5.2. Ionic Liquid System (ILS) Article Design & Manufacturing:

The mechanical design for HYDRA's Ionic Liquid System (ILS) was largely based off of the CARIL team's contactor design. The ILS was a larger version of the CARIL team's contactor with overall dimensions of 23 in. long and a 4 in. outer diameter. HYDRA's final ILS design included 484 hollow fibers, 6 stainless steel support rods, 3 polypropylene disks to support the hollow fibers, 2 spacer rings to create space in the air manifolds, 2 ultra-high molecular weight polyethylene (UHMWPE) end caps, 1 UHMWPE housing for the fibers, and polypropylene NPT compression fittings to integrate the ionic liquid loop and gas loop from AETHER. The system included two inlets for the ionic liquid to flow into the contactor and one outlet. It also included one inlet for air to enter and one outlet for the air. The final design is shown in Figure 20 and Figure 21 below:

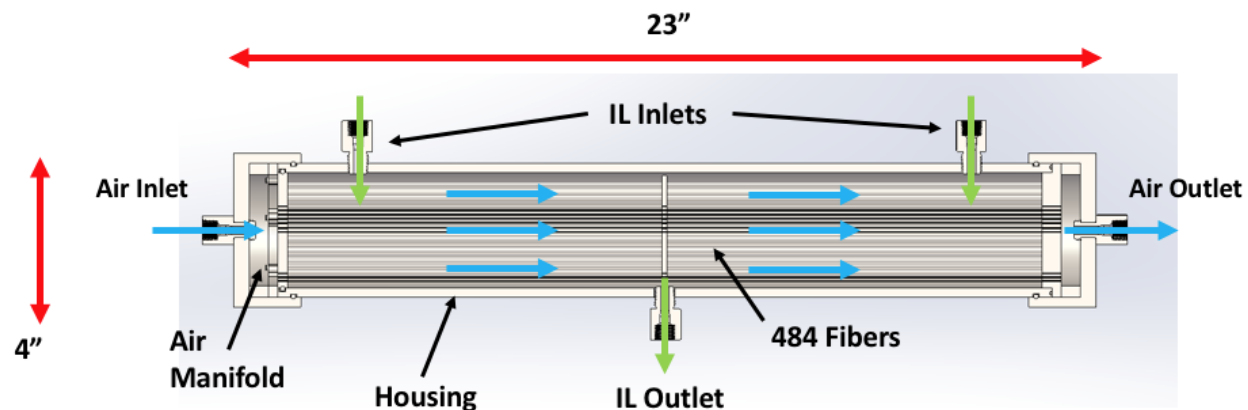


Figure 20. Ionic Liquid System overview.

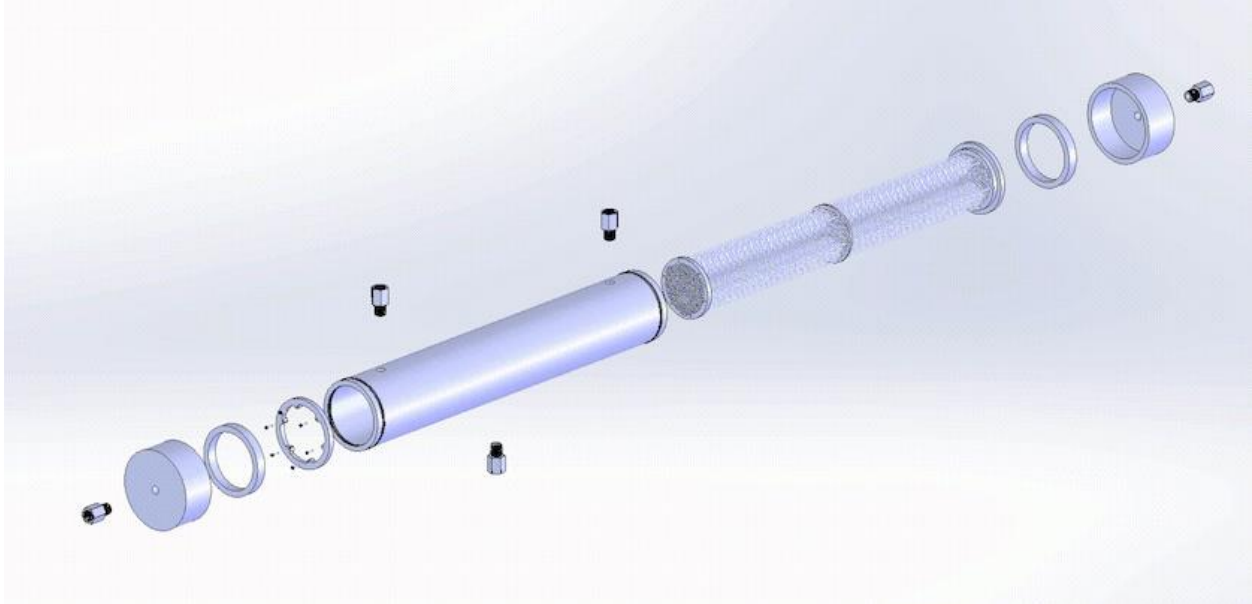


Figure 21. Ionic Liquid System exploded view.

The hollow fibers used were donated to the project by Evoqua Water Technologies under a non-disclosure agreement. Each of the 484 fibers had an outer diameter of 0.0256 in., an inner diameter of 0.0154 in., and a wall thickness of 0.0055 in. The fibers were cut to be 21 in. long for the contactor. These fibers were made out of polypropylene which is not reactive with the ionic liquid chosen and exhibits hydrophobic properties. The hydrophobic properties allowed for the porous fibers to not absorb any of the ionic liquid, which would contaminate the air flowing through the contactor. All of the water gas transfer within the contactor occurs through these fibers. Six 1/16 in. stainless steel support rods (cut to 20.16 in. length) were included in the fiber assembly within the contactor to provide support for the fibers and the three fiber guides.

The three polypropylene fiber guides were used to provide structure and a guidance system for the fibers throughout the contactor. Fiber Guide 1 (as seen farthest to the right in Figure 21 above), was manufactured from a 1/2 in. thick sheet into a disk with an outer diameter of 3.5 in. with 484 #62 holes drilled through it for the fibers and six 1/16 in. holes (0.35 in. deep) for the support rods. It included an axial O-ring groove that sealed with the end face of the fiber guide housing to ensure ionic liquid didn't leak into the air manifold. Fiber Guide 2 (as seen in the middle of the three fiber guides in Figure 21 above), was manufactured from a 1/8 in. thick sheet into a disk with an outer diameter of 2.9 in. and had the same hole pattern from Fiber Guide 1 mirrored onto it (fiber holes and support rod holes). This piece was used to keep the fibers supported in the middle of the contactor so no sag occurred. Its diameter was smaller than the 3 in. inner diameter of the fiber housing in order for flow to be able to flow around it. Fiber Guide 3 (as seen as the farthest left fiber guide in Figure 21 above), was manufactured from a 1/4 in. thick sheet into a disk with an outer diameter of 3 in. and had the same hole pattern from Fiber Guide 1 mirrored onto it for continuity. However, the 1/16 in. holes for the support rods were only 0.25 in. deep and on the opposite side (the air side) six #50 holes (0.130 in. deep) were drilled and tapped for the #2-56 locking screws. A radial O-ring existed on the outer diameter of Fiber Guide 3 that sealed with the inner diameter of the fiber housing in order to seal the ionic liquid from leaking into the air manifold.

The fiber assembly (as seen in Figure 22 below), includes all three fiber guides, 484 hollow fibers, and six 1/16 in. stainless steel rods. Fiber Guide 1, the fibers, and Fiber Guide 3 were all fixed

together via a polyurethane adhesive provided by H.B. Fuller. Fiber Guide 2 was placed in the middle of assembly and was held immobile by friction provided by the support rods. The fibers were all fixed into Fiber Guide 1 and 3 by using the polyurethane adhesive applied using a small syringe. This adhesive wicked well into the #62 holes on the fiber guides and sealed each fiber well, which ensured ionic liquid didn't leak into either air manifold.

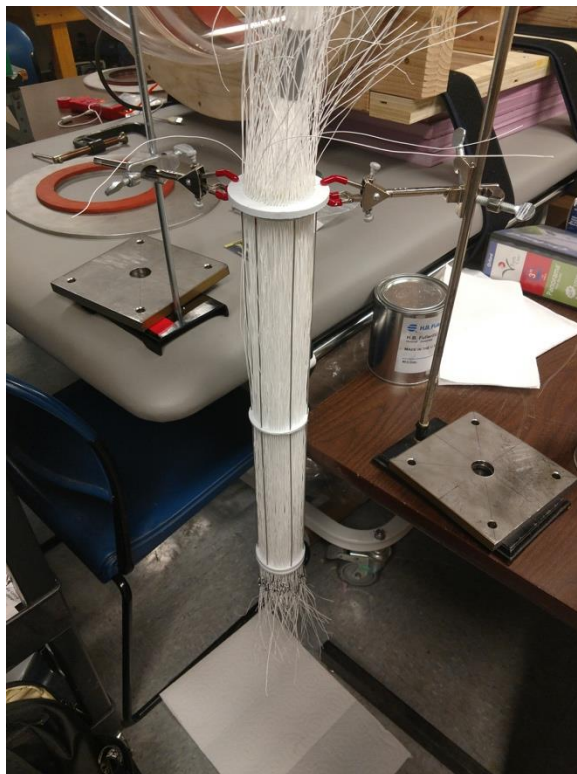


Figure 22. Fiber assembly after fiber potting.

The fiber housing was cut from UHMWPE tubing. The housing was 19.7 in. long, with a 3.5 in. outer diameter, and a 3 in. inner diameter. UHMWPE was chosen as the material due to it being non-reactive with the ionic liquid chosen. Two $7/16$ in. holes and one $37/64$ in. hole were drilled and tapped for NPT compression fittings to be inserted. Once the fiber assembly was inserted into the fiber housing, the Screw Lock Ring was attached to Fiber Guide 3 to keep the fiber assembly fixed in the fiber housing. The Screw Lock Ring (as seen in Figure 23) was manufactured from a $1/4$ in. polypropylene sheet into a disk with a 3.5 in. outer diameter that had six #43 holes drilled through it for the six #2-56 screws to be inserted. Fiber Guide 3 was attached to the Screw Lock Ring via six #2-56 screws (0.375 in. length) that threaded directly into Fiber Guide 3.



Figure 23. Screw Lock Ring with screws.

The two end caps, made of UHMWPE, had an outer diameter of 4 in. and a 3.5 in. inner diameter. They also included a radial O-ring that sealed with the outer diameter of the fiber housing in order to seal the air inside the air manifold from leaking out of the system into the ambient environment. Each end cap also included a 7/16 in. hole drilled and tapped for a NPT compression fitting to be inserted. Two spacers were manufactured from 1/2 in. thick polypropylene disks into disks with an outer diameter of 3.5 in. and a 3 in. inner diameter. These spacers allowed for room in the air manifold so that the ends of the fibers did not get crushed or blocked by the end caps. Finally, four 1/4 in. and one 3/8 in. NPT compression fittings were used to provide the interfaces for the ionic liquid loop and gas loop from AETHER. These fittings were made out of polypropylene also due to it being non-reactive with the ionic liquid chosen. The end caps and NPT compression fittings can be seen below in Figure 24 along with the compression assembly:



Figure 24. Full ILS assembly.

The compression assembly included fully threaded rod, nuts, and two 1/2 in. stainless steel plates. This was used to provide an axial compression force to seal the axial O-ring on Fiber Guide 1 to the end face of the fiber housing. The compression assembly was also useful as a stabilizing structure for the contactor to sit in, which didn't allow the contactor to roll around. Lastly, a manifold was used to diverge the ionic liquid line from the peristaltic pump into two lines continuing to the ILS. This manifold included two 3/8 in. and two 1/4 in. NPT compression fittings. The two 1/4 in. NPT fittings had tubes flowing to the ILS. One of the 3/8 in. fittings had a tube flowing from the pump and the other 3/8 in. fitting housed a thermocouple to measure the ionic liquid temperature. This manifold assembly is shown below in Figure 25:



Figure 25. Ionic liquid manifold.

5.2.1. *ILS Mechanical Considerations*

The design approach for the HYDRA contactor was adopted from the CARIL team's contactor. The initial design was to have all of the O-ring grooves and sealing interfaces machined into the fiber housing as the CARIL team did. The HYDRA team followed in CARIL's footsteps because they had success with their contactor. The original design included a radial O-ring groove on the outer diameter of the fiber housing at both ends, a radial O-ring groove on the inner diameter of the fiber housing where Fiber Guide 3 would be located, and an axial O-ring groove on the face of one end of the fiber housing where the flange of Fiber Guide 1 would be located. All of these grooves can be seen in Figure 26 below:

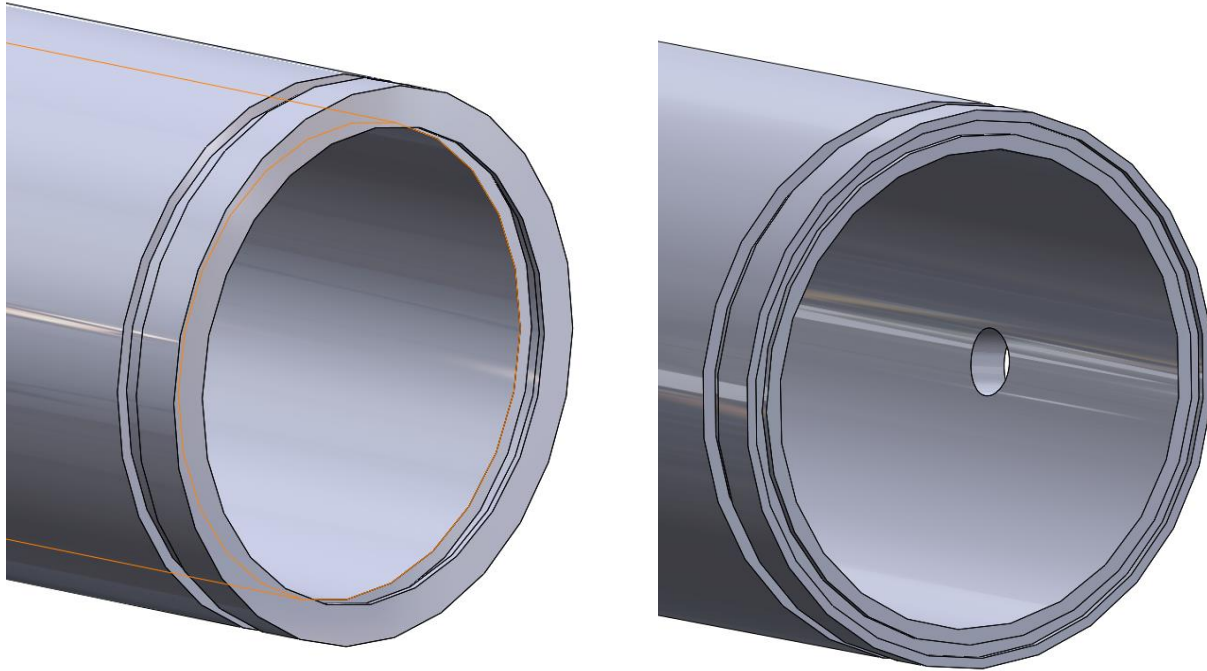


Figure 26. Initial fiber housing design.

This design was presented as the HYDRA team's fiber housing design during the Critical Design Review (CDR). The fiber housing was designed to be 19.7 in. long. This length brought up concern by machinist in the Aerospace Machine Shop because the length would make it difficult to machine the O-ring grooves using a lathe as was done by the CARIL team. The torque on the fiber housing during manufacturing would make the machining difficult because the end of the tube being machined would be suspended around 15 in. away from the chuck. Due to this concern the mechanical design for the fiber housing was modified so that all of the O-ring grooves were moved to other components leaving the fiber housing as a solid piece (except for the holes drilled for NPT fittings). The radial O-ring on the outer diameter of the fiber housing was moved to the inner diameter of the end caps as shown in Figure 27 below:

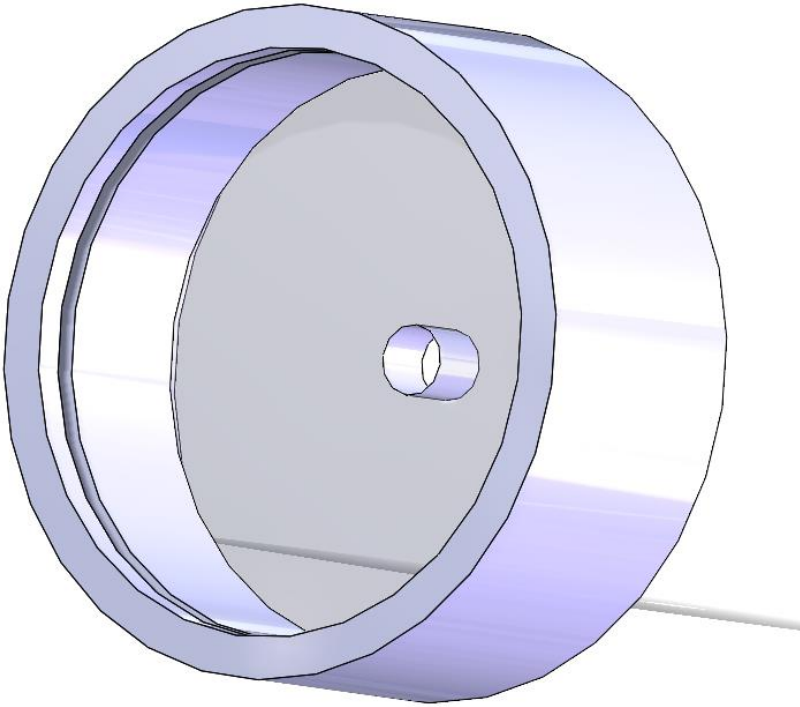


Figure 27. End cap with radial O-ring groove added.

The radial O-ring groove on the inner diameter of the fiber housing was moved to the outer diameter of Fiber Guide 3 as seen in Figure 28 below:

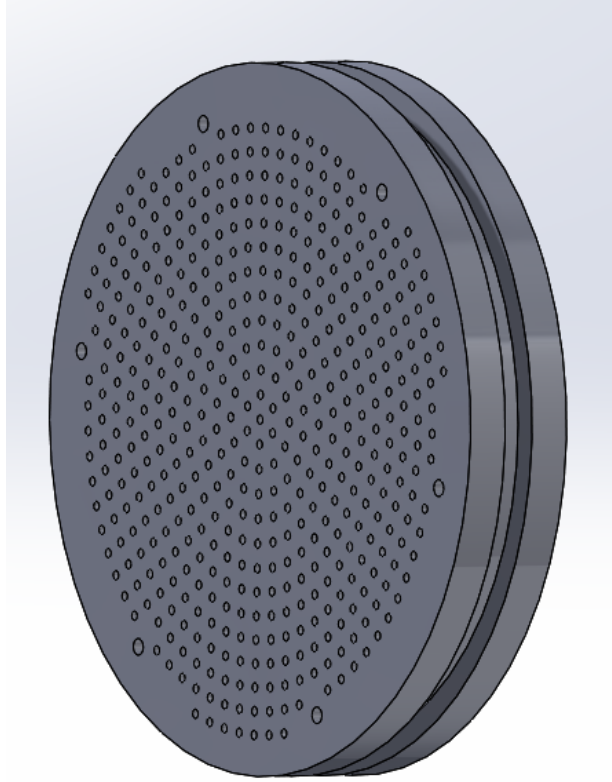


Figure 28. Fiber Guide 3 with radial O-ring groove added.

The axial O-ring groove on the end face of the fiber housing was moved to the flange part of Fiber Guide 1 as seen in Figure 29 below:

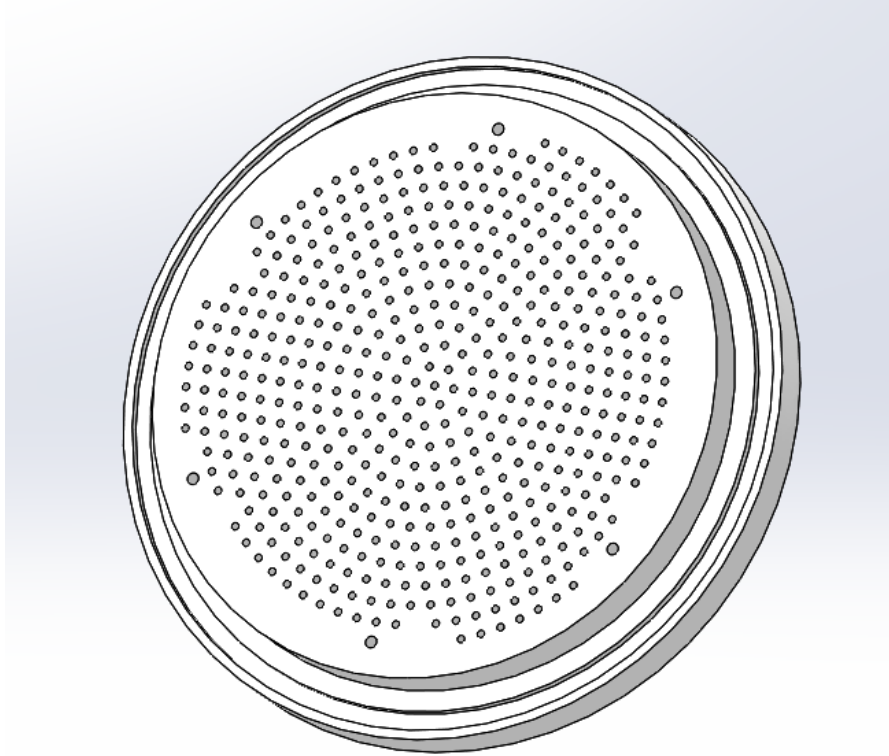


Figure 29. Fiber Guide 1 with axial O-ring groove added.

The remaining mechanical design of HYDRA's contactor was similar to the contactor built by CARIL. One exception was that six supporting rods were used instead of only three. The need for more support within the Fiber Assembly was required because the size of the contactor increased (484 fibers versus 118 fibers).

6. Testing

6.1. AETHER

The Atmospheric and Environmental Test Hub for Experimentation on Revitalization (AETHER) is a test rig designed and operated in the CU Bioastronautics lab. This test rig is a system that allows for air revitalization testing by providing a known and controllable gas stream, and recording upstream and downstream values that characterize the gas stream. HYDRA will be using the AETHER test rig for the majority of the testing. Figure 30 shows the AETHER system with key components pointed out.

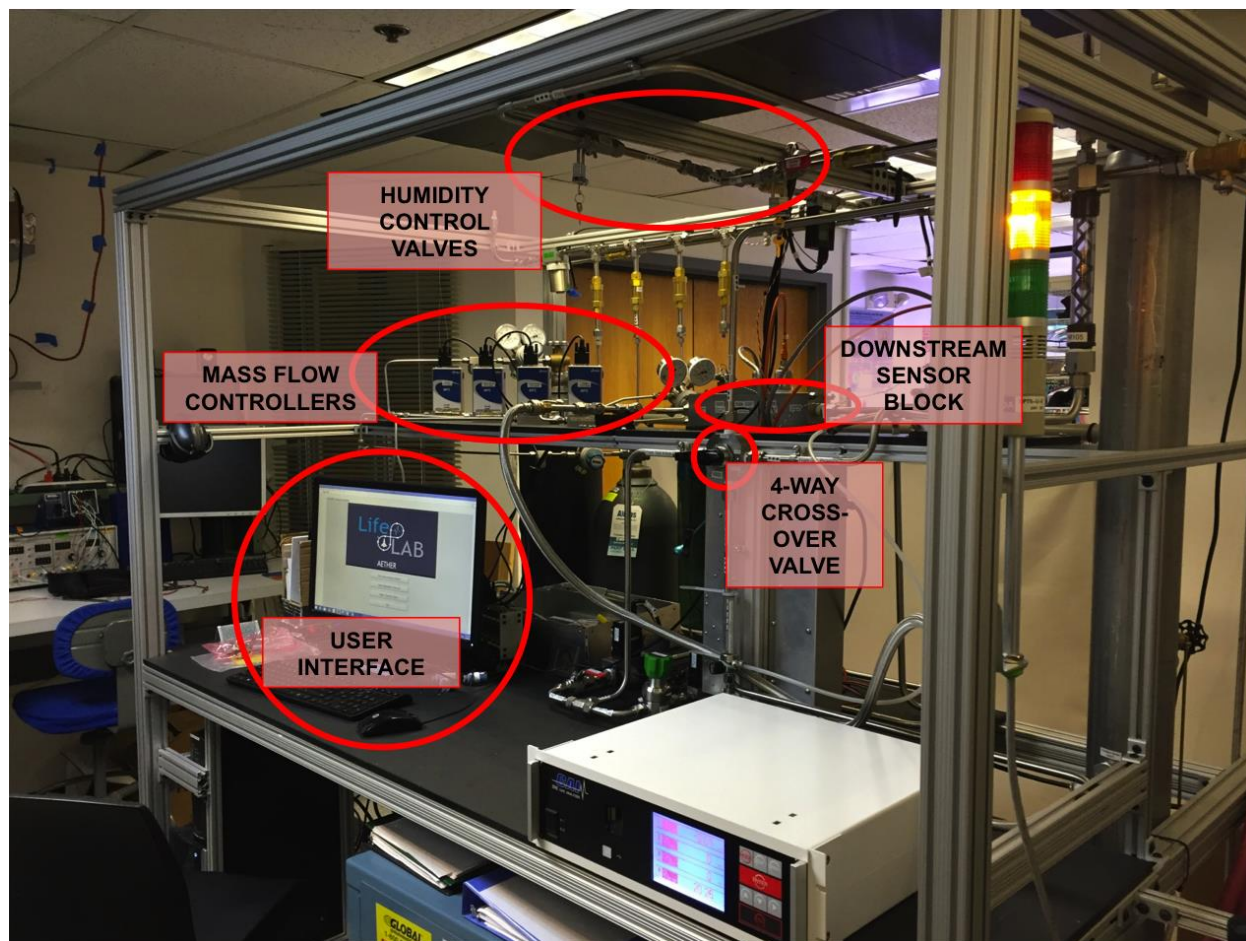


Figure 30. The AETHER Test Rig with Key Components Highlighted.

The AETHER test rig can provide both dry and humid streams of gas, which is beneficial to this project. The humidity control is done by the combination of two quarter turn ball valves. This allows for rather low resolution in terms of controlling the input humidity. This shortcoming of the system will be overcome by accounting for the fact that the input humidity can be anywhere between 25% - 70% RH. AETHER is capable of measuring temperature, pressure, relative humidity, and gas composition. It is also capable of providing gas flow in the range of 0.2 - 400 SLPM. The low flow regime, which all the tests will be conducted in, is from 0.2 - 10 SLPM. The target properties of article input gas are outlined in red in Table 8, which also shows some of AETHER's capabilities. Table 9 shows the list of sensors installed on the AETHER test rig.

Table 8. AETHER capabilities.

Mode	Low Flow	Mid Flow	High Flow	Accuracy
Flow	0.2-9.5 SLPM	10-100 SLPM	100-400 SLPM	+/- 0.5, 3, 15 SLPM
Nitrogen	29-80%	76-80%	77-79%	+/- 5% rel.
Oxygen	17-23%	17-23%	20-22%	+/- 5% rel.
Carbon Dioxide	0-100%	0.03-1.3%	0.03-1.3%	+/- 5% rel.
Humidity	30-70%			+/- 3% abs.
Temperature	Ambient (18-27°C)			N/A
Pressure in Test Article	14.7 psia			+/- 0.25%
Maximum Test Duration	1 day			N/A
Control Program	LabVIEW			N/A
User Ports (Break Out Box)	58 single-ended, 19 differential analog inputs 16 bi-directional digital ports (input or output)			
Resolution	16 bits			
Sampling Rate	0.8 Hz if using AETHER VI			

Table 9. AETHER sensors.

Sensor	FS Range	Accuracy	Operational Range			Life and/or Drift Rate	Warm-Up Time	Response Time
			T (°C)	Humidity (%)	Pressure (psi)			
Temperature Sensor (HS-2000V)	-30 to 100 °C	+/- 0.40 °C	0-70	0-100	N/A	N/A	N/A	50 seconds in slow moving air
Absolute Pressure Sensors (HSCSAND030)	0 to 30 psia	+/- 0.25%	-20-80	0-95	60/120 psia	1 Million Cycles	N/A	N/A
0-3% CO2 Sensor (GMM-221)	0 to 3% CO2	+/- 450 – 1050 ppm	-20-60	0-100	18.85 psia	< +/- 5% per 2 years	Init: 30 s Full: 15 min	20 seconds
Environmental CO2 Sensor (K30)	0 to 10000 ppm	+/- 3% of Reading +/- 30ppm	0-50	0-95	145 psig	15 years	1 minute	20 seconds
O2 Sensor (Max 250)	0 to 100% O2	+/- 4.25%	5-40	5-95	22 psia	Rated at 4 years in standard atmos.	N/A	< 15 seconds

6.2. Test Integration

6.2.1. Sensor and Instrumentation Integration

Dew Point Sensor:

Characterizing the output dew point of the system is the primary goal of the project and this was measured using the Vaisala DMT143. The Vaisala DMT143 was primarily chosen for its available documentation providing confidence in its performance. Initial plans were to integrate the DMT143 into the AETHER LabVIEW code but was ultimately integrated onto an Arduino due to simplicity.

Two of the DMT143 sensors were ordered in case one was damaged due to mishandling or damage during testing. The initial sensor dew point sensor selected was EE355 from E+E but the DMT143 was ultimately chosen due to more confidence in its performance and being simpler to

integrate into the DAQ system. The EE355 may be a viable alternative while being noticeably cheaper.

Relative Humidity Sensor:

Due to how long the AETHER native humidity sensor has been installed, there was concern towards its accuracy. As such a separate humidity sensor was integrated to measure the relative humidity upstream of the test article. The sensor used Omega HX94BV1W although the original sensor selected was the Omega HX15. The Omega HX94BV1W sacrificed some accuracy but was ultimately used due to issues with availability concerning the Omega HX15. Like the dew point sensor, the relative humidity sensor was originally planned to be integrated into the AETHER LabVIEW code but was ultimately integrated onto an Arduino.

Thermistors:

To measure the inner wall temperature of the WCS, thermistors were proven effective in past experiments with Dr. Nabity's heat exchanger experiments. The thermistors selected were the Omega SA1-TH-44006-40-T thermistors by recommendation from Dr. Nabity. Although two were initially planned to measure the temperature of the interior tube of WCS, one thermistor broke just prior to integration so only one was ultimately used. Calibration was performed using room temperature, an ice bath, and boiling water. During testing, it appeared that the calibration was performed improperly as the thermistor reported temperatures that deviated more than 5 °C from our expected. The thermistor was integrated into the Arduino board but was ultimately never used.

Thermocouples:

To simplify integration into the test setup, McMaster 3871K77 were utilized. Originally similar thermocouple probes from Omega were planned but concerns with lead times led to the use of the McMaster thermocouple probes. During the WCS testing, measuring the output air temperature would allow validation of the model developed so a thermocouple was placed immediately downstream of the test article. However, during testing the thermocouple consistently measured temperatures close to room temperature. It is believed that due the thermocouple was unable to measure the air temperature effectively due to the ambient heat due to the environment. Despite the use of insulation and an approximate length of two inches between the WCS outlet and the thermocouple, the downstream air temperature was never able to effectively be measured. During ILS testing the thermocouple was used to measure the temperature of the ionic liquid in order to validate the model. The thermocouple was integrated using a separate NI DAQ and its own separate LabVIEW module due to simplicity in integration. Attempts were made to integrate it into the Arduino board but the thermocouple experienced changes on the order of mV and a signal conditioning circuit was unable to be constructed in a timely manner to have the thermocouple be detectable on the Arduino analog-to-digital voltage converter.

Heat Tape:

There was initially significant concern that the outlet air from the WCS would potentially condensate on the dew point sensor and damage it. Additionally, the accuracy of the dew point sensor has degraded performance when the air is being measured at temperatures below 0 °C. To prevent this, heat tape model HSTAT051004-C from BriskHeat was used to warm up two feet of ¼" stainless steel tubing before the air would reach the dew point sensor. This heat tape was chosen for having its own temperature controller in addition to being flexible enough to be able to bend to ¼" tubing. During testing the air heated close to ambient temperatures before reaching the dew point sensor so the heat tape was moved to the inlet of the WCS to prevent the inlet from freezing before the interior tube. The heat tape's built in temperature controller appeared ineffective at regulating temperature so a Variac was utilized as a means of manually controlling the heating. The Variac was borrowed from the Aerospace Engineering Instrumentation Lab.

6.2.2. Test Article Integration

During the manufacturing process both the WCS and ILS were designed with $\frac{1}{4}$ " compression fittings as the interface. In efforts to make test article integration as simple as possible, $\frac{1}{4}$ " tubing FEP was used as the consistent tubing between AETHER, the test article, and all sensors. Various combination of NPT pipe interfaces and compression fittings were used to house sensors and interface between the sensors. The NPT threads were sealed with either PTFE tape or the use of pipe sealant. A combination of either stainless steel or plastic parts were used depending on if the manufacturer recommended using stainless steel interfaces to the sensor. Due to the size of the test articles, the test article was housed in secondary containment on the ground near AETHER. This required the use of significant amount of tubing and approximately 10 ft. of the $\frac{1}{4}$ " FEP tubing was used over the entire portion of testing.

Dew Point Sensor Integration:

Figure 31 below shows how the dew point sensor was integrated into the test setup. The DMT143 comes in a form with $\frac{1}{2}$ " NPT threading for mounting. A $\frac{1}{2}$ " NPT T-joint is used as the sampling cell to mount the dew point sensor while pipe nipples and adapters are used to integrate the T-joint to and from the $\frac{1}{4}$ " tube size.

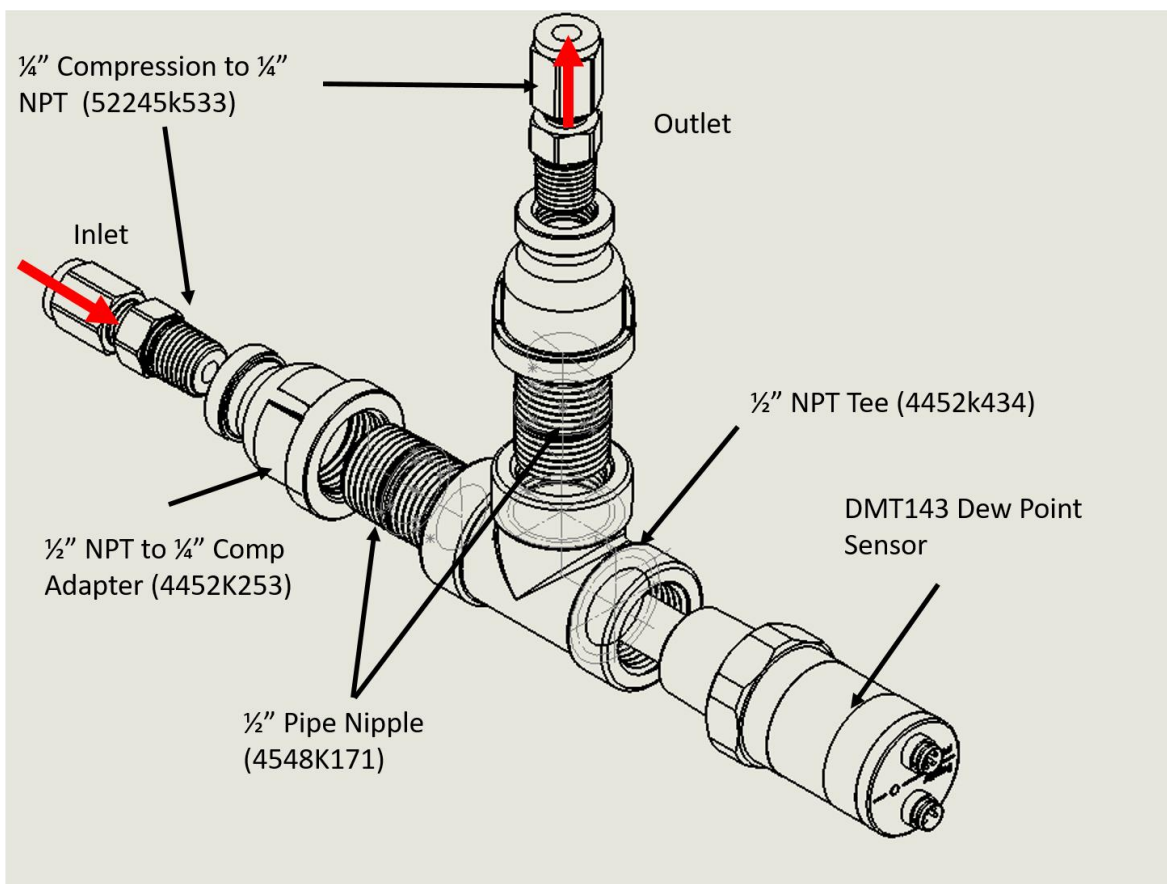


Figure 31. CAD drawing of the dew point sensor block.

Relative Humidity Sensor Integration:

Figure 32 below shows how the relative humidity sensor was integrated into the system. The probe on the sensor has an outer diameter of $\frac{3}{4}$ " so a compression fitting was utilized to integrate the system into a 1" NPT T-joint. Similar to the relative humidity sensor, pipe adapters were utilized to maintain the $\frac{1}{4}$ " tubing interface between parts of the test setup.

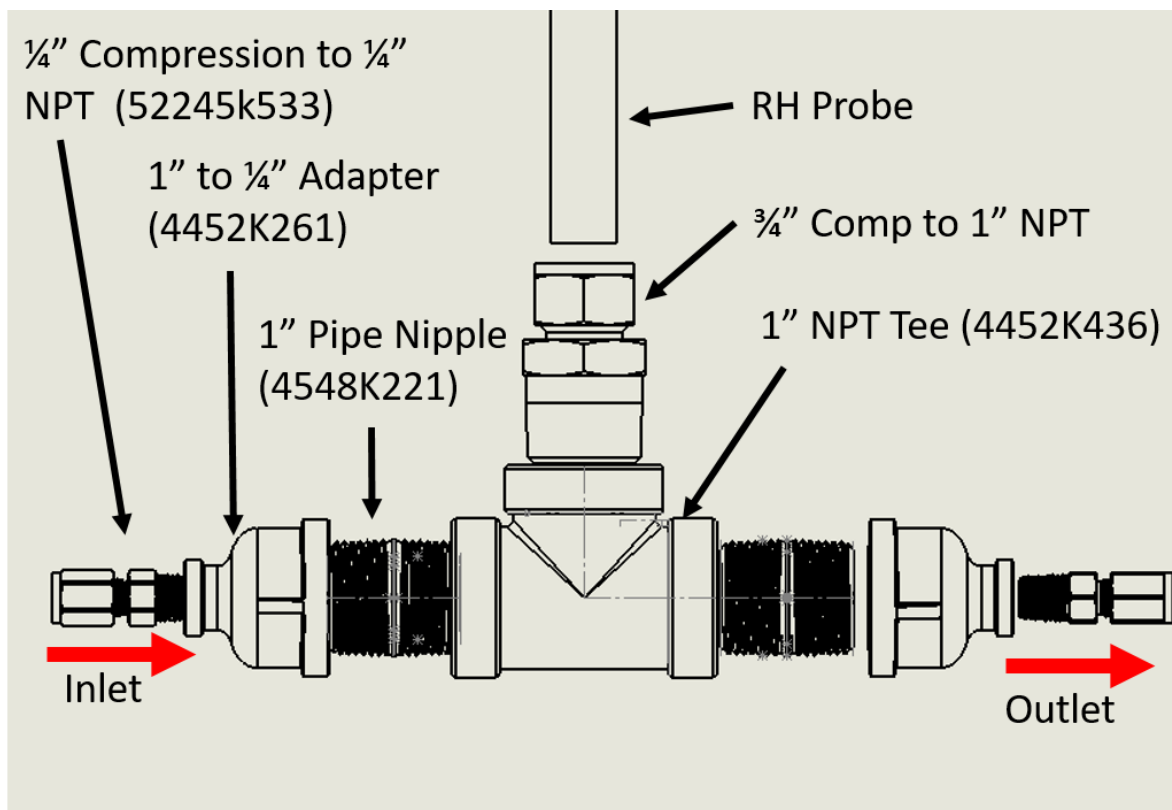


Figure 32. CAD drawing of the relative humidity sensor block.

Thermistor Integration:

The thermistors were attached to outer wall of the interior tube in the WCS using JB weld. A feedthrough hole on the outer tube was drilled and filled with JB weld to seal the feedthrough hole. During testing a minor amount of coolant leaked through the feedthrough hole as temperature of the coolant decreased. This leak was not present when the test article was at room temperature so this is most likely the result of the different materials and their different rates of thermal expansion and contraction.

Thermocouple Integration:

Figure 33 below shows how the thermocouple was integrated to measure the downstream air temperature. The thermocouple probe is a $\frac{1}{4}$ " so a compression fitting was utilized similar to how the relative humidity sensor was integrated. However, because the thermocouple probe matched the size of the $\frac{1}{4}$ " tubing being used between items in the test setup, a standard $\frac{1}{4}$ " compression T-joint was used as the housing.

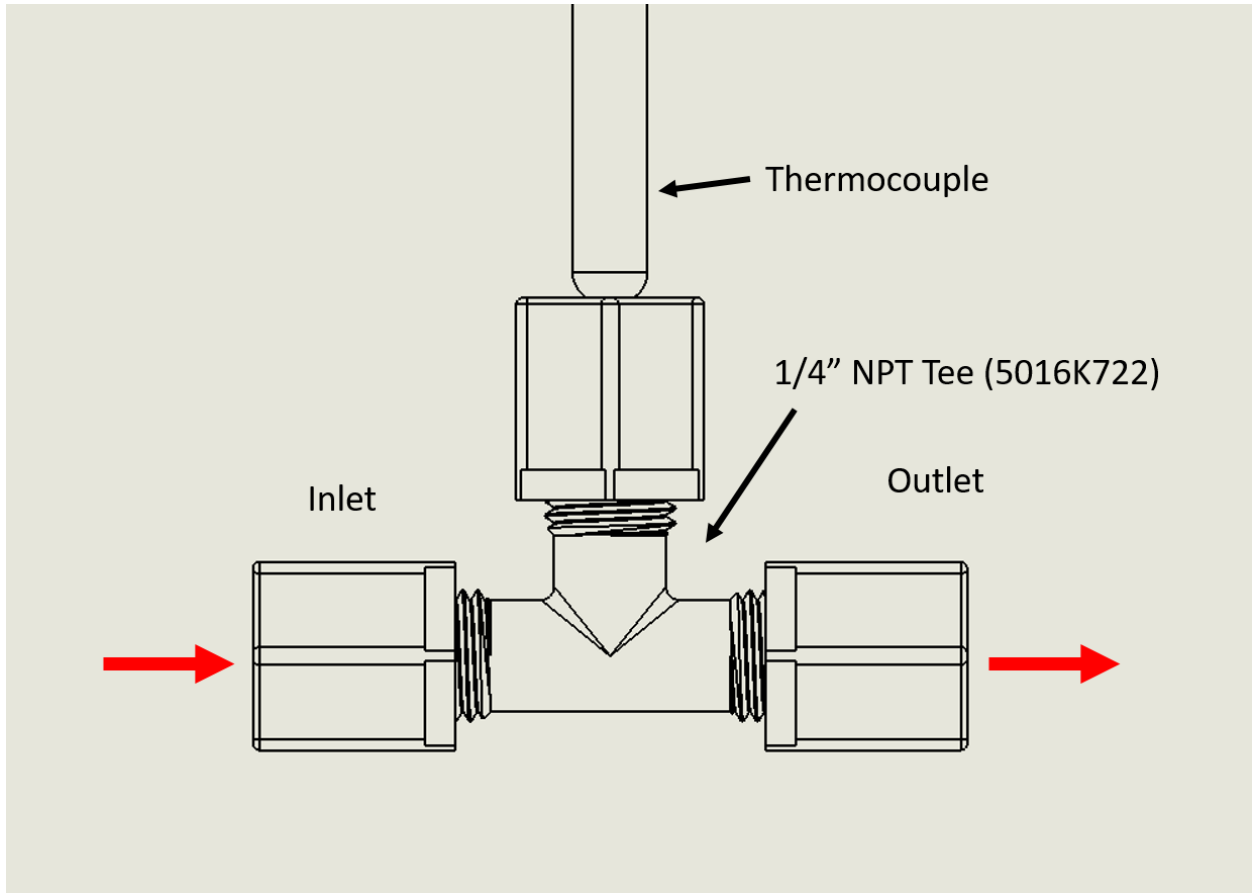


Figure 33. CAD drawing of the thermocouple integration to measure the downstream air temperature of the WCS.

Figure 34 below shows how the thermocouple was integrated into the manifold to measure the temperature of the ionic liquid during testing. This manifold design was borrowed from the CARIL team last year but instead of plugging the extra hole, a 3/8" NPT to 1/4" compression fitting was used to integrate the thermocouple. Only one thermocouple was used to measure the ionic liquid temperature as the ionic liquid was recirculated during testing and the temperature was not expected to change significantly over one pass over the membrane.

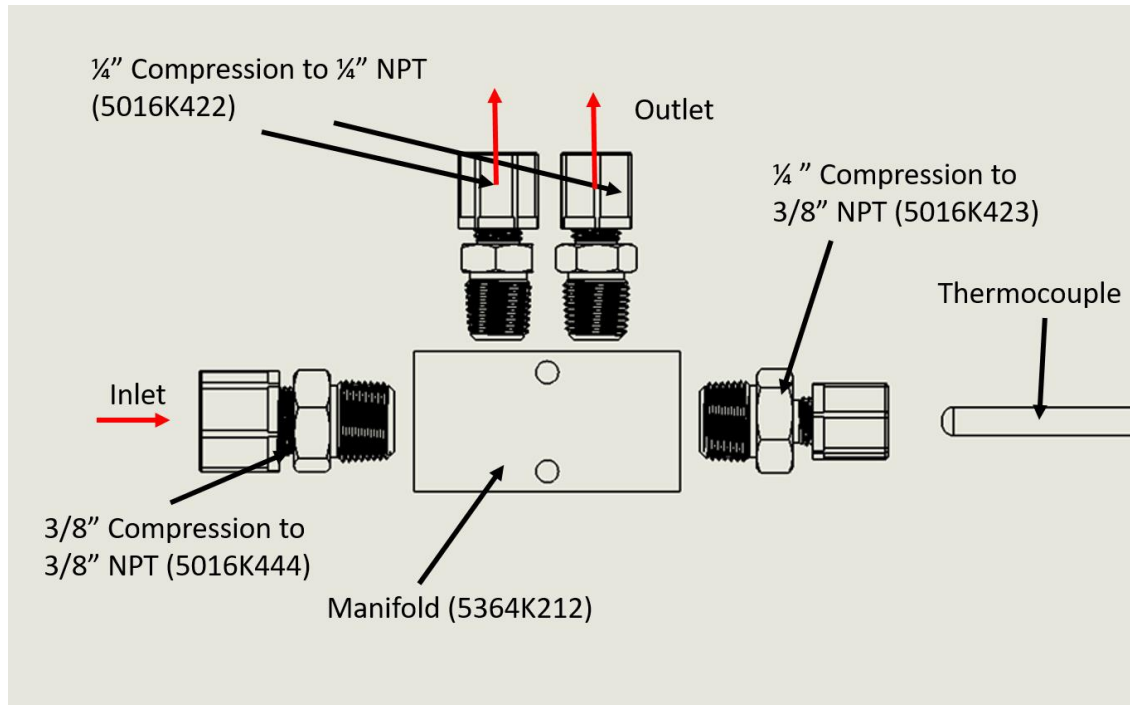


Figure 34. CAD drawing of the thermocouple integrating into the manifold of the ILS.

6.2.3. Integration Difficulties

Air Leaks:

When setting up for initial testing and all the sensors were integrated together with the WCS, approximately 20% of the airflow was leaking between the AETHER upstream sensor block and the downstream sensor block. A significant amount of the leaks were due to not engaging the ferrule in the compression fittings enough. As such a significant amount of leaking was reduced by tightening down on all the compression fittings. However, the largest leak was due to a nut on the top on the relative humidity sensor not being tightened completely. The process of removing leaks from the system took an extensive amount of time and effectively took about a few of the testing time to get the test article and all the sensor connections to a point where testing was viable. Coupled with issues faced with the DAQ and AETHER troubleshooting, it took about a week to begin collecting data for AETHER.

Ambient Heating:

During the initial testing, the chiller would stabilize at a temperature of approximately -24 °C after approximately 1.5-2 hours from startup. The chiller has reportedly been operated to approximately -30 °C. It is believed that due to the size of the system and the amount of hosing used between the chiller and the test article that ambient heating was significant and prevented the coolant from reaching the targeted -30 °C. Ambient heating also appeared to be an issue for the downstream thermocouple on the WCS as the thermocouple consistently measured temperatures close to ambient.

6.2.4. Recommended Improvements

For the relative humidity and dew point sensor, the use of an NPT T-joint as a sampling cell operated as necessary but the significant number of pieces to house each sensor caused issues

when trying to find the leaks of the system. In the future it is recommended that each sensor to be integrated with minimal interfacing as each interface point is a potential leak and would allow for simpler troubleshooting during test setup. Particularly, there was concern that a leak from on the NPT interfaces was being missed when the primary leak coming from the relative humidity sensor probe was the cause. By removing the amount of points a leak could occur, troubleshooting should become easier and leaks should be easier to identify.

To interface all the components in the test setup, the ¼” tubing was established as the connection between all points. However, there was merit in the use of varying tube sizes to reduce the number of interfaces. AETHER is normally a ½” sizing so two adapters were used from the outlet of the dew point sensor block to AETHER but was probably unnecessary and complicated the interfaces. Additionally, more elegant sensor integrations could probably be designed by manufacturing the test article with sensor integration in mind. Particularly, a smaller thermocouple could potentially have been mounted into the WCS air stream if designed to.

6.3. Experimental Design and Testing Configuration

6.3.1. Overview

The primary objective of the WCS/ILS testing was the characterization of time and flow rate dependent performance metrics. Experimental design was influenced by AETHER capabilities and limitations.

6.3.2. WCS

6.3.2.1 Nitrogen purging

The initial step for each WCS test was to perform a dry nitrogen purge using AETHER provided gas to establish minimize test article moisture before each test iteration.

6.3.2.2 Chiller verification

The chiller, filled with 60:40 (volume) mixture of propylene-glycol to water, has a minimum temperature set point of -50 degrees Celsius. Flow rate settings varied from low, medium, to high. An initial verification test was performed to verify the WCS wall temperature at a chiller set-point of -35 degrees Celsius. Chiller verification iterations showed that to reach the required wall temperature, the chiller needed to be set to -50 degrees Celsius and the high flow rate setting.

6.3.2.3 Test Matrix

The goal of WCS testing was to characterize ice accumulation in the inner wall. Flow rates varied from 0.2 to 9 LPM of total gas flow (standard atmosphere compositions) and humidity was calibrated to 70%RH.

Test	Flow Rate (L/min)	Humidity (%RH)	End Criteria
1	0.2	70	Stable outlet dew point (stable within 0.1 C for 10 minutes)

2	0.2 → 3	70	Stable outlet dew point (stable within 0.1 C for 10 minutes)
3	0.2 → 9	70	Stable outlet dew point (stable within 0.1 C for 10 minutes)
4	9	70	6 hour time elapsed or outlet dew point reaches -10 °C

6.3.3. ILS

6.3.3.1 Peristaltic Pump Verification

The peristaltic pump was the primary method of transporting the ionic liquid in the required cross-flow orientation. Prior to ILS operations, flow tests were performed to characterize the pump settings.

6.3.3.2 IL circulation

Before each test, the ionic liquid was circulated to mitigate variability due to stagnation.

6.3.3.3 Nitrogen purging

The initial step for each ILS test was to perform a dry nitrogen purge using AETHER provided gas to establish minimize test article moisture before each test iteration.

6.3.3.4 Test Matrix

The goal of ILS testing was to characterize levels of water saturation in the ionic liquid. Flow rates varied from 0.2 to 9 LPM of total gas flow (standard atmosphere compositions) and humidity was calibrated to 30 or 70%RH. An added test for the ILS was a vacuum desorption to compare pre and post water content in the IL. Repeated trials were conducted as necessary for model validation.

Test	Flow (L/min)	Rate	Humidity (%RH)	End Criteria
1a	0.2		70	Stable outlet dew point (stable within 0.1 C for 10 minutes)
1b	4		70	Stable outlet dew point (stable within 0.1 C for 10 minutes)
1c	9		70	Stable outlet dew point (stable within 0.1 C for 10 minutes)
Bake out	0		0	Vacuum desorption (50 mTorr) for 24 hours
1a, trial 2	0.2		70	Stable outlet dew point (stable within 0.1 C for 10 minutes)

1b/c, trial 2	9,4	70	Stable outlet dew point (stable within 0.1 C for 10 minutes)
2a	9→4→ 0.2	70	30 minutes at each flow rate
2b	9→4→ 0.2	25-30	30 minutes at each flow rate

6.3.4. Auxiliary Tests

Auxiliary tests were performed to either obtain experimental data for model validation for material safety validation.

6.3.4.1 Equilibrium Distribution Coefficient (EDC) Test

The initial EDC experiment characterized the ionic liquid's propensity to adsorb water vapor out of ambient air. The initial EDC estimate was obtained using a flask containing 30 mL of IL. The flask was closed in a self-sealing plastic container and positioned on top of a magnetic stirrer. This allowed agitation of the IL over the course of the experiment. The IL was agitated in the closed container for 18 hours, with humidity and temperature measurements taken at regular intervals. Pre and post mass measurements taken to assess the percent mass change due to water adsorption. Results of the initial EDC test are discussed on pg. 28.

6.3.4.2 Hollow Fiber Pressure Testing

As discussed earlier, the ILS features a series of hollow fibers to facilitate air flow through the ionic liquid. The HYDRA team determined it was necessary to characterize the risk of over-pressurization leading to fiber damage. AETHER supplies gas at roughly 1 atm (14.7 psia), therefore the pressure testing levels were set to test levels with an added safety factor of 1.5 (1.5 atm, ~22.1 psia). Pressurized nitrogen was supplied to the hollow fiber via a 25-gauge syringe needle. Due to an operator error, the testing pressures were set to 22.1 psi gauge instead of 22.1 psi absolute. However, even at these higher than intended pressures, there were no observable marks of damage to the hollow fiber due to over pressurization.

7. Experimental Results and Model Validation

7.1. Water Cryocooler System (WCS) Model Validation

7.1.1. Data Analysis Procedures

During testing, the thermistors intended to measure the wall temperature either malfunctioned or gave erroneous readings so the wall temperature had to be estimated. This was done by noting that the chiller achieved a temperature of -24°C and the temperature of the outer wall of the outer pipe was -21°C. These two values were used to bound the wall temperature. Wall temperature for each trial was estimated by assuming that the output dew point at 0.2 L/min, the lowest flowrate the test rig could produce, was equal to the wall temperature. This assumption is supported by the model predictions and first principle calculations.

7.1.2. Error Analysis Procedures

The uncertainty on the dew point sensor used is 2 °C and the uncertainty on the flow rate produce by AETHER is 0.5 L/min. These two values were the primary sourced of error on experimental measurements. In figures where the dew point deviation from the wall temperature is plotted the uncertainty on the deviation is 4 °C because an extra 2 °C must be added for uncertainties in the wall temperature measurement.

The 3 standard deviation model uncertainty was obtained by running Monte Carlo simulations similar to that described in the WCS modelling section. A simulation was run for several values across the range of possible flow rates (assuming no flow rate variation since that is captured in the experimental error) and the standard deviation of each simulation was recorded and used to create the model uncertainty bounds.

7.1.3. Results Summary

7.1.3.1 Flowrate Sensitivity

The results of the first experiment showing output dew point versus air flowrate along with a power series fit of the data are shown in Figure 35. All data was taken with an input humidity of 70%RH. For comparison to the model Figure 37 shows the dew point values of each trial minus the wall

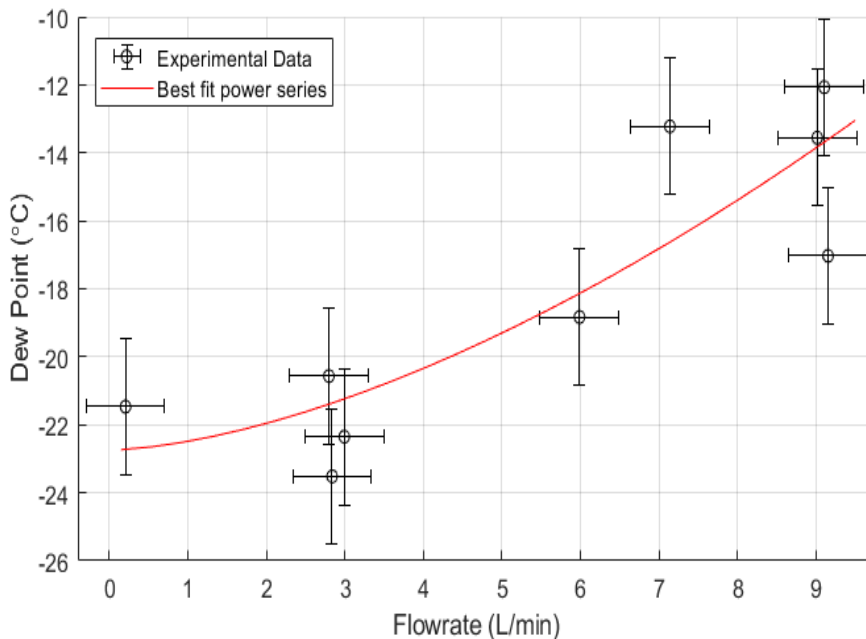


Figure 35. Experimental data and best fit power series of output dew point vs air flowrate. Input humidity was 70%RH.

temperature for that trial as well as the model prediction and the 3 standard deviation model uncertainty. The model comparison in Figure 36 shows that the model can adequately predict the output dew point as a function of air flowrate. Thus, the model is capable of informing preliminary full-scale system design.

7.1.3.2 Transient Behavior

The experimental data for output dew point

versus time is given in Figure 36. The light bands surrounding the data points represent the error bounds. The end of the test marks when the inner tube became completely blocked with ice. In Figure 37 the data is plotted against the model prediction and the y-axis represents the dew point

change from the dew point measurement at the start of testing. The band around the model prediction represents the 3 standard deviation model uncertainty.

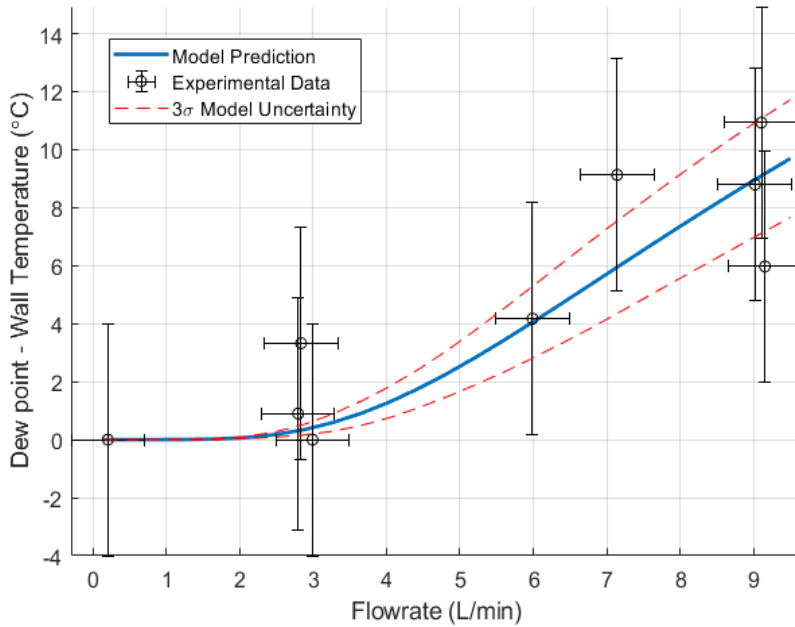


Figure 36. Experimental data and model prediction of output dew point minus wall temperature vs air flowrate.

The model predicts that the output dew point should rise slowly at a rate of about 1 °C every two hours. This is in direct contrast to the experimental results where not only did the dew point change much more rapidly (5°C over 45 minutes), it also decreased rather than increased. Additionally, the model predicted that the tube would freeze shut after approximately 120 hours whereas the experimental setup froze shut in less than 1 hour. All this suggests that the current method of modelling ice accumulation

on the tube walls is inadequate both in terms of volume of ice accumulated and the effects of this accumulation on the output dew point.

There are several possible factors that could account for the inadequacies of the modeled ice accumulation. The first is the assumed density of the ice collecting on the tube walls. The model assumed an ice density of 917 kg/m³ but frost can potentially have a density as low as 82 kg/m³ and that density is not constant over time [Kandula, 2011]. Figure 38 shows a picture taken of the inside of the tube after a short test at low flow rates and gives an illustration of the complexity of ice formation in the system.

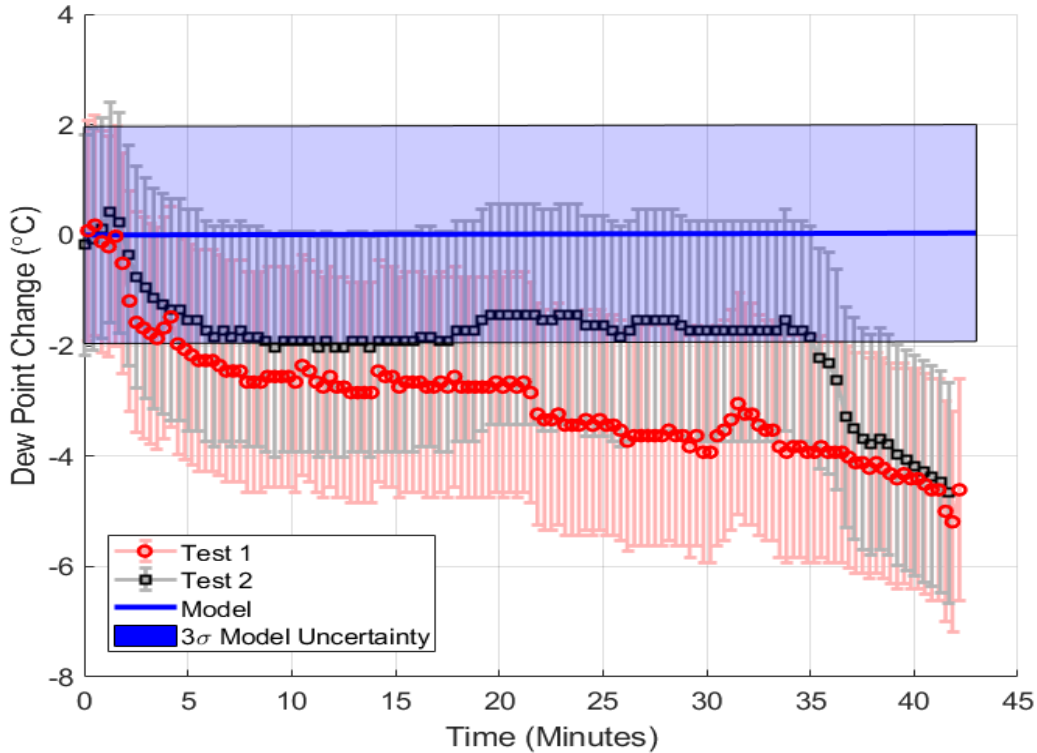


Figure 37. Experimental data and model prediction of dew point vs time at 9 L/min. Input humidity was 70%RH.

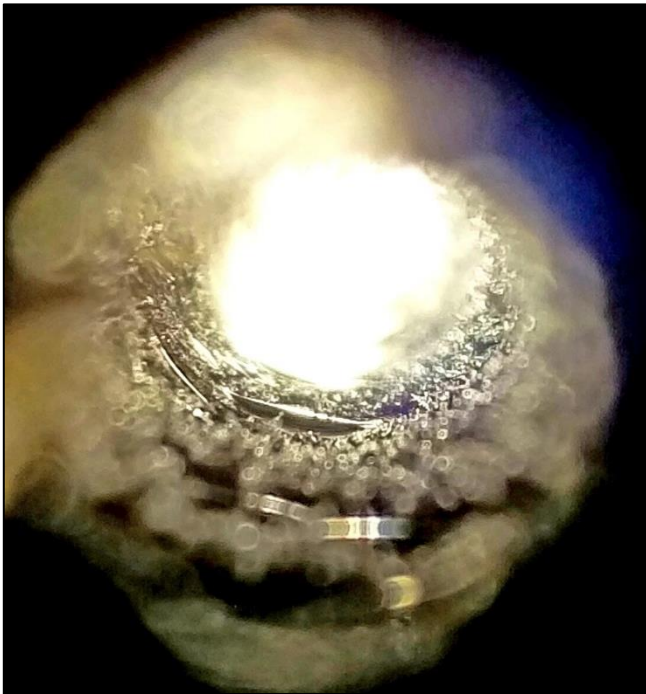


Figure 38. Ice accumulation after approximately 1 hour of testing at flow rates below 3 L/min.

Another contributing factor may be the effects of frost on the mass transfer coefficient. It is possible that the rough, porous surface created by the frost greatly increases rates of mass transfer by increasing the effective surface area of the tube wall. It also may be the case that frost will more readily form on other frost than it will on the metal tube walls. Both of these factors could help explain why the output dew point decreased as frost accumulated.

7.1.4. Flight Scale Design

The results of the WCS experiments give confidence in the ability of the model to predict the behavior of a flight-scale system, at least in regards to nominal output and preliminary sizing. The full scale flowrate for a crew of 4 is approximately 30 cubic feet per minute. The lowest practical wall temperature for the system is -70°C as anything lower than that would risk freezing carbon dioxide out of the air stream. Using these inputs along with an assumed input humidity of 70 %RH Figure 39 shows a range of

possible tube sizes and the output dew point they would produce. Each line represents a different inner diameter with the smallest being 15.5 mm and the largest being 250 mm. One possible design point has been chosen which corresponds to an inner diameter of 88 mm and a length of 5.1 m. Assuming two tubes are needed to support the two-bed design that gives an estimated system volume of 0.25 m³ and an estimated system mass of 60 kg assuming the tubes are made of copper. The total cooling power required by the system is calculated to be about 2 kW, however almost all of this power could come from the space thermal environment or other passive sources. Assuming the system operation would be similar to that of a two-bed CO₂ cryocooler the practical full scale system power would be on the order of 30 W [Belancik, 2017]. It should be noted that, for a given output dew point and air flow rate, the total cooling power requirements are the same regardless of tube dimensions. This means that cycle time will be an important factor in system sizing. No attempt was made here to estimate full scale system cycle time because the model currently overestimates the time to ice blockage by several orders of magnitude.

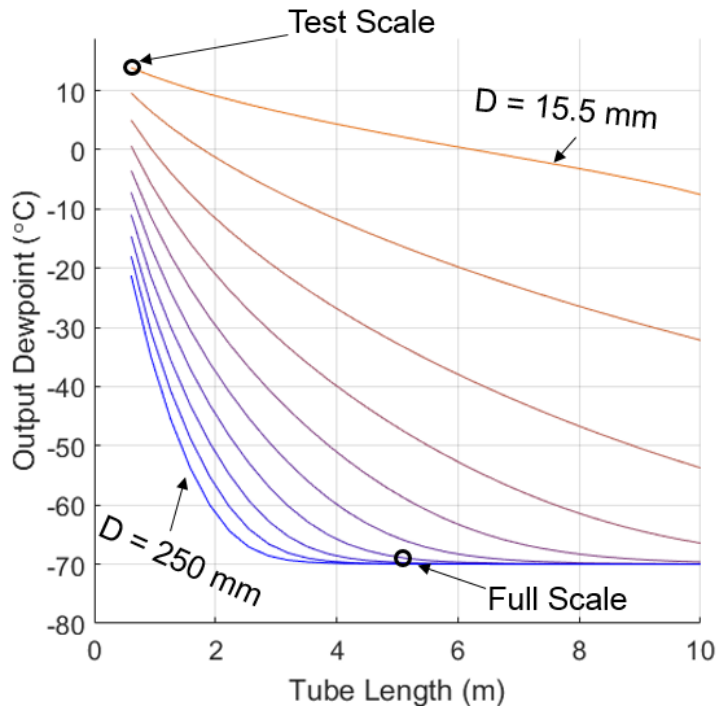


Figure 39. Scaling analysis for the WCS. Air flowrate is 30 cfm, wall temperature is -70°C and input humidity is 70 %RH.

7.2. Ionic Liquid System (ILS) Model Validation

7.2.1. Water Accumulation in the Ionic Liquid

As discovered in the modelling efforts, the primary driver of ILS performance is the concentration of water in the ionic liquid. The concentration of water was estimated using two independent methods: by tracking the water in the inlet air stream and outlet air stream, and by measuring the conductivity of the ionic liquid after each test.

The first method utilized the upstream relative humidity sensor and the downstream dew point sensor, along with the volumetric flow sensor. The upstream and downstream water measurements were converted into concentration in moles/m³ as shown in Figure 40. The concentration difference multiplied by the volumetric flow rate (in m³/s) provided the molar uptake of water per second. The equation is written as:

$$\dot{n} = (C_{in} - C_{out})\dot{V} \quad [\text{mol/s}] \quad (15)$$

Integrated over the entirety of testing and divided by the volume of ionic liquid in the system provided the concentration of water as shown in Figure 41.

The second method involved taking a sample of ionic liquid after each test for conductivity measurements. The conductivity has been related to the concentration of water in the ionic liquid by Vila et al. (2006). The measurements are shown in Figure 42.

When converted into molar fractions, these two methods provided very similar results, as shown in Figure 43.

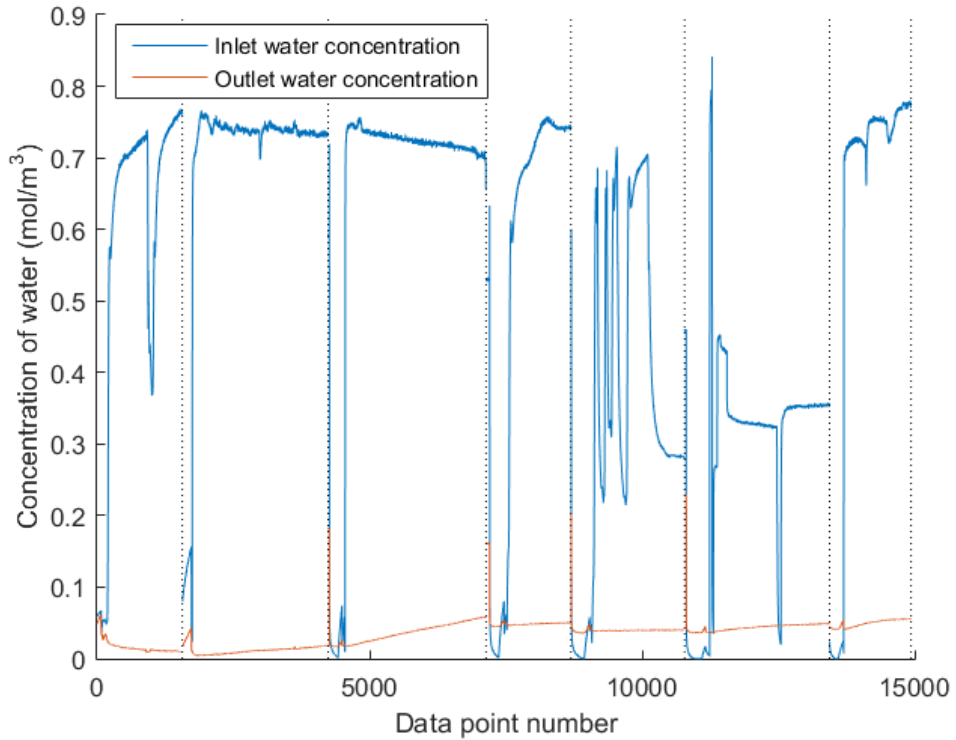


Figure 40: Inlet and Outlet Water Concentration during ILS Testing

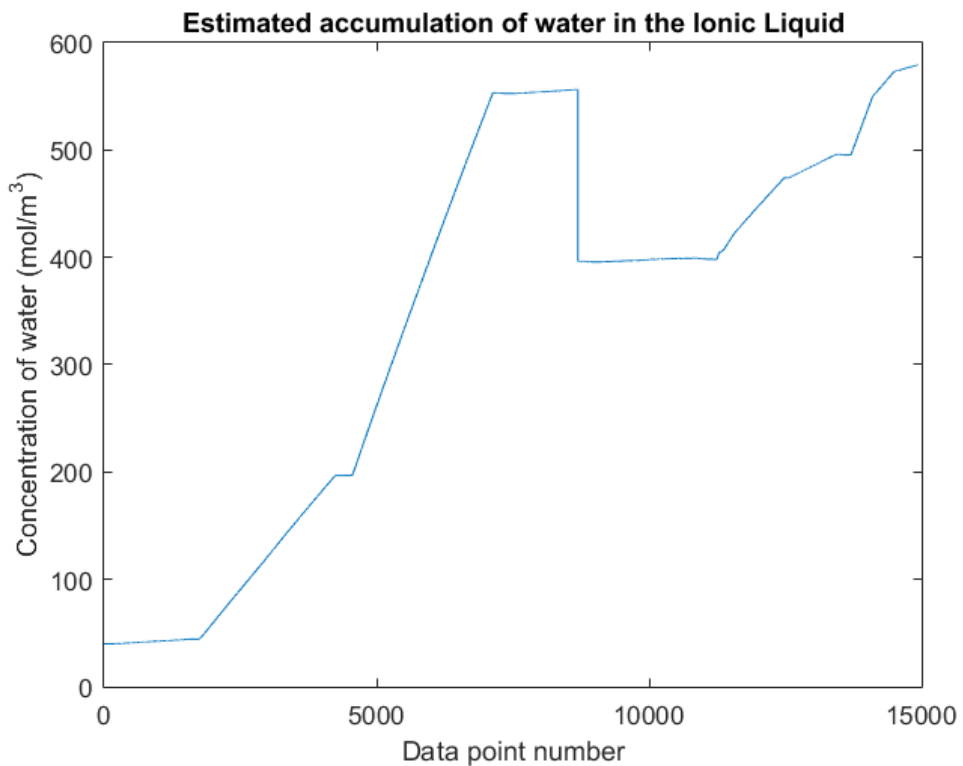


Figure 41: Estimated Accumulation of Water in the ILS during Testing

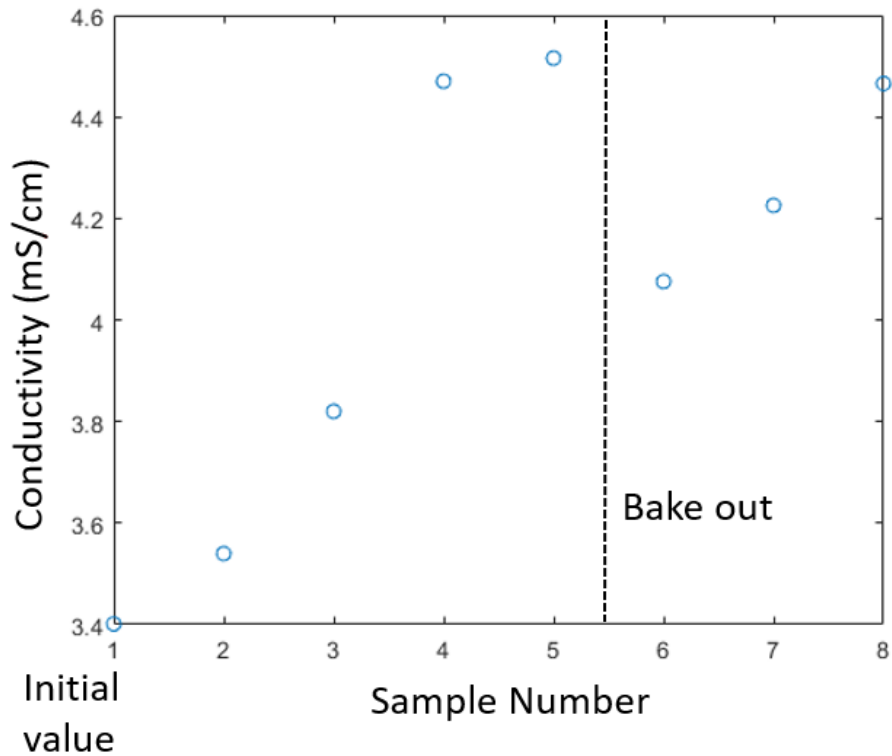


Figure 42: Electrical Conductivity Measurements during ILS Testing

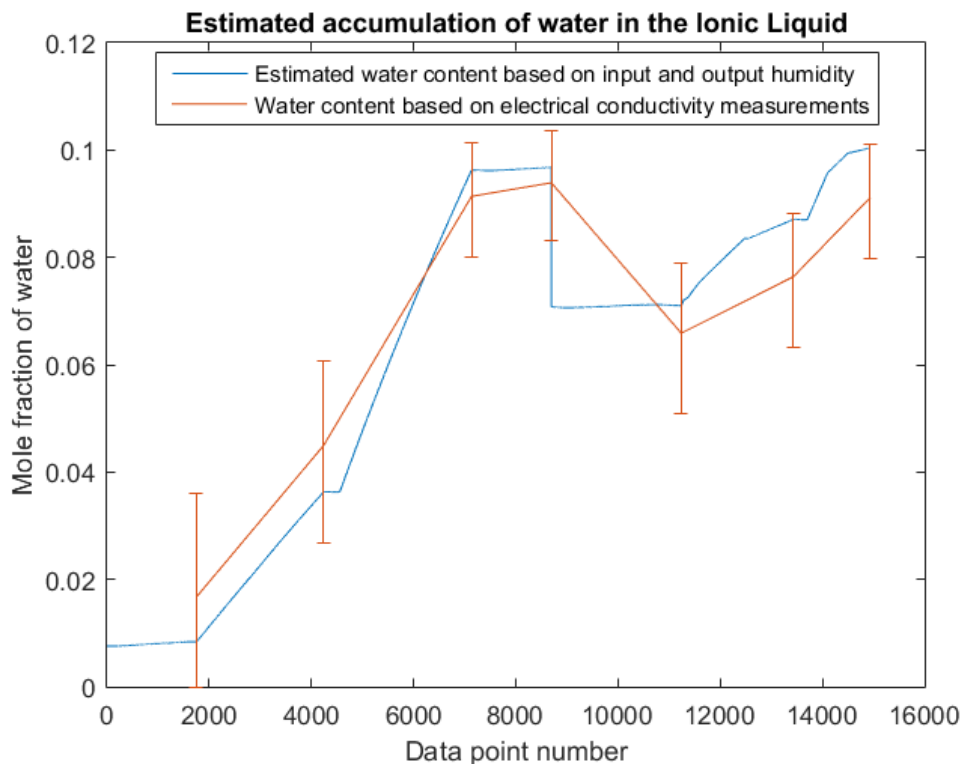


Figure 43: Water Accumulation in the ILS During Testing

7.2.2. Ionic Liquid Bake Out

After test number 4, the ionic liquid was drained from the system and left in a vacuum chamber for 24 hours. The amount of water removed from the ionic liquid was estimated using both conductivity measurements and post bake out performance. The concentration of water dropped from 555 moles/m³ to 395 moles/m³, a decrease of approximately 29%. This was less effective than expected, however the bake out was done in less than ideal circumstances: the ionic liquid was left in their bottles with very little exposed surface area, the ionic liquid was static instead of being agitated, and it was not heated.

7.2.3. ILS Performance

The ILS achieved its best performance during the first test run due to the low initial concentration of water in the ionic liquid. The outlet air reached a dew point of -36°C despite not performing a nitrogen purge of the system before the first test, nor desorbing the ionic liquid beforehand. The nitrogen purge during the second test dropped the outlet air to below -40°C, which was likely at equilibrium with the ionic liquid. The outlet air dew point continued to track the same pattern as the water content in the ionic liquid despite testing at various flow rates and inlet humidity values. This matches the model quite well as shown in Figure 43. Since all evidence suggests that the water in the air and the ionic liquid reached equilibrium before reaching the end of the contactor, it was not possible to validate the efficacy of the mass transfer rate within the contactor.

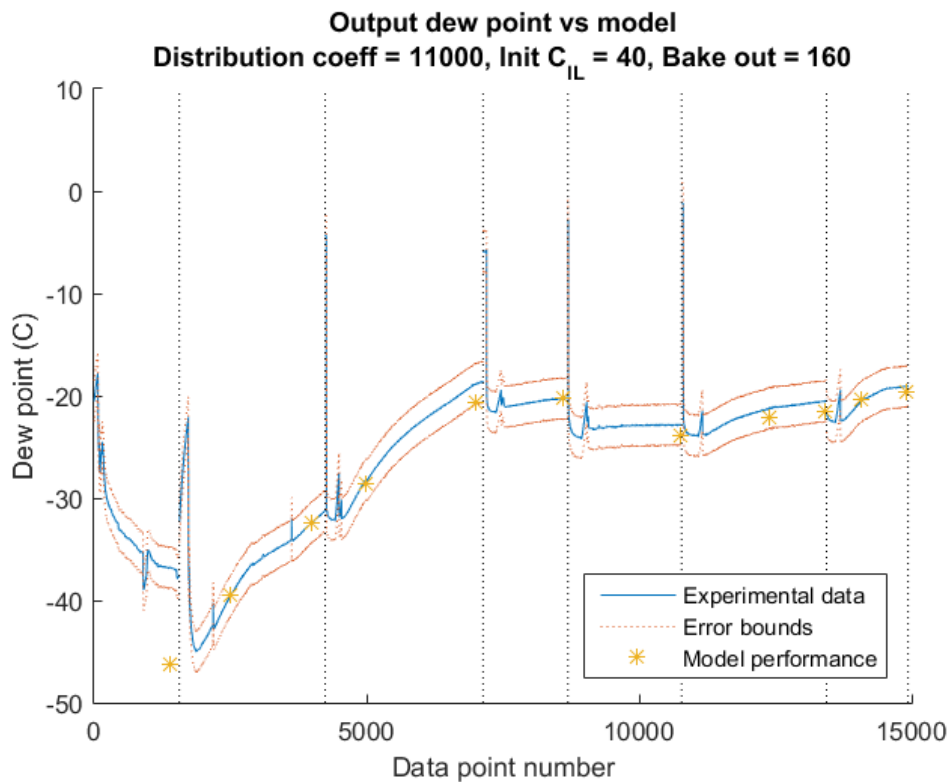


Figure 44: Outlet Dew Point during ILS Testing

7.2.4. Interaction of Carbon Dioxide in the ILS

Given concerns about ionic liquid removing carbon dioxide from the air stream, the inlet and outlet concentrations were measured, as shown in Figure 45. The outlet concentration of carbon dioxide was actually measured to be higher than the inlet concentration, however this was within the error bounds of the sensors. Therefore, no detectable amount of carbon dioxide was removed by the ILS.

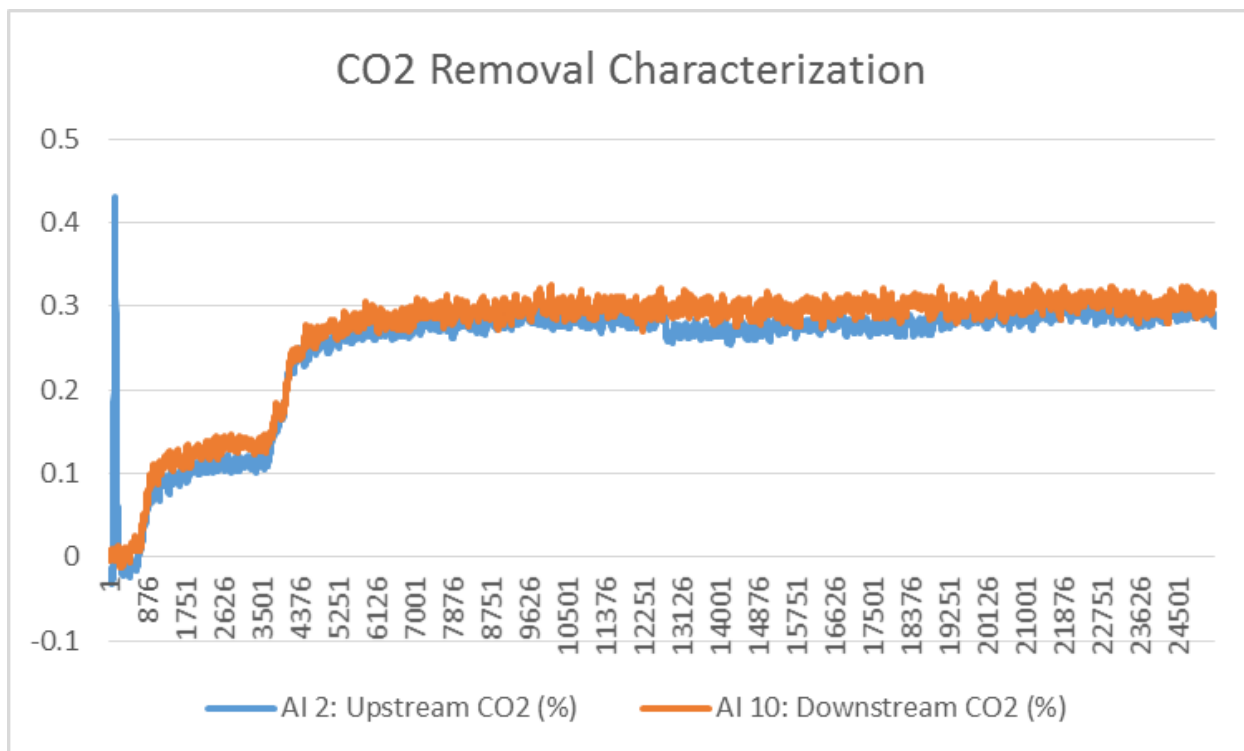


Figure 45: Carbon Dioxide Concentration Upstream and Downstream of the ILS

7.2.5. Results Summary

ILS article testing confirmed the model's indication that the primary driver of ILS performance is the concentration of water in the ionic liquid. However, due to the equipment available to the team, efficient, effective ionic liquid drying was not possible. Because of this, the ILS produced the lowest outlet dew point in the initial tests and bottomed out at 36°C despite not performing a nitrogen purge of the system before the first test, nor desorbing the ionic liquid beforehand. The outlet air dew point continued to track the same pattern as the water content in the ionic liquid despite testing at various flow rates and inlet humidity values. This matches the model quite well as shown in Figure 43. Since all evidence suggests that the water in the air and the ionic liquid reached equilibrium before reaching the end of the contactor, it is likely that the article was over engineered both geometrically (in that it could have been smaller and had fewer fibers) and operationally (in that the IL flowrate could have been lower). A smaller contactor with a lower IL flow rate could have produced the same output dew point for a given flowrate of humid simulated cabin air.

It should also be noted that, given the data displayed in Figure 45, it can be concluded that the ionic liquid sorbed a negligible quantity of carbon dioxide. This further justifies the choice of [EMIM] [EtSO₄] for dehumidification applications.

7.2.6. ILS Scaling Analysis

For a full scale version of the ILS, it would be required to function at an air flow rate of 30 scfm, approximately 100 times higher than the flow rates tested. Based on model performance, the contactor would only need to be 4x larger by volume, assuming it had 10x more fibers and an

ionic liquid flow rate of 10 times higher than the HYDRA contactor. The dry mass of this contactor would be approximately 25 kg. It is difficult to know for sure whether this size would be optimal given that the rate of mass transfer within the HYDRA contactor was not characterized experimentally (only lower bounds were determined). Assuming that the contactor is sized sufficiently to allow for the concentration of water in the air and the ionic liquid to reach equilibrium by the end of the fibers, performance becomes limited by the amount of ionic liquid in the system. The more ionic liquid is in the system, the longer it will take to saturate, or degrade to a given performance and need to be cycled.

For a given desired output dew point, the cycle time scales linearly with the mass of ionic liquid. For example, a target dew point of -20°C can be maintained for 6 hours with 500 kg of ionic liquid, or 3 hours with 250 kg of ionic liquid. Level 3 success (-90°C) is not practically achievable, as performance degrades above that target in a matter of seconds even with large quantities of ionic liquid. Level 2 success (-43°C) can be maintained for 37 minutes with 500 kg of ionic liquid before cycling would be required. Further performance characteristics for a given cycle time can be found in Figure 46.

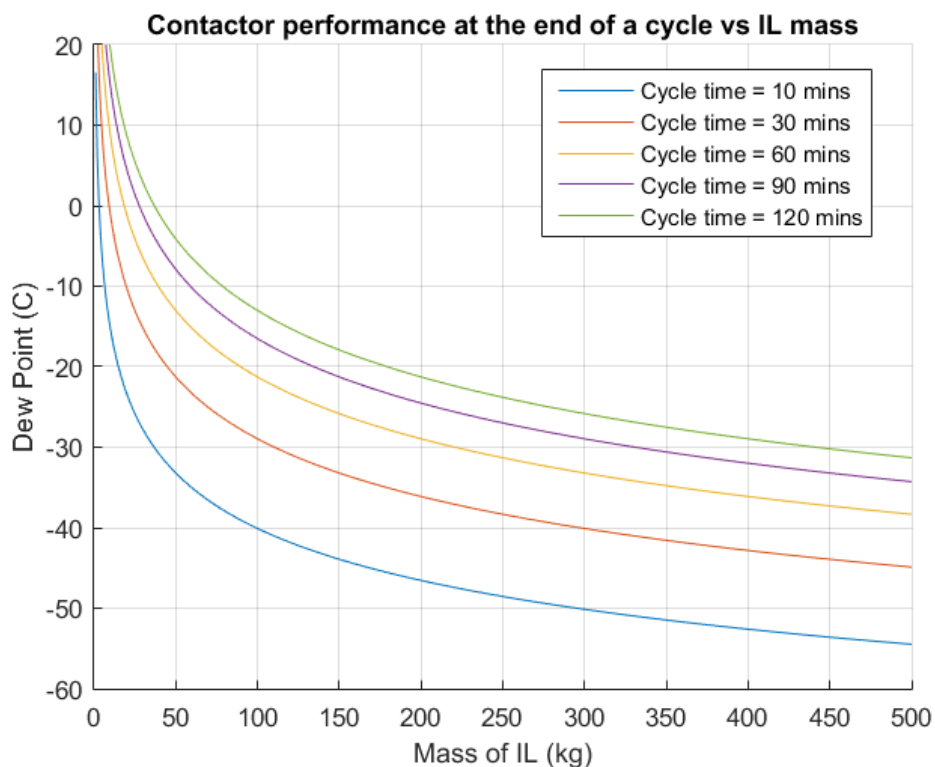


Figure 46: Contactor Performance at the End of a Cycle given the Cycle Time

8. Recommended Future Work

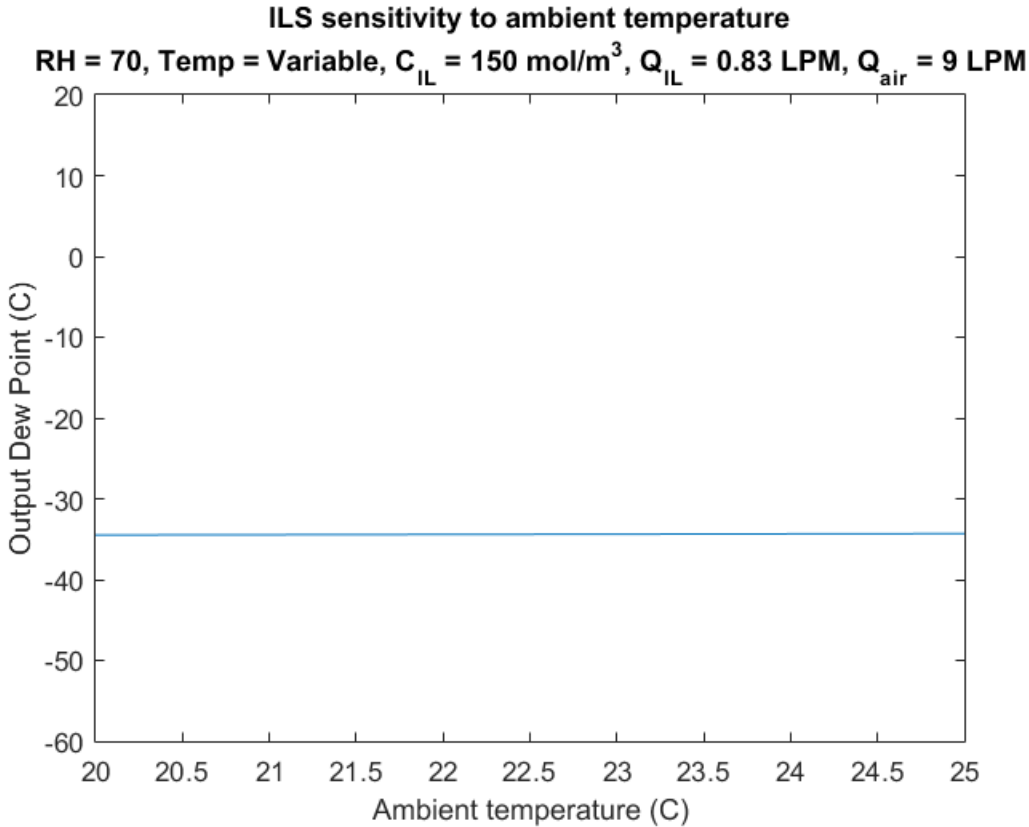
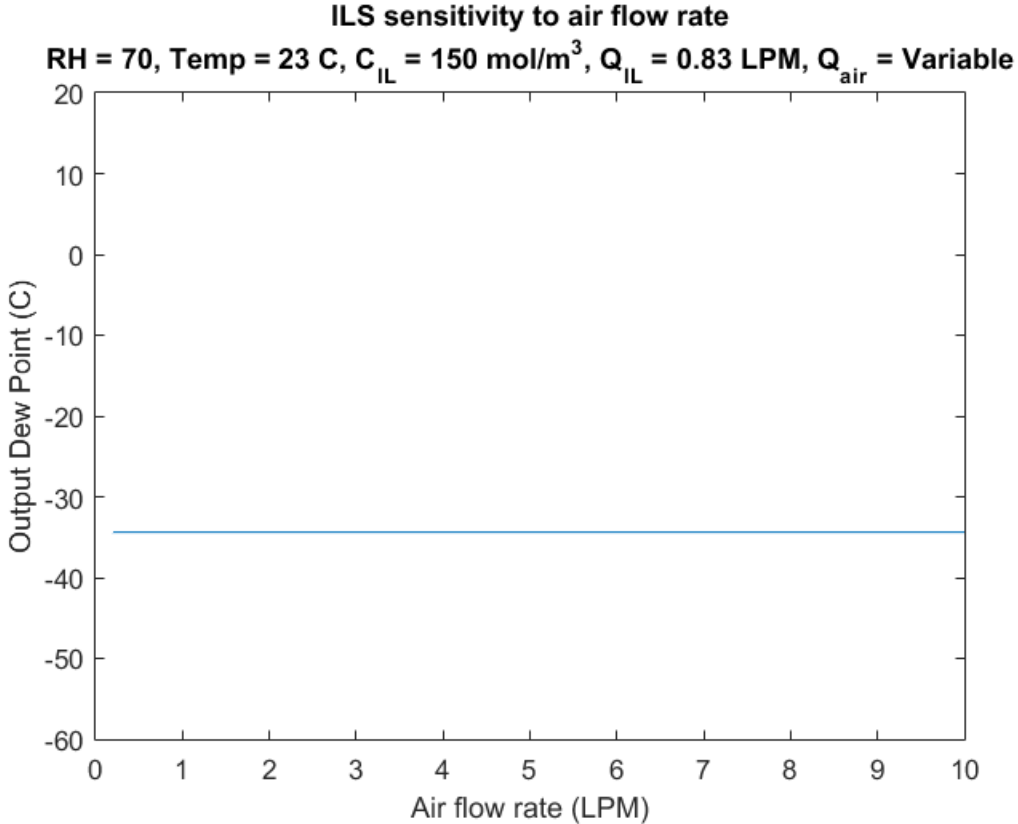
In the lab, water recovery from the WCS was as easy as allowing the system to warm and tipping it up on one end such that the water could drain out. However, water collection and recovery in the micro-gravity environment of space is non-trivial. Steps should be taken to characterize the process of transferring the water ice from the inside of a WCS operating in micro-gravity to storage or to a reclamation loop.

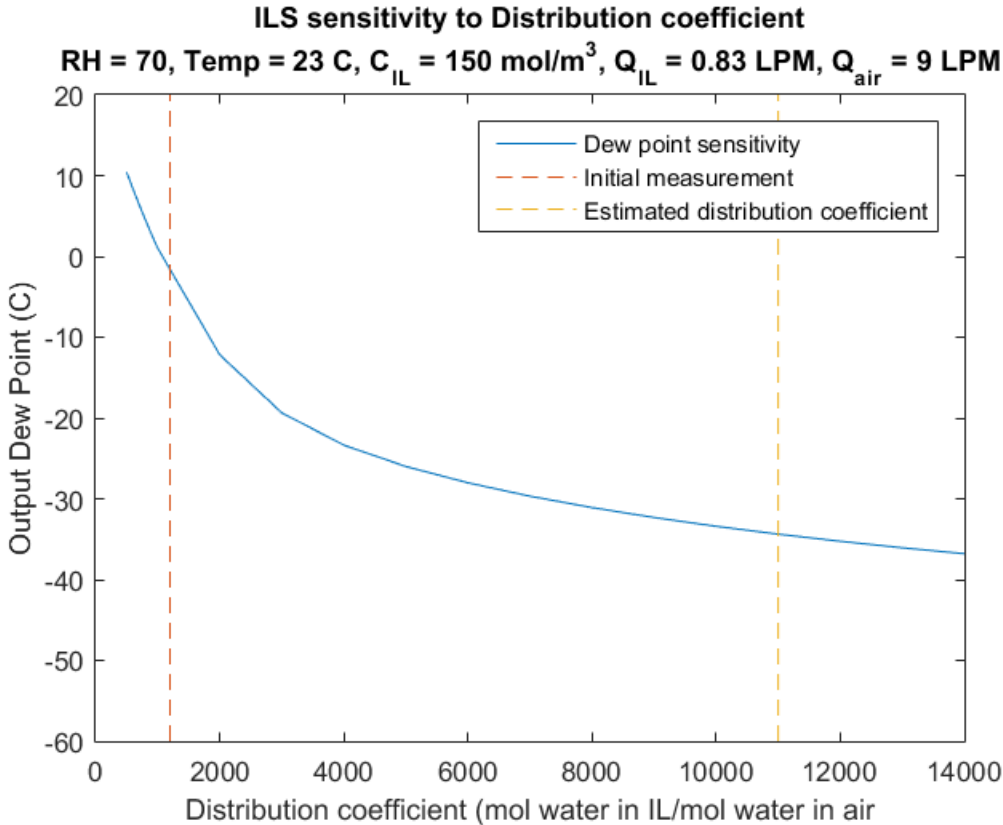
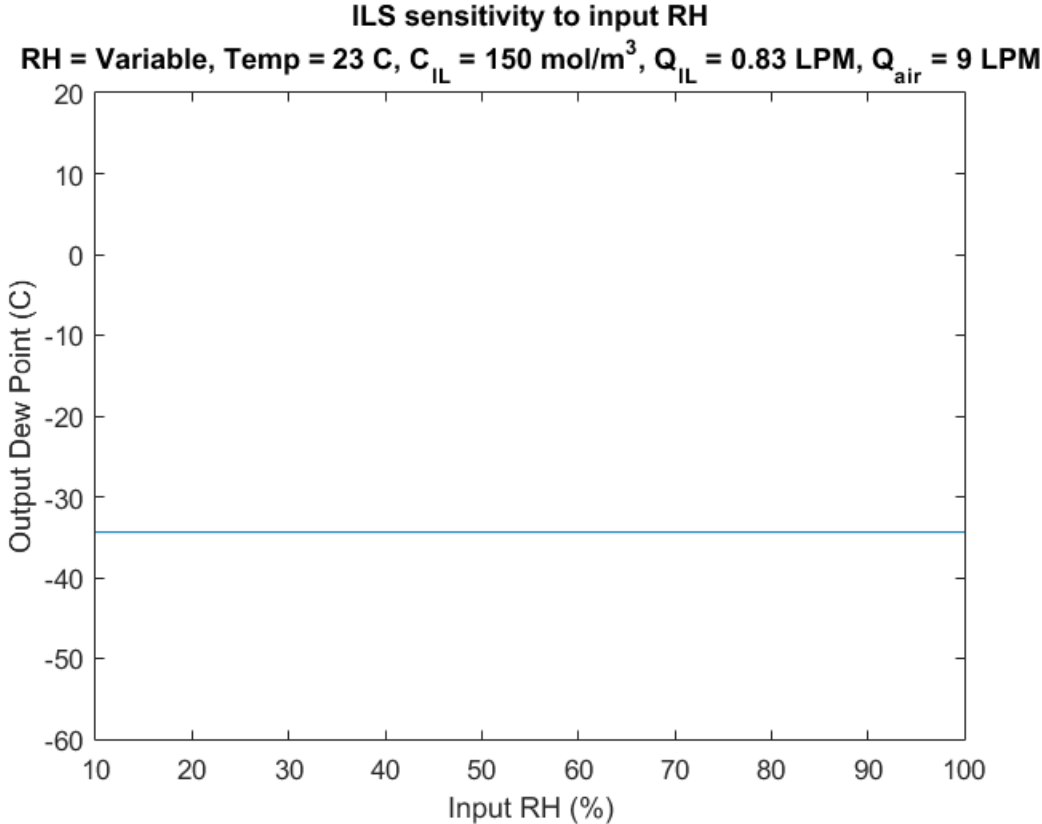
The ILS performance is driven primarily by water concentration within the IL, so it is of paramount importance going forward to determine a way to integrate an ionic liquid regeneration process into the ILS. Operating with the driest possible IL will minimize the size of the contactor, number of fibers within the contactor, and the volume of IL required to flow through the contactor.

One of the main goals of this project was to identify a few promising technologies for air dehumidification in life support applications. Both the WCS and the ILS show potential from operational principle standpoint. However, only rudimentary scaling analysis was conducted for each the WCS and ILS in this project. This will have to be done in greater detail to truly determine technology feasibility in a spaceflight environment.

9. Works Cited

- Belancik Grace. Characterizing Cryogenic Carbon Dioxide Capture Support Systems. 47th International Conference on Environmental Systems, Charleston, SC, 16-20 July 2017.
- Chambliss, J., Sweterlitsch, J., Swickrath, M. J., "Potential Uses of Deep-Space Cooling for Exploration Missions", AIAA 2012-3638, July 2012.
- Cussler, E. L. Diffusion: Mass Transfer in Fluid Systems. Cambridge University Press, 1997.
- Dindore, V, et al. "Modelling of Cross-Flow Membrane Contactors: Physical Mass Transfer Processes." *Journal of Membrane Science*, vol. 251, no. 1-2, Jan. 2005, pp. 209–222., doi:10.1016/j.memsci.2004.11.017.
- Kandula, M. "Frost growth and densification in laminar flow over flat surfaces", John F. Kennedy Space Center. 2011
- Muntaha, A., Haider, M., Rahman, A., "Modelling of Frost Formation and Growth on Microstructured Surface", American Institute of Physics, 2016
- Rausch, Michael Heinrich, et al. "Mutual Diffusion in Binary Mixtures of Ionic Liquids and Molecular Liquids by Dynamic Light Scattering (DLS)." *Physical Chemistry Chemical Physics*, vol. 13, no. 20, 2011, p. 9525., doi:10.1039/c1cp20208a.
- Rodríguez, Héctor, and Joan F. Brennecke. "Temperature and Composition Dependence of the Density and Viscosity of Binary Mixtures of Water Ionic Liquid." *Journal of Chemical & Engineering Data*, vol. 51, no. 6, 2006, pp. 2145–2155., doi:10.1021/je0602824.
- Vila, J., et al. "Great Increase of the Electrical Conductivity of Ionic Liquids in Aqueous Solutions." *Fluid Phase Equilibria*, vol. 247, no. 1-2, 2006, pp. 32–39., doi:10.1016/j.fluid.2006.05.028.
- Wieland, P. "Living Together in Space: The Design and Operation of the Life Support Systems on the International Space Station." NASA, vol. 1, 1998, p. 95.
- Xanthopoulos, G., Mitropoulos, D., Lambrinos, G., "Estimation of Heat and Mass Transfer Coefficients During Air-Freezing of Cucumber", *International Journal of Food Properties*, Volume 15, 2012 – Issue





Appendix B: WCS Detailed Manufacturing and Assembly

The pieces of the WCS were manufactured and assembled in three distinct phases. The phases were the building of the custom flange, the assembly of the outer pipe, and the final assembly. The custom flange deserves its own focus because of the significant amount of design work necessary and it was the only piece that was manufactured in house. The outer pipe assembly consists of the outer pipe, the bosses, the NPT tube fittings, and the outer flanges. The final assembly looks at how these processes were combined with the inner pipe, outer flanges, O-rings and nuts and bolts to create finished design.

Custom Flange:

The custom flange was cut from a 5 inch diameter, 5 inch long stock of 303 stainless steel (seen in Figure 49). The stock for the flange was cut into two pieces using a horizontal band saw. The two pieces were machined separately in the CNC lathe and cut to be 1 inch in length and 4.25 inches in diameter. Four 5/8 in. unthreaded bolt holes were drilled to match the ones on the off-the-shelf inner flange. A hole that was 3/4 inch in diameter was drilled 1/2 inch deep into the center of the flat face of the flange. A second centered hole was drilled into the bottom of the first drill hole. The second hole was cut through the opposite end of the flange and cut 1/4 inch to fit the 1/4 inch NPT compression fitting.



Figure 49. Custom flange stock.

Outer Pipe Assembly:

Outer Pipe:

The Outer pipe was originally 36 inches in length. To cut it down to its designed size, the outer pipe was cut down to 24 inches using a horizontal band saw. Once it was cut, it was edged so it was perpendicular to the length of the pipe, and sanded, to prepare it for welding.

Inner Flanges:

Once the outer pipe was cut and prepared, the inner flanges were welded to the ends of each pipe using a TIG welder. The flanges were placed the flat part of the flange was facing outwards. This can be seen in the pictures of the Outer Pipe Assembly in Figure 50 and Figure 51.

Bosses:

The bosses were $\frac{3}{4}$ inch square rods that were cut and chamfered to fit snugly on the outer pipe.

These pieces used an acceptable piece of available material from the machine shop and were cut to size using a CNC mill. Once the bosses were cut, they were welded on opposite sides of the pipe (both axially and radially) as seen in Figure 51. The bosses were placed as close as was possible to the ends of the pipes without disturbing the welding, about $\frac{1}{4}$ inch. After the bosses were welded, a $\frac{1}{2}$ inch hole was drilled through both the bosses and the outer pipe that was underneath them. These holes were to allow coolant flow through the system. The hole was tapped to fit NPT threading. The $\frac{1}{2}$ inch NPT tube fittings were screwed into the system once the entire WCS had been assembled. A picture of the complete outer pipe assembly can be seen in Figure 51.



Figure 50. One end of WCS outer pipe assembly.



Figure 51. Outer pipe assembly.

Final Pipe Assembly:

Once the outer pipe assembly and the custom flange were built, it was possible to construct the entire WCS.

Inner Pipe:

The inner pipe needed to be fitted properly to allow a seal between the two flanges on each side of the system. To make sure the inner pipe was cut to the correct length, it was measure how deep the pipe went into the flange, and that was added to the amount that was able to fit into the outer pipe assembly with one flange attached, and marked. Using the marking it was possible to cut the inner pipe slightly above the correct size of 25 inches. The pipe was then edged and sanded to create a good seal with the gaskets and radial O-rings.

Bolts:

One of the bolts needed to be cut due to the alignment of the flange and the boss. This cut shortened the length of the bolt by $\frac{3}{4}$ inch and allowed for the nut to be screwed on successfully. This was done using a hand Dremel rotary tool. Once the cut was complete, the bolt was sanded to allow the nut to be screwed on.

Assembly:

Once all of the construction was completed, the assembly could begin. The first step of the assembly was to place the O-rings and gasket on one of the custom flanges and place the inner pipe in the custom flange. Next, the outer pipe assembly was placed over the inner pipe, creating the concentric circles, and bolted in place. Once this was completed, the O-rings and gasket on the other custom O-ring were put into place, the rest of the system was placed on it. The

penultimate step was to screw the final bolts in place and ensure a tight fit via a water test. The last step was to attach all the NPT fittings and drill a hole for the thermistor to measure the temperature of the coolant. It was important that this hole was small and only went through the outer wall, so it did not cause leaks and could be easily sealed with JB Weld. The completed Water Cryocooler System can be seen in Figure 52.



Figure 52. Completed WCS.

Appendix C: ILS Detailed Manufacturing and Assembly

The mechanical design for HYDRA's Ionic Liquid System (ILS) was largely based off of the CARIL team's contactor design. The ILS was a larger version of the CARIL team's contactor with overall dimensions of 23 in. long and a 4 in. outer diameter. HYDRA's final ILS design included 484 hollow fibers, 6 stainless steel support rods, 3 polypropylene disks to support the hollow fibers, 2 spacer rings to create space in the air manifolds, 2 ultra-high molecular weight polyethylene (UHMWPE) end caps, 1 UHMWPE housing for the fibers, and polypropylene NPT compression fittings to integrate the ionic liquid loop and gas loop from AETHER. The system included two inlets for the ionic liquid to flow into the contactor and one outlet. It also included one inlet for air to enter and one outlet for the air.

Ionic Liquid System Components

Hollow Fibers:

The hollow fibers used were donated to the project by Evoqua Water Technologies under a non-disclosure agreement. Each of the 484 fibers had an outer diameter of 0.0256 in., an inner diameter of 0.0154 in., and a wall thickness of 0.0055 in. The fibers were cut to be 21 in. long for the contactor. These fibers were made out of polypropylene, which is not reactive with the ionic liquid chosen and exhibits hydrophobic properties, and had a porosity of 60-70%. The hydrophobic properties allowed for the porous fibers to not absorb any of the ionic liquid, which would contaminate the air flowing through the contactor. The test gas from AETHER flowed through the fibers while the ionic liquid flowed around them.

Fiber Guide 1:

Fiber Guide 1 was manufactured from a 1/2 in. thick polypropylene sheet. It was designed to hold the fibers at one end of the contactor. It included 484 #62 thru-holes for the fibers and 6 1/16 in. diameter holes (0.35 in. deep) for the support rods. Fiber Guide 1 is broken down into essentially two parts, an outer flange with the O-ring groove and an inner part that inserts into the fiber housing. The outer flange is 1/4 in. thick with a 3.5 in. diameter. It has an axially oriented O-ring groove cut to fit a -042 EPDM O-ring on the flange. The rest of Fiber Guide 1 is 1/4 in. thick also and has an outer diameter of 3 in. to fit into the fiber guide housing. The fibers were fixed into Fiber Guide 1 using a polyurethane adhesive. Fiber Guide 1 was manufactured using a CNC Milling Machine. The milling operation took around 6 hours to complete due to the lengthy time required to drill the 484 thru-holes for the fibers.

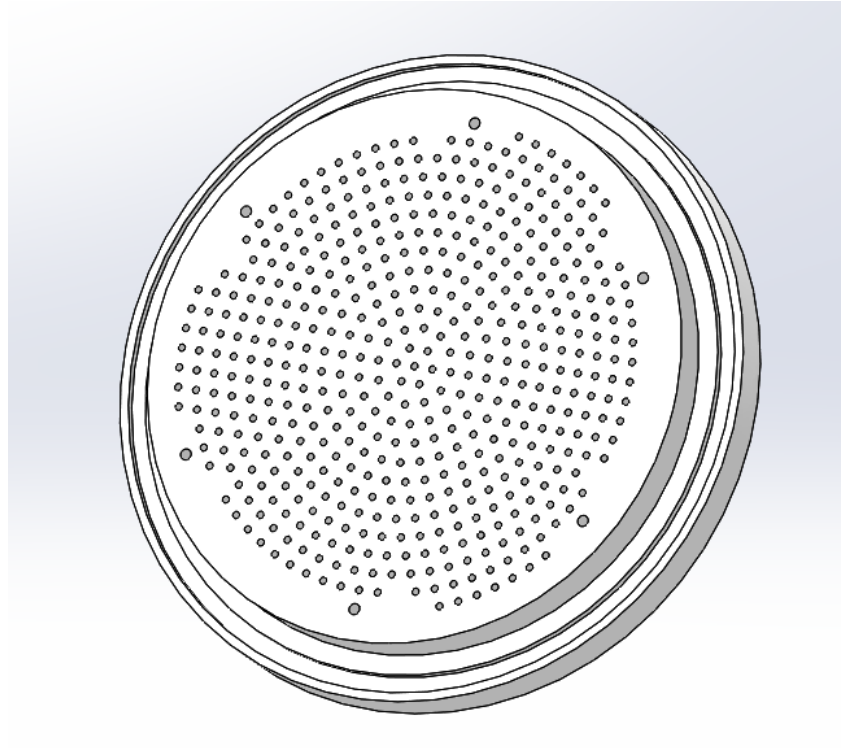


Figure 53. Fiber guide 1.

Fiber Guide 2:

Fiber Guide 2 was manufactured from a 1/8 in. thick sheet of polyethylene. It was cut into an outer diameter of 2.9 in. and had the same hole pattern from Fiber Guide 1 mirrored onto it (#62 holes thru-holes for the fibers and 1/16 in. thru-holes for the support rods). This piece was used to keep the fibers supported in the middle of the contactor so no sag occurred. Its outer diameter was smaller than the 3 in. inner diameter of the fiber housing in order for flow to be able to flow around it and not cause compartmentalization of the flow in the contactor. Fiber Guide 2 was manufactured on a CNC Milling Machine. The milling operation took around 4 hours to complete due to the extensive amount of fiber holes being drilled.



Figure 54. Fiber guide 2.

Fiber Guide 3:

Fiber Guide 3 was manufactured from a 1/4 in. thick sheet of polyethylene. It had an outer diameter of 3 in. and had the same hole pattern from Fiber Guide 1 mirrored onto it for continuity (#62 thru-holes for the fibers and 1/16 in. holes for the support rods). However, the 1/16 in. holes for the support rods were only 0.25 in. deep and on the opposite side (the air side) six #50 holes (0.130 in. deep) were drilled and tapped for the #2-56 locking screws. A radial O-ring existed on the outer diameter of Fiber Guide 3 that sealed with the inner diameter of the fiber housing in order to seal the ionic liquid from leaking into the air manifold. The radial O-ring groove was cut to fit a square -232 Viton O-ring. A special part was made in order for Fiber Guide 3 to be made. This part seen below in Figure 55 was made so that the piece could be flipped over after machining the first side to drill the #2-56 holes and cut the radial O-ring groove. This piece was machined out of a scrap block of aluminum. The aluminum was squared and made on a CNC Milling Machine. 1/16 in. diameter holes were drilled and then 1/16 in. pins were pressure fit into the holes. This process took about 2 hours to complete. Fiber Guide 3 was then manufactured on a CNC Milling Machine. After the first side of the piece was machined it was flipped over and pressed onto the pin supporting piece. Then the #50 holes were drilled in and the axial O-ring groove was cut. Lastly, the #50 holes were tapped with a #2-56 tap. The overall process took about 6 hours.

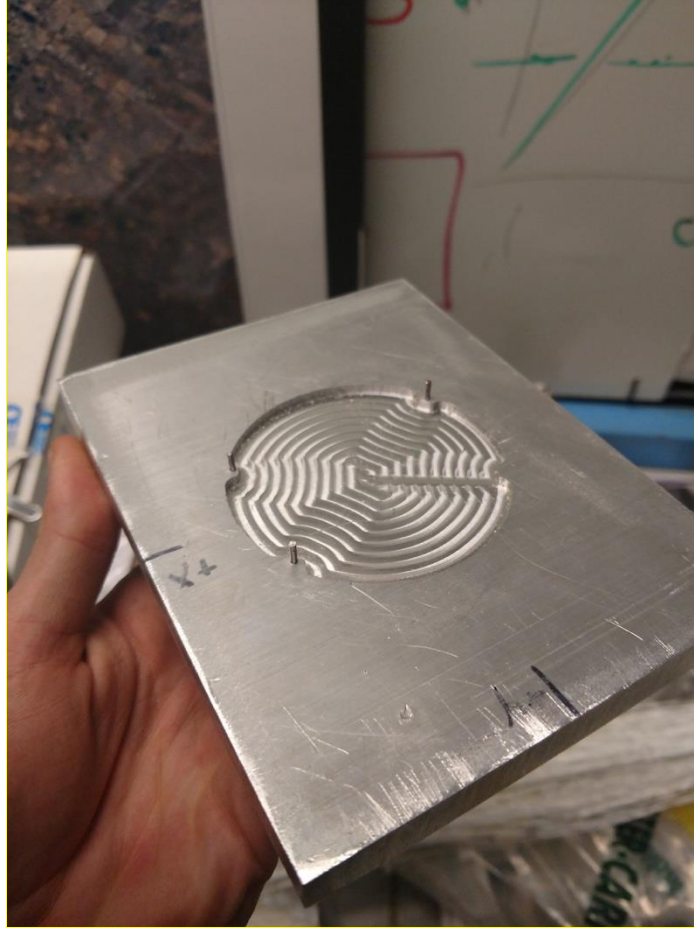


Figure 55. Pin supporting piece.

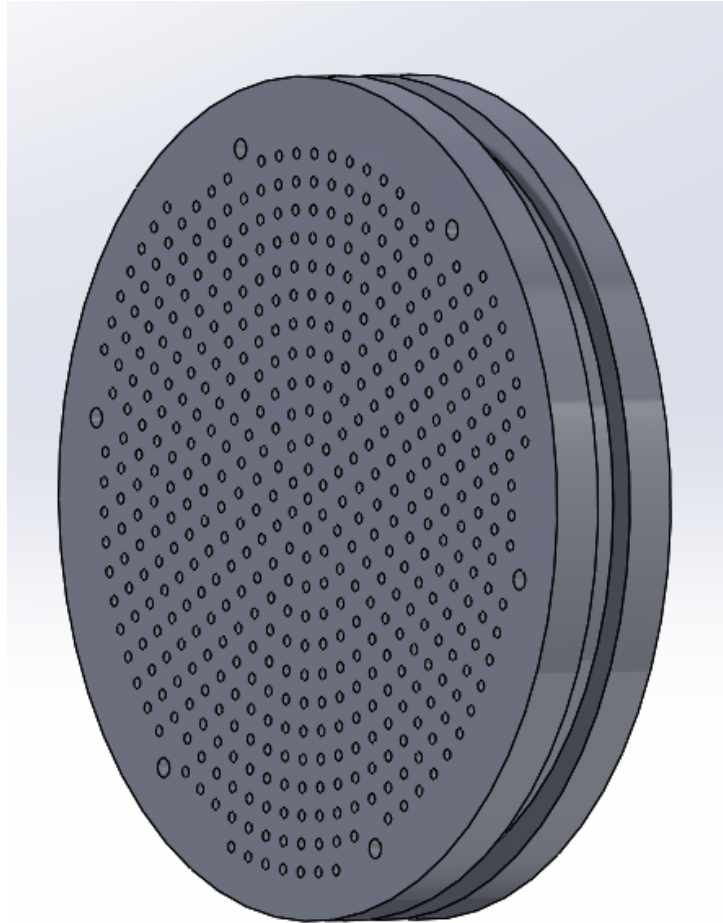


Figure 56. Fiber guide 3.

#2-56 Stainless Steel Socket Head Screws:

Six #2-56 screws (0.325 in. length) were used to attach the Screw Lock Ring to Fiber Guide 3. They required a 5/64 in. hex key to tighten and were purchased from McMaster Carr (Part #: 92196A079).

Support Rods:

Six 1/16 in. stainless steel rods were used as the support rods. These were ordered from McMaster Carr (Part #: 88915K11). These rods were cut to a length of 20.16 in. using heavy duty wire cutters and then grinded down to make flat ends. These were fixed into the fiber guides without the use of adhesives because the tight fit didn't allow the rods to slide out once inserted into the fiber guides.

Screw Lock Ring

The Screw Lock Ring was manufactured from a 1/4 in. polypropylene sheet. It was used to attach to Fiber Guide 3 via six #2-56 screws in order to secure the fiber assembly into the fiber housing. It had a 3.5 in. outer diameter with six #43 holes drilled through it for the six #2-56 screws to be inserted. Fiber Guide 3 was attached to the Screw Lock Ring via six #2-56 screws (0.375 in. length) that threaded directly into Fiber Guide 3. The Screw Lock Ring was manufactured using CNC Milling Machine. This operation took approximately 30 minutes.

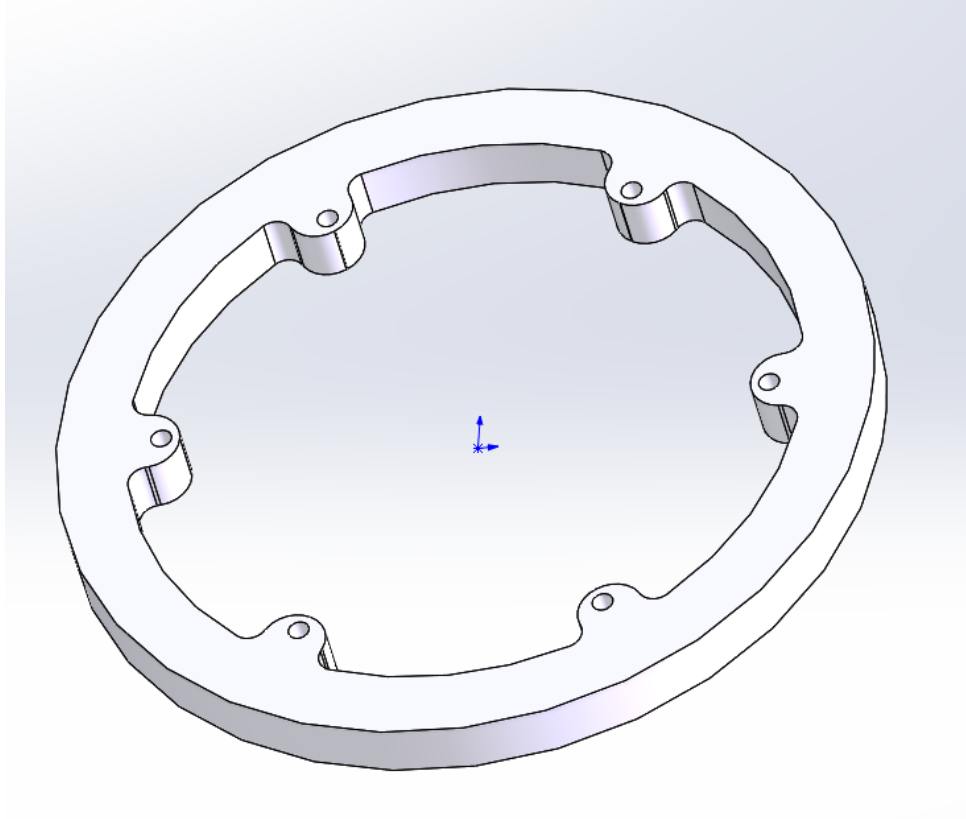


Figure 57. Screw lock ring.

Adhesive:

The adhesive used to pot the 484 hollow fibers was the polyurethane adhesive UR-2187 provided by H.B. Fuller. This is a 2-part adhesive that mixes with a ratio of 2:1 (2 parts of A: 1 part of B). This adhesive was used by the CARIL team and was found to wick down the #62 holes for the fibers very well. The adhesive proved to seal well for CARIL so it was chosen again to be used. The HYDRA team found this adhesive to once again seal well and was easy to use even when potting 484 fibers versus 118 fibers. This adhesive set in approximately 10 minutes and fully cured in a few hours. All fiber potting adhesive was left to cure for at least 3 hours each time.

Spacer:

Two spacers were manufactured from a 1/2 in. thick polypropylene sheet. They had an outer diameter of 3.5 in. and a 3 in. inner diameter. These spacers allowed for room in the air manifold so that the ends of the fibers did not get crushed or blocked by the end caps. The spacers were cut using a CNC Milling Machine. The total operations time for both spacers together was around 30 minutes.

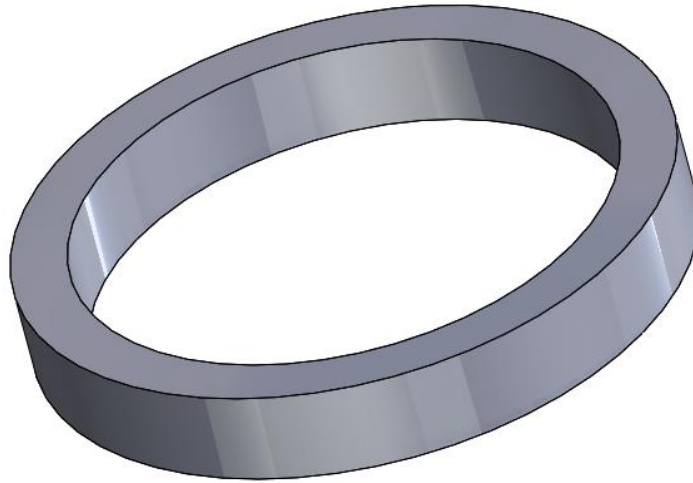


Figure 58. Spacer.

End Cap:

Two end caps, made of UHMWPE, had an outer diameter of 4 in. and a 3.5 in. inner diameter. They also included a radial O-ring that sealed with the outer diameter of the fiber housing in order to seal the air inside the air manifold from leaking out of the system into the ambient environment. The O-ring groove was dimensioned to fit a -238 Viton square profile O-ring. Each end cap also included a 7/16 in. thru-hole drilled and tapped for a 1/4 in. NPT compression fitting to be inserted. First, a 4 in. diameter stock of UHMWPE was cut into two 1.75 in. lengths and then each length was faced using a lathe. Then each piece was machined using a CNC Milling Machine. Lastly, the 7/16 in. hole was tapped using a 1/4 in. NPT tap. The overall machining process for both end caps to be finished was completed in around 5 hours.

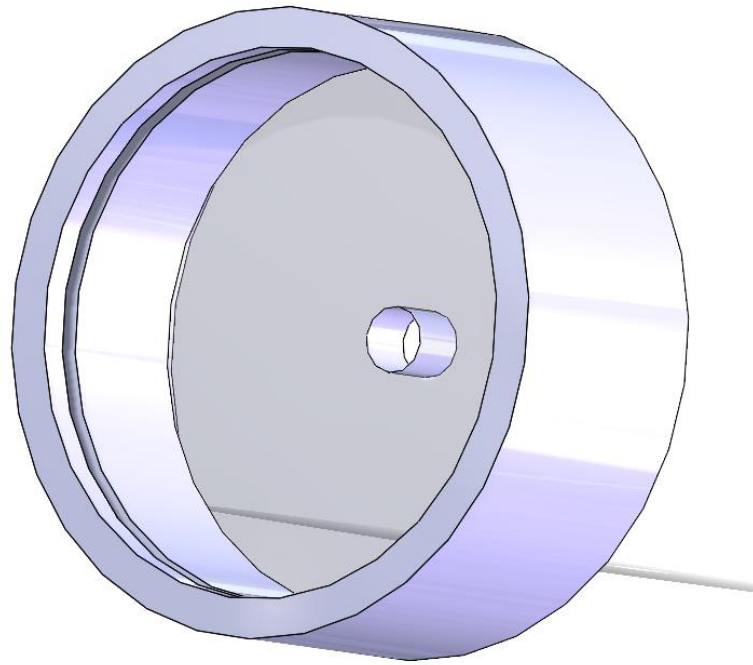


Figure 59. End caps.

Fiber Housing:

The fiber housing was cut from UHMWPE tubing. The housing was cut to 19.7 in. long, with a 3.5 in. outer diameter, and a 3 in. inner diameter. UHMWPE was chosen as the material due to it being non-reactive with the ionic liquid chosen. Two 7/16 in. holes and one 37/64 in. hole were drilled and tapped for NPT compression fittings to be inserted. The UHMWPE tubing was cut to length using a band saw and then the ends were faced using a belt sander. Usually parts are faced using a lathe but the length of this piece did not allow for that. The holes were then drilled using a drill press and then tapped using the corresponding NPT taps. This whole process was completed in around 2 hours.

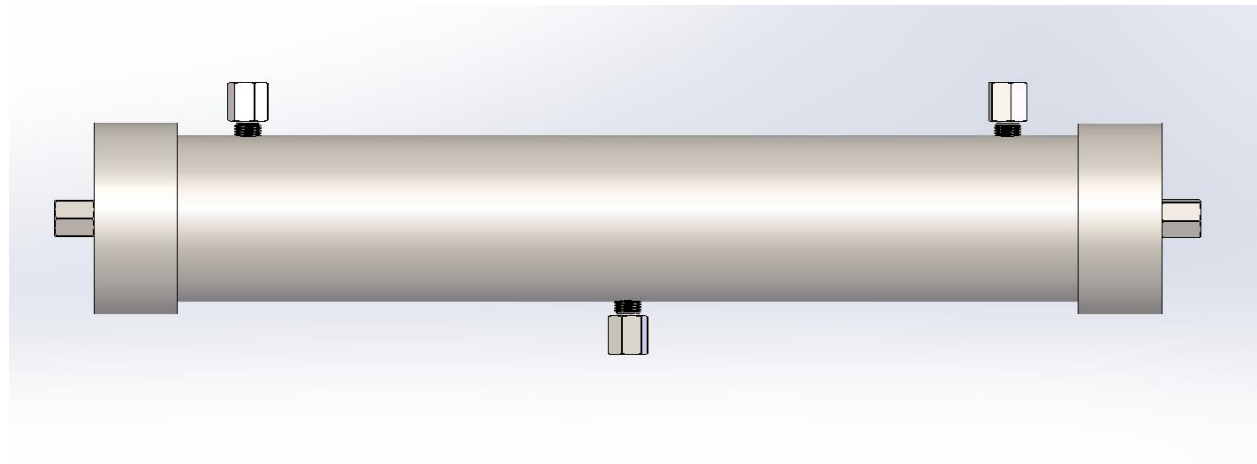


Figure 60. Fiber housing.

O-rings:

Three different sizes of O-rings were used within the contactor. The axial O-ring on Fiber Guide 1 was a 1/16 in. thick -042 EPDM O-ring (McMaster Carr Part #: 9557K133). The radial O-ring on Fiber Guide 3 was a 1/8 in. thick -232 square Viton O-ring (McMaster Carr Part #: 1170N105). The radial O-ring in the end caps was a 1/8 in. thick -238 square Viton O-ring (McMaster Carr Part # 1170N112). The square O-ring profiles were chosen because these are less likely to experience rolling when being assembled. Rolling can lead to damage being done to the O-ring or complete rupture. The seals from both of the axial O-rings in the end caps and on Fiber Guide 3 proved to not work as designed so other sealing methods were explored (this is explained later on).

5/16 – 18 All Thread:

Four 5/16 – 18 fully threaded rods were used to apply compression on the contactor via the compression assembly. This axial force was used to create the seal between Fiber Guide 1 and the fiber housing. Each of these rods were 27 in. long and were not cut from their stock length.

5/16 – 18 Nuts:

Eight 5/16 – 18 nuts were used to apply compression on the contactor. The nuts were threaded onto the fully threaded rods on the outside of the compression plates and contactor. They essentially sandwiched the plates around the contactor.

Compression Plates:

Two compression plates (6 in. x 6 in.) were manufactured from a 1/2 in. plate of stainless steel. These plates were used to provide an axial compression force on the contactor. Each plate had four 3/8 in. diameter holes drilled in each corner and one 1 in. diameter hole in the center for the 1/4 in. NPT compression fitting to extrude from the end cap. The stock for each plate was cut from a 6 in. x 12 in. stainless steel plate using a band saw. Then the thru-holes were drilled using a drill press. The 1 in. hole was done by stepping from a 3/8 in. drill bit to a 3/4 in. drill bit and then finally to a 1 in. drill bit. This process took around 2 hours.

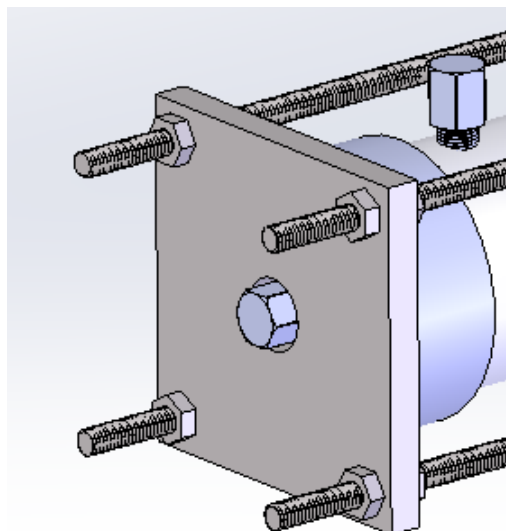


Figure 61. Compression plate and assembly.

Manifold:

One polypropylene manifold was used to diverge ionic liquid flow from the peristaltic pump into two tubes acting as the ionic liquid inlets to the ILS. The manifold selected had two 3/8 in. NPT ports and two 1/4 in. NPT ports. The manifold was purchased from McMaster Carr (Part #: 5364K212).

1/4 in. FEP Tubing:

1/4 in. FEP tubing was used to transport ionic liquid from the manifold to the inlets of the ILS. It was purchased from McMaster Carr (Part #2129T13).

L/S 15 Masterflex Tubing

L/S 15 Masterflex silicone tubing was used to attach the outlet of the ILS to the inlet to the ionic liquid manifold. This tubing was also ran through the peristaltic pump. It was purchased from Cole-Parmer.

NPT to Compression Fittings:

Two different sizes of NPT fittings were used: 1/4 in. NPT to 1/4 in. compression and 3/8 in. NPT to 3/8 in. compression. The NPT fittings used were made of polypropylene due to its material compatibility with the ionic liquid chosen. A total of six 1/4 in. NPT fittings were used (McMaster Carr Part #: 5016K422) and a total of three 3/8 in. NPT fittings were used (McMaster Carr Part #: 5016K444). PTFE tape was used to thread these into the ILS in order to create proper seals.

Assemblies

A description of how some of the sub-assemblies were put together is included below before the final assembly is discussed.

Fiber Assembly:

The Fiber Assembly included Fiber Guide 1, Fiber Guide 2, Fiber Guide 3, six support rods, 484 hollow fibers, and polyurethane adhesive. Two support stands with clamps on them were used to help assemble the Fiber Assembly once all of the fibers were threaded through all three fiber guides. The first step included threading all six of the support rods through each of the fiber guides until the structure of the Fiber Assembly was built.



Figure 62. Structure of the fiber assembly.

From here each fiber was individually threaded through all three fiber guides using tweezers. It was ensured that each fiber was being threaded through the same corresponding hole on each fiber guide so that no holes were skipped. This process took an astonishing 24 hours to complete.



Figure 63. Threading fibers through the fiber guides.

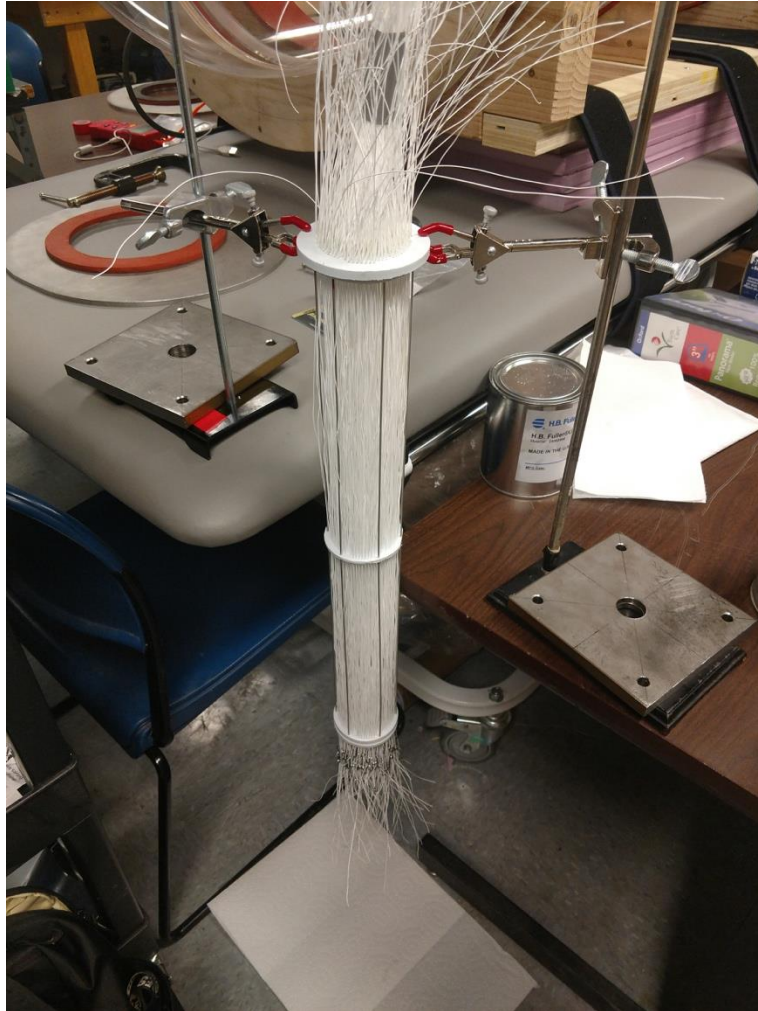


Figure 64. Fiber Assembly fully threaded.

After all of the fibers were threaded through, the adhesive was applied to the air side of Fiber Guide 1 first. Small disposable cups were used to measure out and mix the adhesive prior to application. UR-2187 A was measured up to the bottom of the blue section in one cup while UR-2187 B was measured up to halfway between the bottom of the cup and the bottom of the blue section in another cup. The two parts were then mixed in a different cup. Both parts of the adhesive were poured into the mixing cup at the same time to promote uniform mixing. The parts were then mixed with a popsicle stick for a few minutes prior to application. The Fiber Assembly was then hung vertically and adhesive was applied to Fiber Guide 1 via a small syringe. The top surface of the fiber guide was coated in adhesive and it was checked that adhesive had begun wicking down all of the holes before it was left to dry for at least 3 hours.



Figure 65. Cup used to mix adhesive.

Once the fibers had cured in Fiber Guide 1, the Fiber assembly was then taken out of the vertical holding stand in order to complete the next step. The fibers were then all individually weighted with a 1 oz. fishing weight in order to provide enough tension on the fibers when potting Fiber Guide 3. This tension allows the fibers to hang straight down so that the amount of fibers touching within the contactor was minimized.



Figure 66. Adding fishing weights to fibers.

Once each fiber had a fishing weight attached to it the Fiber Assembly was once again hung vertically in the support stand so that Fiber Guide 3 was close to the ground and the fishing weights were pulling the fibers down in tension. Another batch of the adhesive was then mixed and applied via a syringe to Fiber Guide 3. This adhesive was then left to dry for at least 3 hours.

Lastly, the extra length of fibers at both ends of the Fiber Assembly were cut using an X-Acto knife in efforts to not close off the ends of the fibers. Due to how soft the material of the fibers is, when cut the ends of the fibers can sometimes become blocked. With this known issue, the fibers were visually checked after cutting to see if an opening was still existing. If there wasn't an opening a needle was used to reopen the fiber. Due to the large number of fibers, it was expected that some fibers were missed and not open during testing.

Manifold Assembly:

The manifold was assembled prior to the final assembly of the ILS. Two 3/8 in. NPT to 3/8 in. compression and two 1/4 in. NPT to 1/4 in. compression fittings were wrapped in PTFE tape prior to being threaded into the manifold. These fittings were tightened using a crescent wrench.

Final Assembly Process

The entire ILS system was then assembled by combining the Fiber Assembly, fiber housing, O-rings, the Screw Lock Ring, socket screws, spacers, end caps, and fittings. The compression assembly including the two compression plates, four fully threaded rods, and eight nuts was then

placed around the contactor. The manifold along with tubing was then installed last to complete the full system assembly and deem the ILS prepared for testing.

First, one of the spacers was inserted into one of the end caps. The radial O-ring for the end cap was inserted before the Fiber Guide 1 side of the Fiber Assembly was then inserted into the end cap. Then the Fiber Assembly was inserted into the end cap with the axial O-ring already installed on Fiber Guide 1.

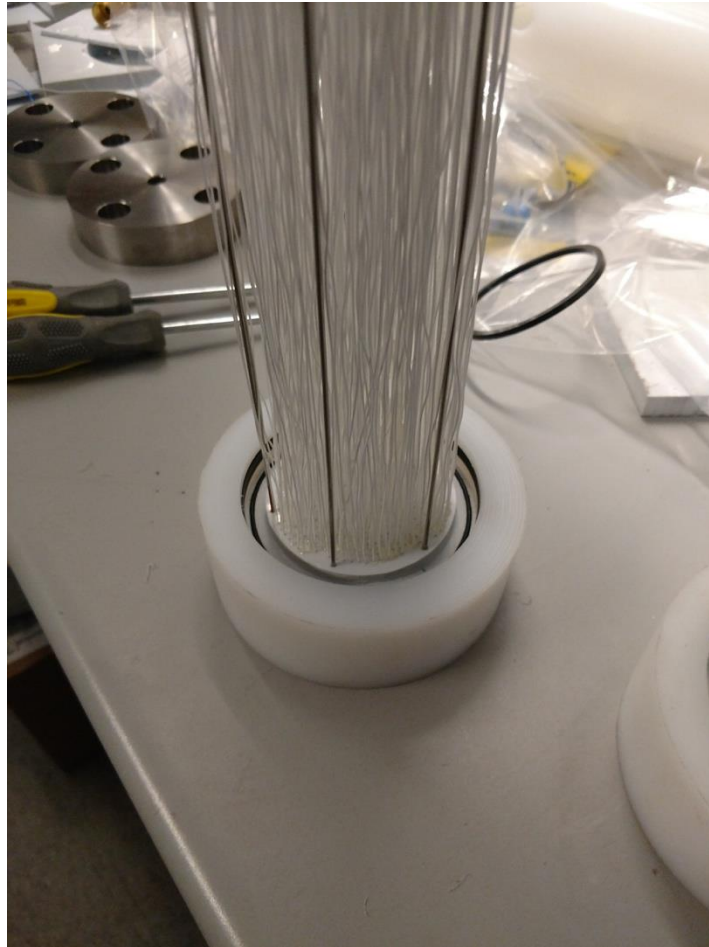


Figure 67. Fiber Assembly inserted into one end cap.

The fiber housing was then slid over the Fiber Assembly until the housing was flush against the axial O-ring on Fiber Guide 1. Due to manufacturing tolerance issues with the ordered fiber housing the radial O-ring on Fiber Guide 3 would not fit in the housing. The housing was received with an inner diameter 0.15 in. smaller than the nominal 3 in. inner diameter designed for. Therefore, both Fiber Guide 1 and Fiber Guide 3 had to be sanded down to fit within the housing. Instead of the radial O-ring on Fiber Guide 3 a JB Weld epoxy was used to fix and seal Fiber Guide 3 into the fiber housing. The epoxy was left to cure for a few hours.

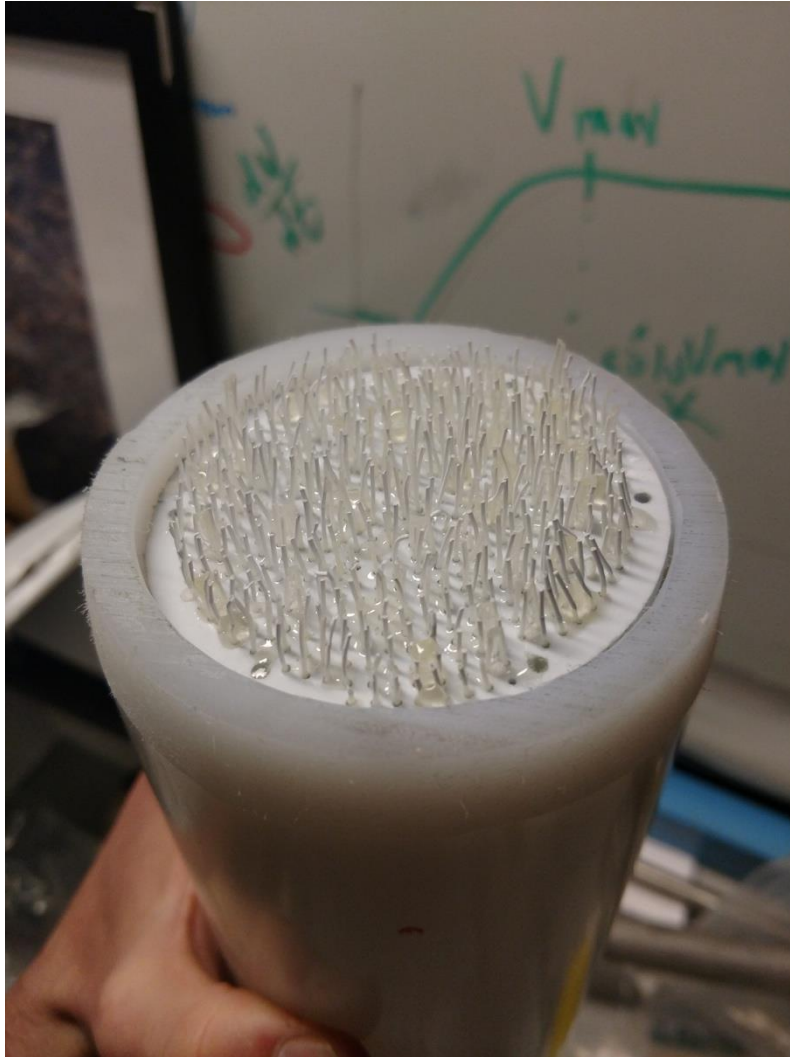


Figure 68. Fiber Guide 3 fitting snugly into the fiber housing.

Next, the Screw Lock Ring was attached to Fiber Guide 3 via the six #2-56 screws. The other spacer was then inserted into the other end cap (with the radial O-ring installed) and then slid over the Screw Lock Ring/fiber housing. From here, four 1/4 in. NPT to 1/4 in. compression and one 3/8 in. NPT to 3/8 in. compression fittings were wrapped in PTFE tape before being threaded into the ILS. These fittings were then installed using a crescent wrench.



Figure 69. ILS assembly without compression assembly.

The compression assembly was then placed around the contactor by placing each compression plate at either end with the 1/4 in. NPT fitting sticking through the 1 in. thru-holes in the center of each plate. Then the four 5/16 – 18 fully threaded rods were inserted through each plate at all four corners and then tightened on using the 5/16 – 18 nuts.



Figure 70. ILS contactor with compression assembly installed.

After installing the compression assembly around the contactor a preliminary leak test was conducted by flowing air through the ILS from AETHER while monitoring the upstream and downstream flow rates to determine if any air leaks were occurring. It was determined that the O-ring seals between the end caps and the fiber housing were not fully sealing so we disassembled the contactor to look at the end caps. It was found that O-ring grooves in the end caps were not

equal in depth. This was believed to happen due to a tooling set-up error by the manufacturing team when setting up the CNC Milling Machine for the operation. In order to be able to still remove the end caps if needed, silicone sealant was used around the interface between the end caps and fiber housing. This sealant was found to provide an air tight sealant.

The manifold was then added by installing a section of 1/4 in. FEP tubing between both of the 1/4 in. compression fittings on the manifold and both of the 1/4 in. compression fittings on the contactor. Lastly, a section of L/S 15 Masterflex tubing was installed between the 3/8 in. compression fitting on the contactor and the 3/8 in. compression fitting on the manifold. The system was then ready for testing.



Figure 71. ILS final assembly.

Lessons Learned

Machining Difficulties:

While machining the various parts for the ILS a few difficulties arose. The drill bit size required for the fiber holes in the three fiber guides was a #62, which is very small. Due to the small bit size the bit is very easy to bend and break while machining so we pre-drilled each fiber hole with a 1/16 in. drill bit to act as a pilot. Then each hole was then drilled through with the #62 bit using a pecking pattern. Pecking allowed for the drill bit to only be pressed into the material a little bit at a time, which would minimize the stress on the bit. Pre-drilling and pecking the holes caused for

the drilling process to take a lengthy amount of time versus just drilling straight through the material in one motion.

Another problem arose when drilling the small fiber holes. Polypropylene and polyethylene melt easily when machining. This became a problem because during the hole drilling process on the fiber guides the machining had to be stopped often to clear the bit of melted material. It was a concern with material building up on the #62 drill bit because the extra material could cause an excessive torque on the bit and possibly break the bit. The material melting was also a problem during drilling because some material would stay connected inside the hole after the drill bit was pulled out. This caused us to have to go back through and clear out some of the holes with a small needle prior to being able to thread the fibers through.

Both members of the manufacturing team did not have experience with using SolidCAM, a CNC g-code producing software using with the CNC Milling Machines, and this proved to be time consuming at first when learning how to use it. The problem was that the only computers with this software available were in the Aerospace Machine Shop so the time available to work on the SolidCAM code was limited to shop hours during the day. Due to the team's inexperience with SolidCAM a lot of time was spent waiting for shop employees to be available to teach and help with the programming. In addition, the manufacturing team had to often wait for senior projects teams to be done using the computers and CNC machines. Both of these battles caused for a lot of time spent idling and waiting.

The UHMWPE stock tubing used for the fiber housing came with horrific tolerances from McMaster Carr (± 0.320 in. for the inner diameter and outer diameter). The tube received had the nominal outer diameter of 3.5 in. but the inner diameter was around 0.1 in. smaller than the nominal 3 in. inner diameter. This bad tolerance created major complications for the manufacturing team because the fiber guides had already been made by time the tube was received. So Fiber Guide 1 and Fiber Guide 3 had to be sanded down in order to fit into the fiber housing. This did not allow for the radial O-ring seal on Fiber Guide 3 to be used and epoxy was used instead. In the future, the tube should have been ordered sooner so that the design or size of the fiber guides could have been altered if needed prior to manufacturing and thus retaining the functionality of the radial O-ring seal. Other suppliers could also be sought out that claim better tolerances.

Fiber Assembly Manufacturing:

Assembling the Fiber Assembly was an arduous task. Individually threading 484 fibers through three fiber guides was tedious and very time consuming, taking 24 hours to complete. The task of adding fishing weights to each of the fibers was also very time consuming, taking 6 hours to complete. There is no easy way to accelerate the potting process except for using less fibers and larger fibers for easier handling. An alternate contactor design would have the ionic liquid flowing through larger diameter fibers and air flowing around them. This would decrease the number of fibers required and increase their size in diameter. The contactor may be larger in size but the complexity would decrease immensely with less fibers and larger fibers. The potting process would be much easier and take much less time.

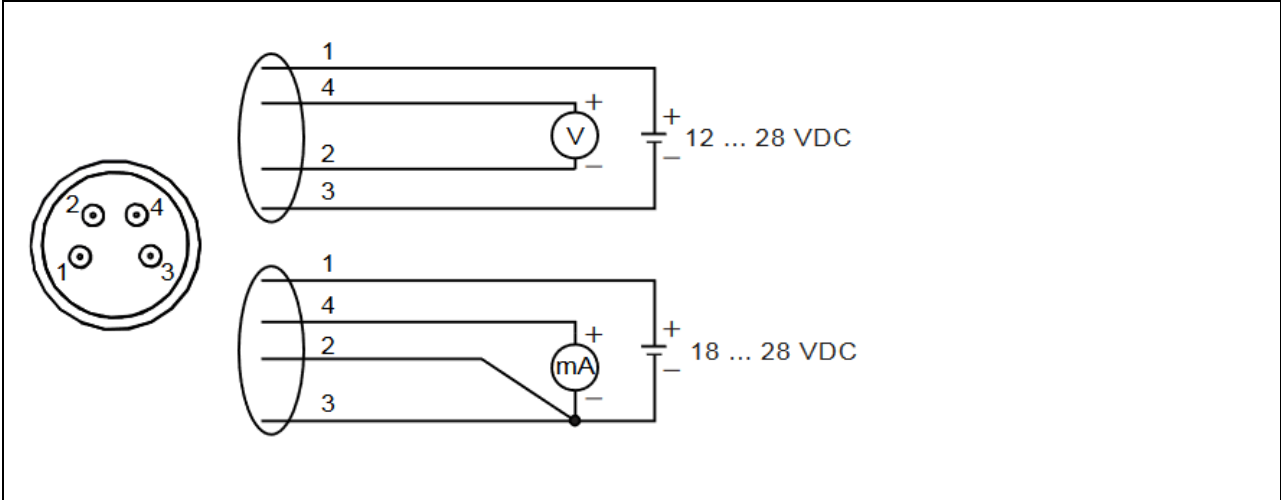
Appendix D: Sensor Specifications

Dew Point Sensor:

General Performance

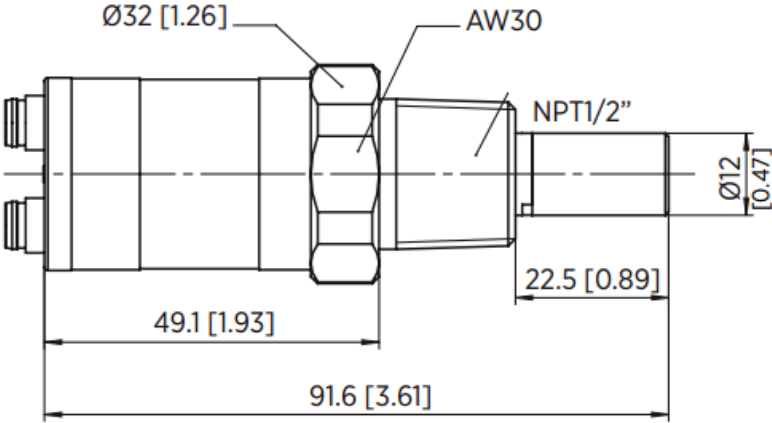
HYDRA Project Spring 2018 Final Report

Measurement Range	-70 to 60 °C		
Accuracy in air or N2	±2 °C (see plot below)		
Analog Output	-80 to 20 °C		
Response time to 63% [90%] at 20 °C	-60 to -20 °C:	5 s	[15 s]
	-20 to -60 °C:	45 s	[10 min]
Operating Temperature	-40 to 60 °C		
Sample Flow Rate	Any flow rate with no effect on accuracy		
Electrical / Mechanical Inputs			
Analog output (scalable)	0-5V, other voltage outputs and current output possible		
Voltage Resolution	0.3 mV		
Input Power Supply	12 V (Voltage Output), 18 V (Current Output)		
Connector Pinouts and Wiring:			
Pin	Analog connector	Digital connector	Wire color
1	VDC supply+	VDC supply+	Brown
2	Ch-	RS-485 D0-	White
3	GND	GND	Blue
4	Ch+	RS-485 D1+	Black



Mechanical Specifications:

Housing Material: Stainless Steel
 Mechanical Connection: NPT 1/2
 Weight: 3.5 oz



Dimensions in mm (inches)

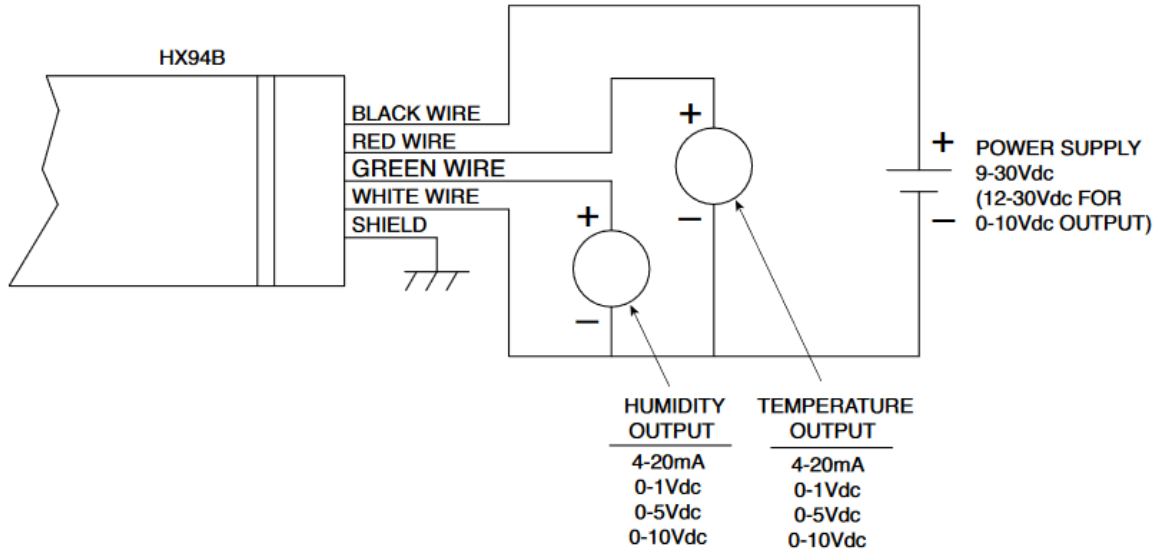
Relative Humidity Sensor:

General Performance	
Measurement Range	0 to 100 °C 0 to 100% RH
Accuracy	±0.6 from 0 to 50 °C ±1.25 from 50 to 100 °C ±2.5 from 20 to 80% RH ±3.5 from 5 to 20% to 80% to 95% RH ±4 from 0 to 5% and 95 to 100% RH
Response Time	Temperature: 5-30 s

HYDRA Project Spring 2018 Final Report

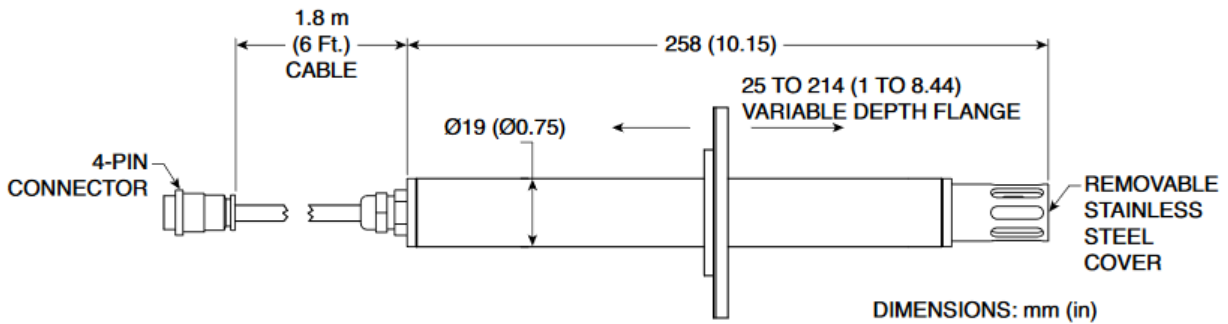
	Relative Humidity: 8s
Operating Temperature	0 to 100 °C
Electrical / Mechanical Inputs	
Analog output	0-5V, other voltage outputs and current output possible
Power Source	12 V

Connector Pinouts and Wiring:



Mechanical Specifications

Enclosure Housing: 316 Stainless Steel
Weight: 200 g (7 oz)



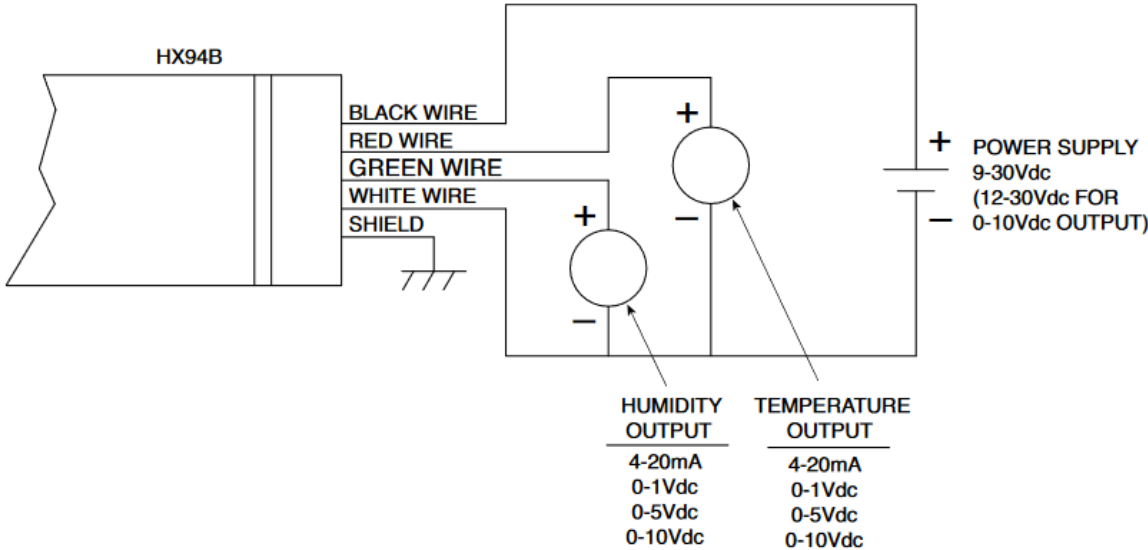
*Note that the sensor is designed to be able to be mounted into a duct so a mounting flange and setup (not pictured) is included with the sensor. The mounting system was not used in favor of a compression fitting due to the sensor having an outer diameter of 3/4 inch.

General Performance	
Measurement Range	0 to 100 °C

HYDRA Project Spring 2018 Final Report

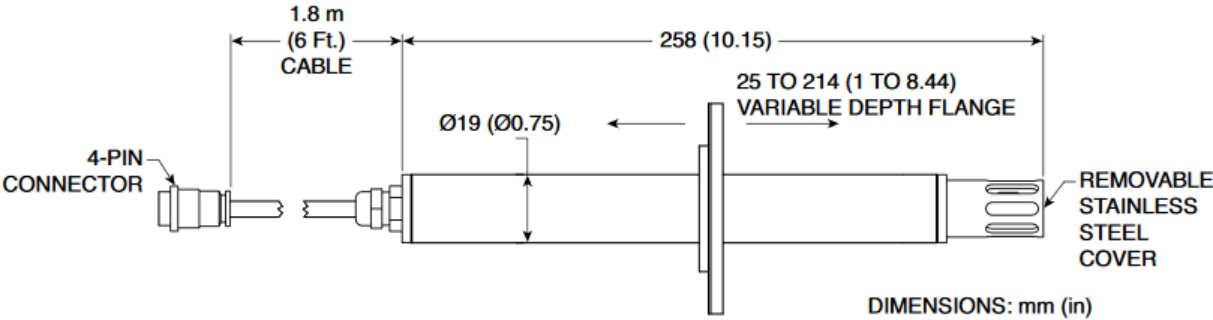
	0 to 100% RH
Accuracy	± 0.6 from 0 to 50 °C ± 1.25 from 50 to 100 °C ± 2.5 from 20 to 80% RH ± 3.5 from 5 to 20% to 80% to 95% RH ± 4 from 0 to 5% and 95 to 100% RH
Response Time	Temperature: 5-30 s Relative Humidity: 8s
Operating Temperature	0 to 100 °C
Electrical / Mechanical Inputs	
Analog output	0-5V, other voltage outputs and current output possible
Power Source	12 V

Connector Pinouts and Wiring:



Mechanical Specifications

Enclosure Housing: 316 Stainless Steel
 Weight: 200 g (7 oz)

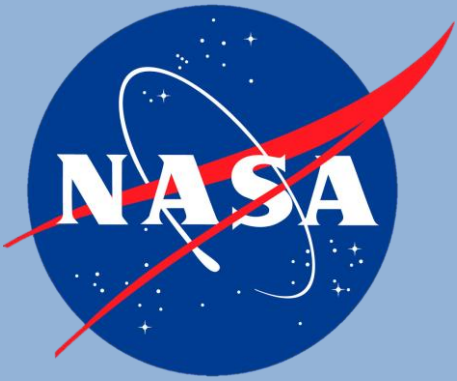


HYDRA Project Spring 2018 Final Report

*Note that the sensor is designed to be able to be mounted into a duct so a mounting flange and setup (not pictured) is included with the sensor. The mounting system was not used in favor of a compression fitting due to the sensor having an outer diameter of 3/4 inch.

Thermistors:

General Performance	
Max Stability Measurement Range	-80 to 120 °C
Accuracy	±0.2 °C
Max Operating Temperature	150 °C



NASA X-Hab Challenge: Final Presentation University of Colorado - Boulder



HYbrid Dehumidification and Reclamation Apparatus (HYDRA)

Project team members:

Mitchell Woolever	(Project Manager)
Jonathan Eble	(Systems Engineer)
Thomas Pearson	(Modeling Lead)
Lee Huynh	(Mechanical Design Lead)
Grant Vincent	(Manufacturing Co-Lead)
Mario Maggio	(Manufacturing Co-Lead)
Zachary Fester	(Testing Lead)



Project Advisers

University of Colorado:

Graduate Project Advisers

Prof. Jim Nabity, PhD

Rick Hieb

Katya Arquilla

Daniel Phillips

PhD Students

Emily Matula

Jordan Holquist

Mike Lotto

Christine Escobar

CU Shop and Lab Staff

Bobby Hodgkinson

Trudy Schwartz

Matt Rhode

Reaction Systems, LLC:

Dr. Dave Wickham

NASA:

Grace Belancik

Dr. Jeff Sweterlitsch

Dr. Jim Knox

Tracy Gill

Thank you!

Presentation Outline

1. Project Background
2. Design / Manufacturing Recap
3. Test Facility Readiness
4. Test Article Integration
5. System Test / Model Validation
6. Budget and Schedule
7. Project Takeaways
8. Questions



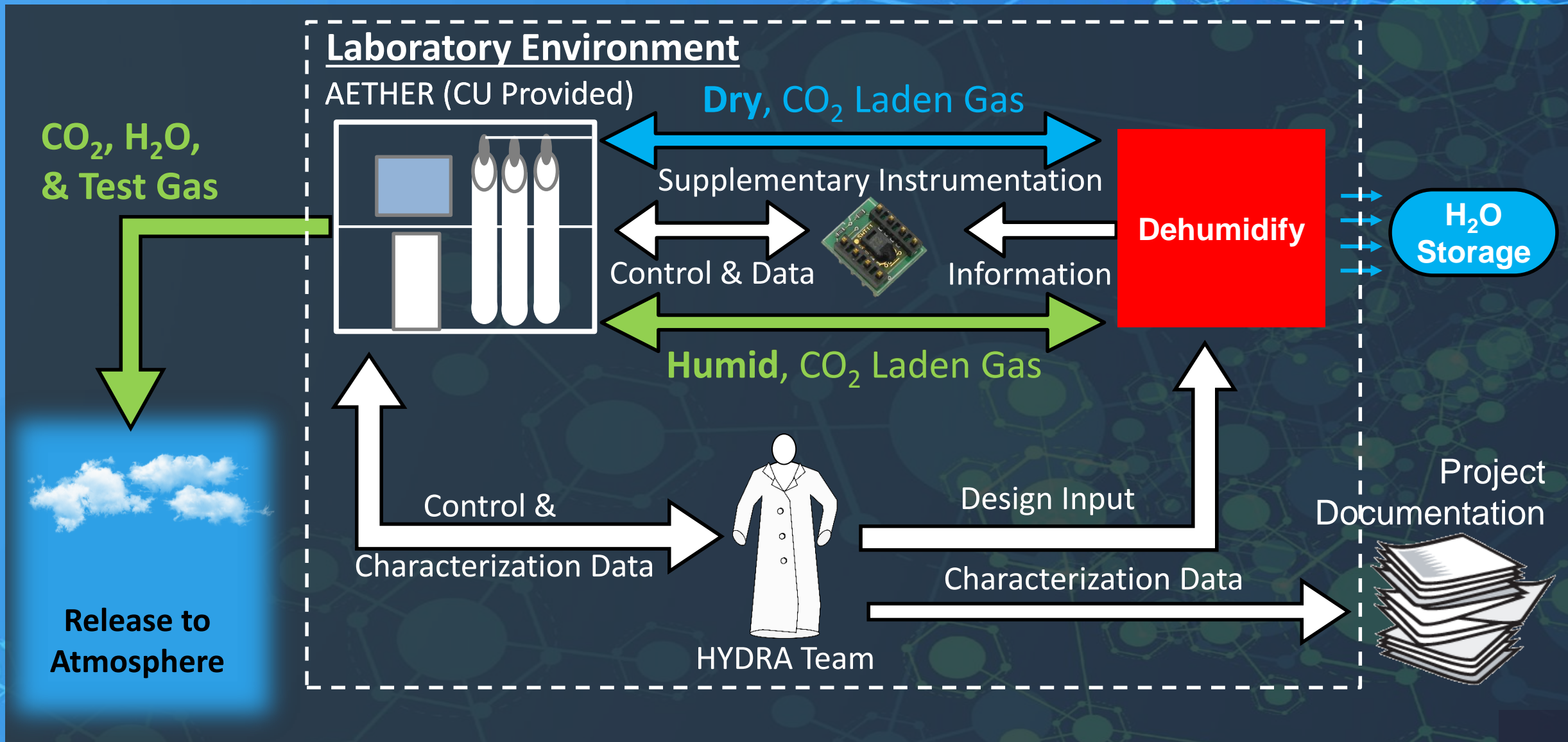
Project Background

Project Need

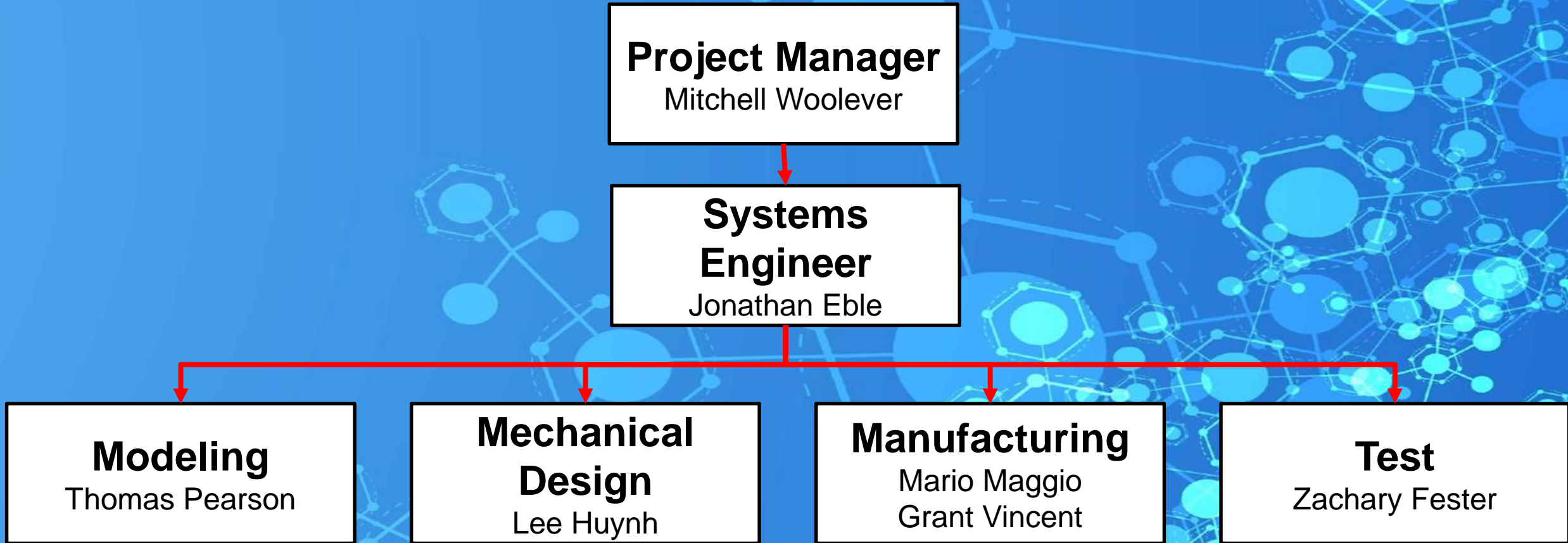
NASA seeks new methods for cabin air CO₂ removal that build on the success of legacy systems

- Carbon Dioxide Removal Assembly (CDRA)
 - Current state of the art installed on ISS
- Direct CO₂ removal using ionic liquids
 - CARIL: 2016-17 CU X-Hab team
 - Reaction Systems, LLC
- Cryogenic CO₂ removal tested at NASA Ames Research Center
 - Cryocooler lowers air temperature below freezing point of CO₂
 - **Air must first be dehumidified to prevent ice buildup**
 - ISS Condensing Heat Exchanger insufficient, only reaches ~2°C dew point

Project-Level ConOps



HYDRA Organization Chart



Project Objectives and Success Criteria

- Project Objectives:

- PO1: **Design, build and test** a dehumidification system for air revitalization
- PO2: **Characterize** H₂O transport
- PO3: Report any **change in flow composition** including CO₂ and contaminants
- PO4: **Justify chosen flow rate** to be scalable to 30 scfm
- PO5: **Estimate the power** required to operate the system

- Levels of Success:

- Level 1: $\leq 0^{\circ}\text{C}$ Dew point (90+% of H₂O removed from the gas stream)
- Level 2: $\leq -43^{\circ}\text{C}$ Dew point (99+% of H₂O removed from the gas stream)
- Level 3: $\leq -90^{\circ}\text{C}$ Dew point (Virtually all of H₂O removed from the gas stream)



Design / Manufacturing Recap

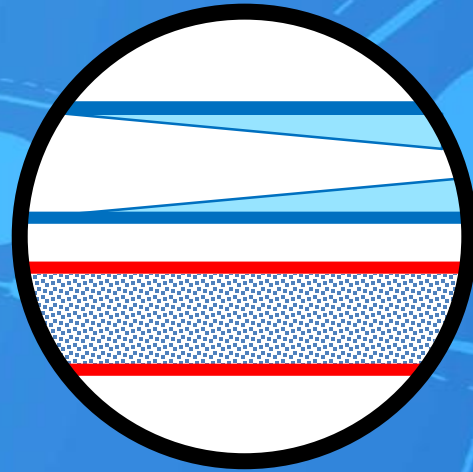
Design Introduction

Methods:

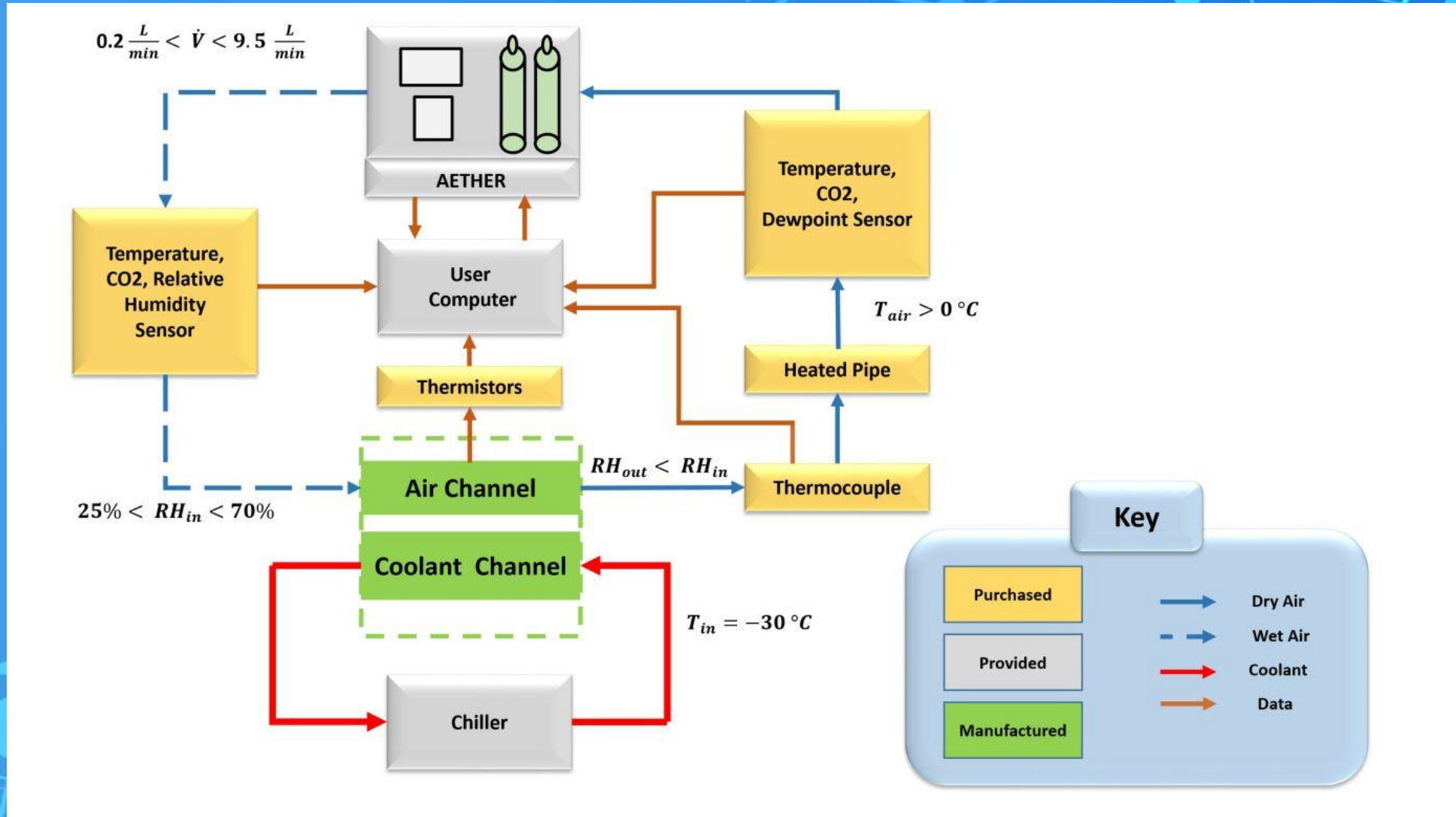
Water Cryocooler System (WCS)

Ionic Liquid System (ILS)

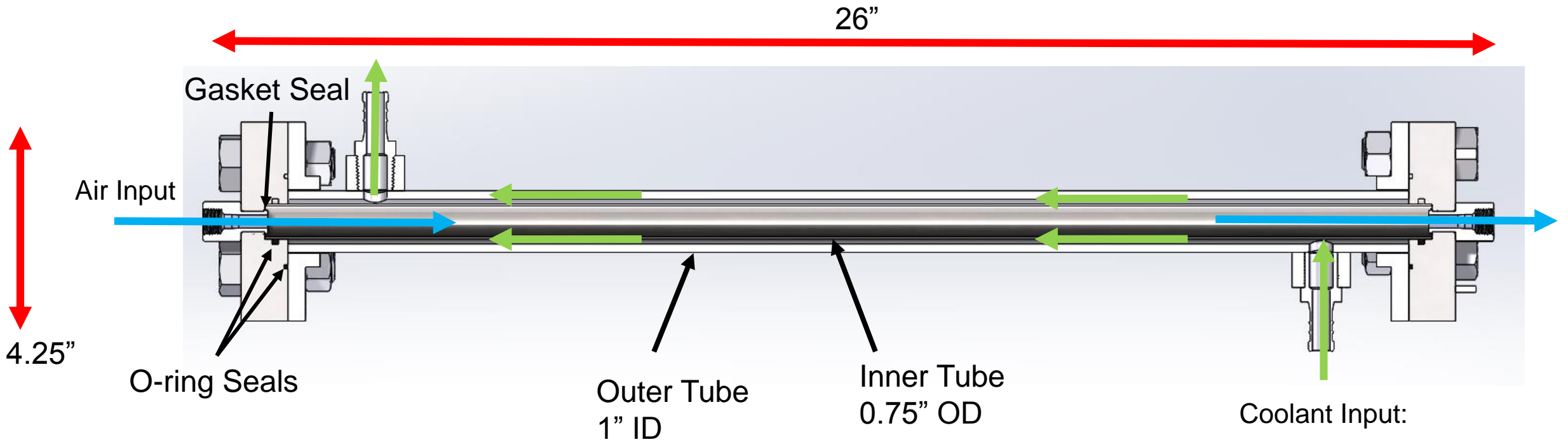
Water Cryocooler System (WCS) Mechanical Design



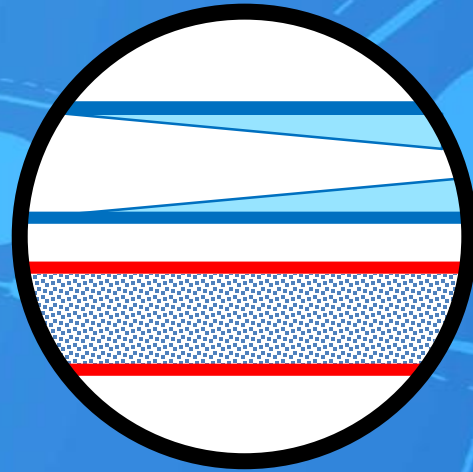
WCS Block Diagram



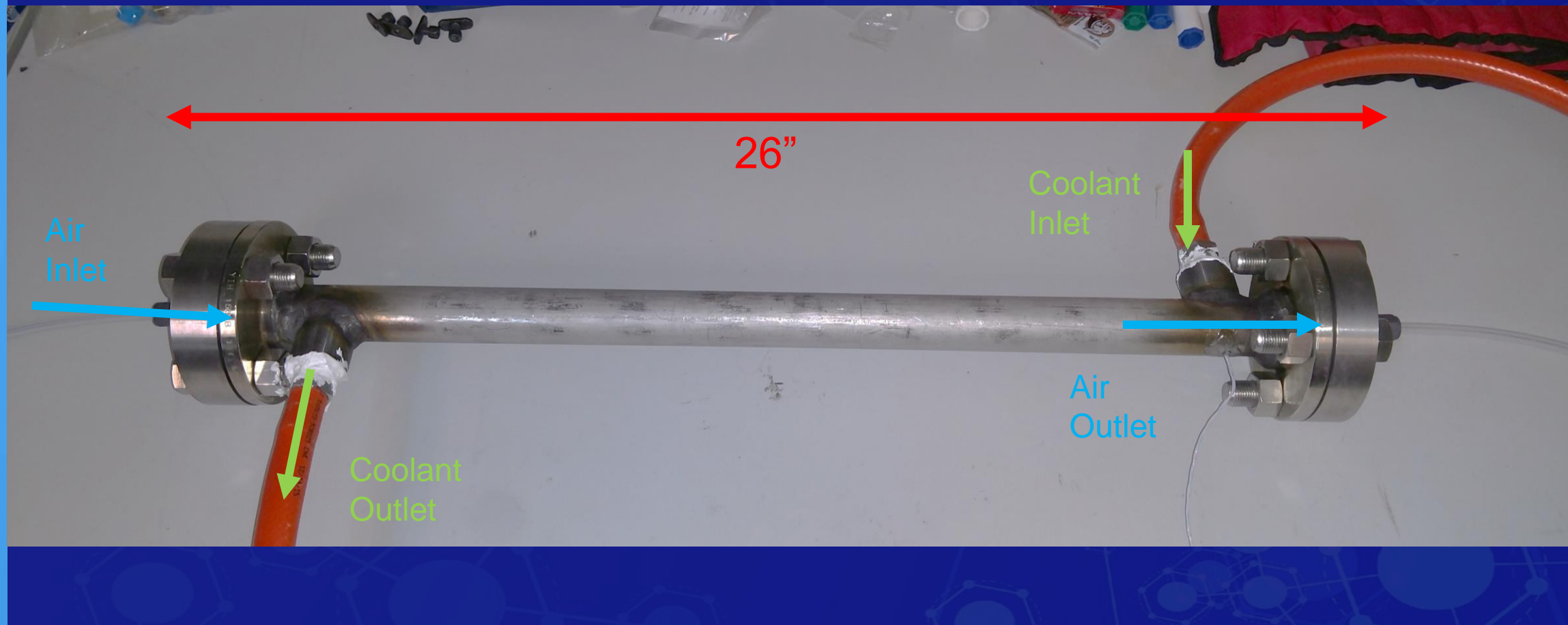
WCS Design



Water Cryocooler System (WCS) Manufacturing



Integrated WCS

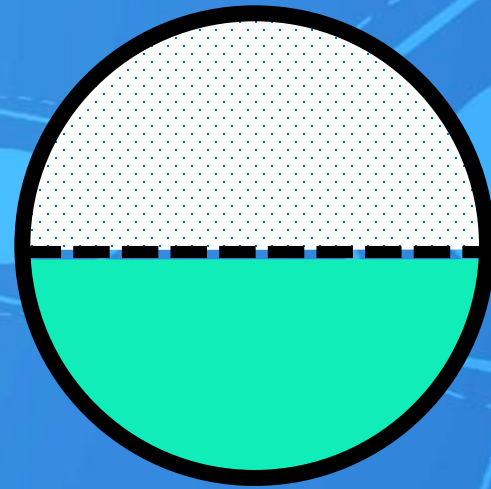


Design Complications

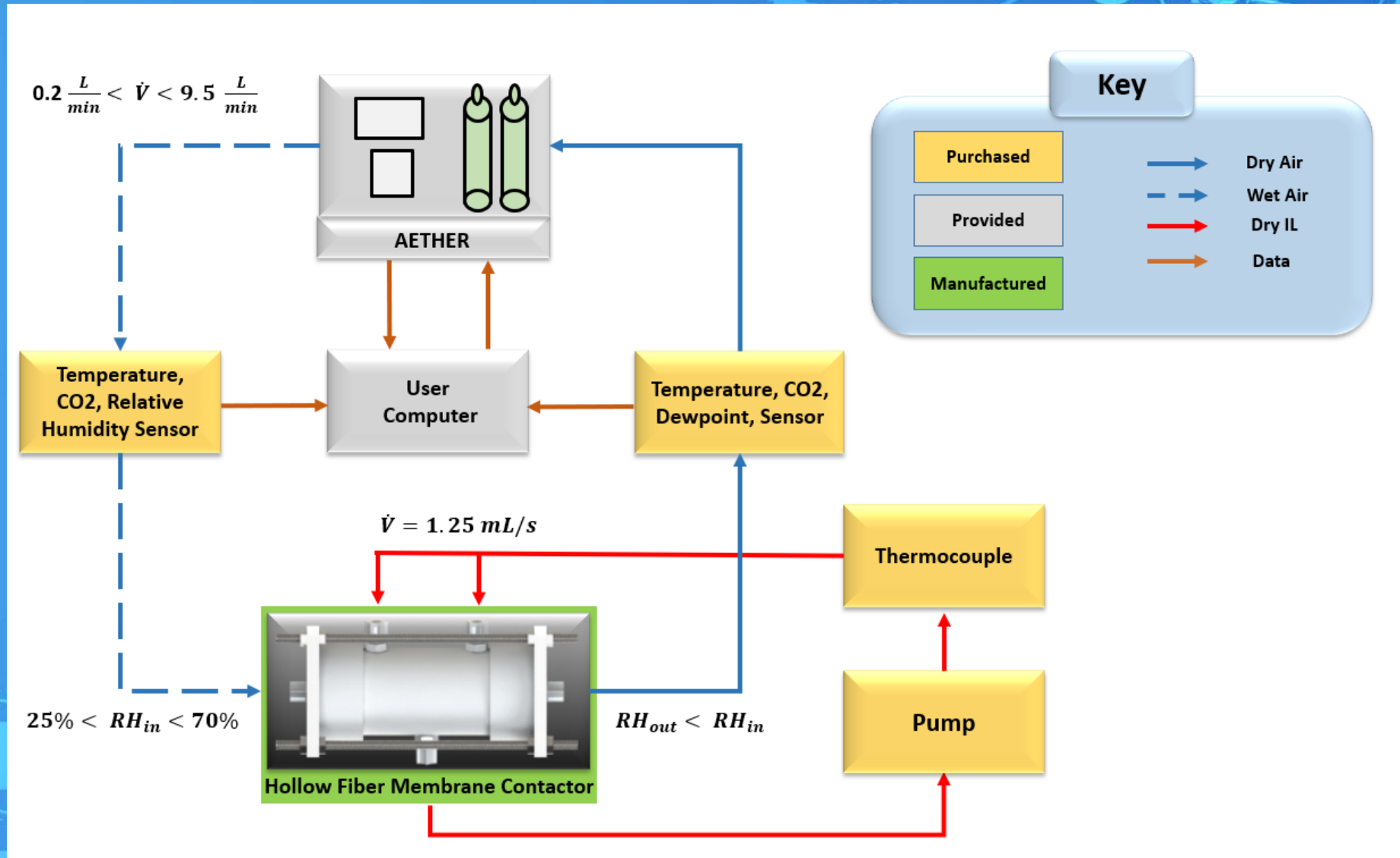
- Minor leaks of propylene glycol/water cooling mixture from ½" NPT fitting
 - Never fully mitigated
 - Did not affect overall testing
 - No intermixing of cooling mixture and airflow
 - Believed to occur due to varying thermal expansions/contractions
- Ambient Heating
 - Mitigated by adding insulation



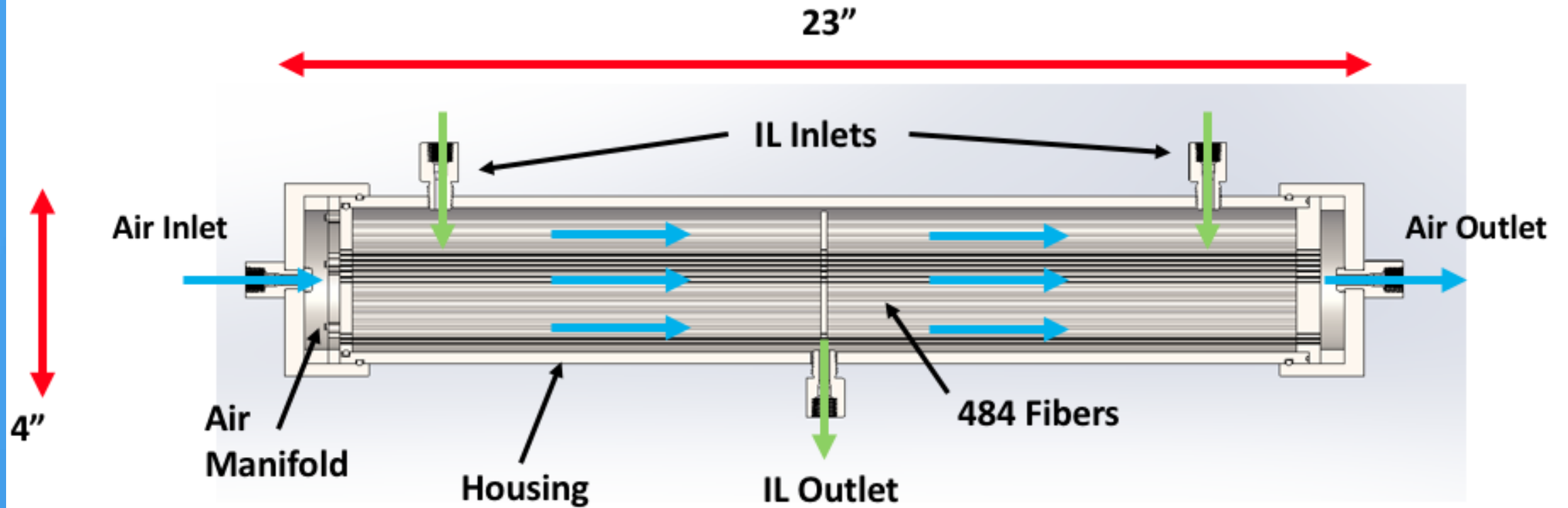
Ionic Liquid System (ILS) Mechanical Design



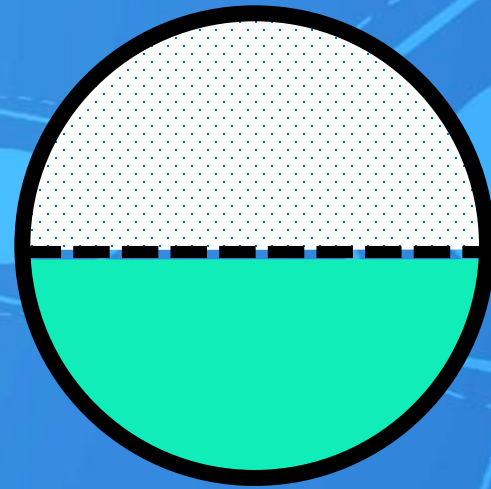
ILS Block Diagram



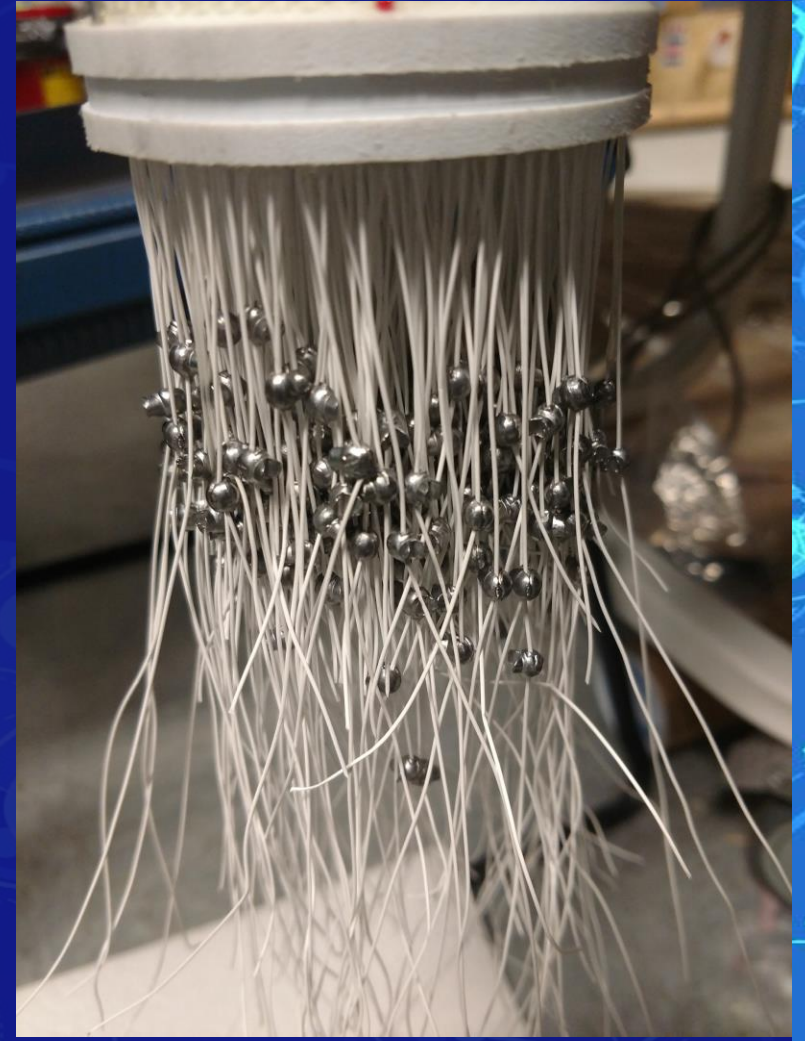
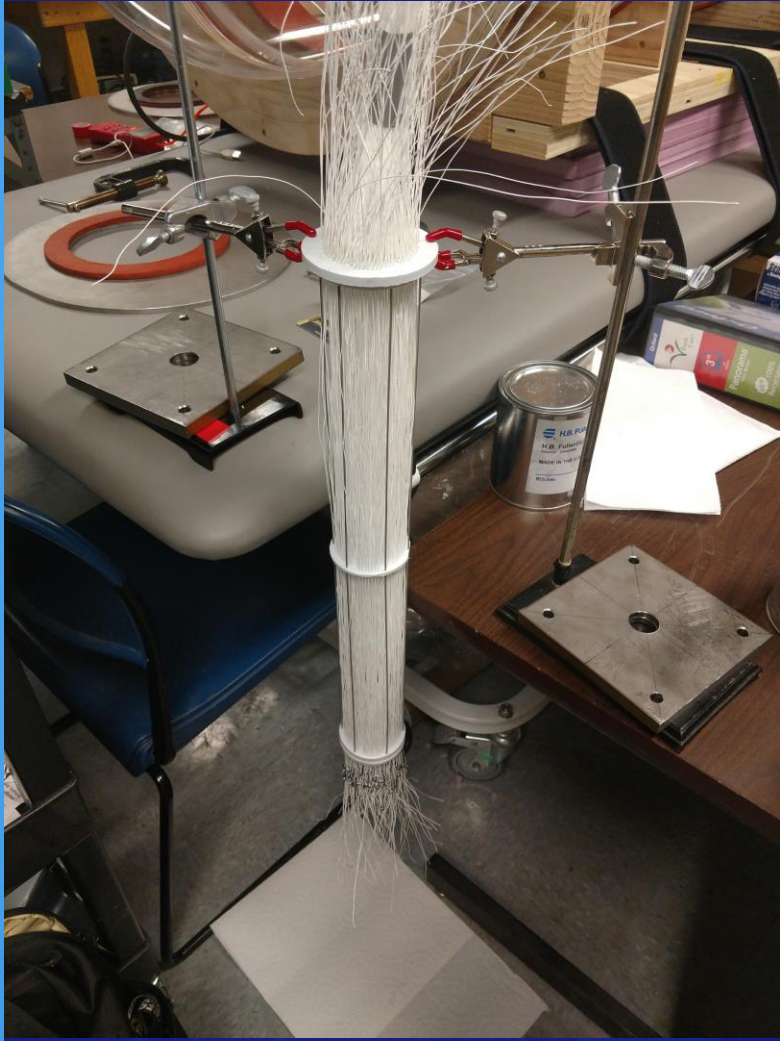
ILS Design



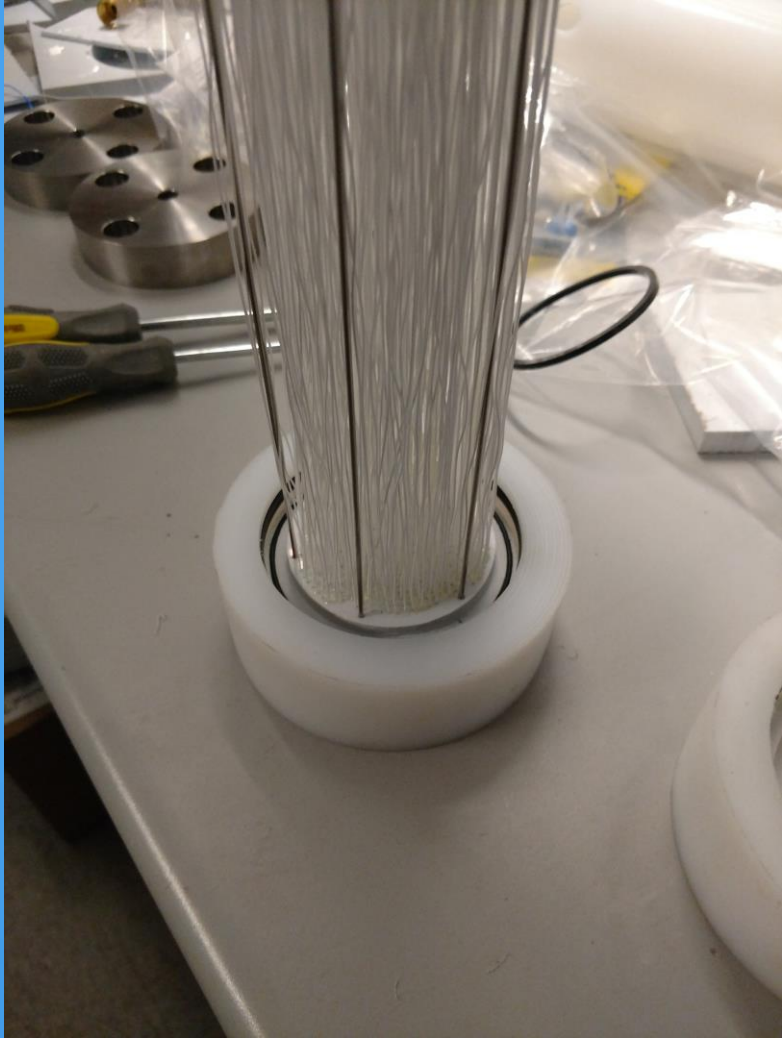
Ionic Liquid System (ILS) Manufacturing



Fiber Potting

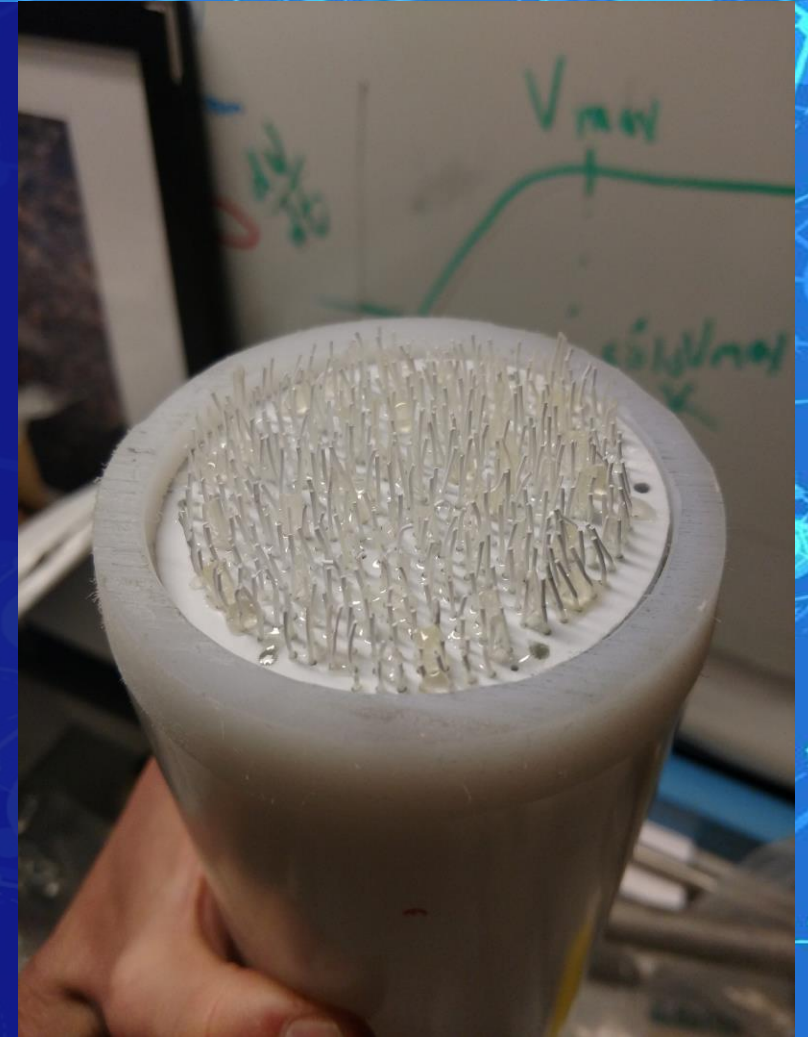


Final Assembly



Design Complications

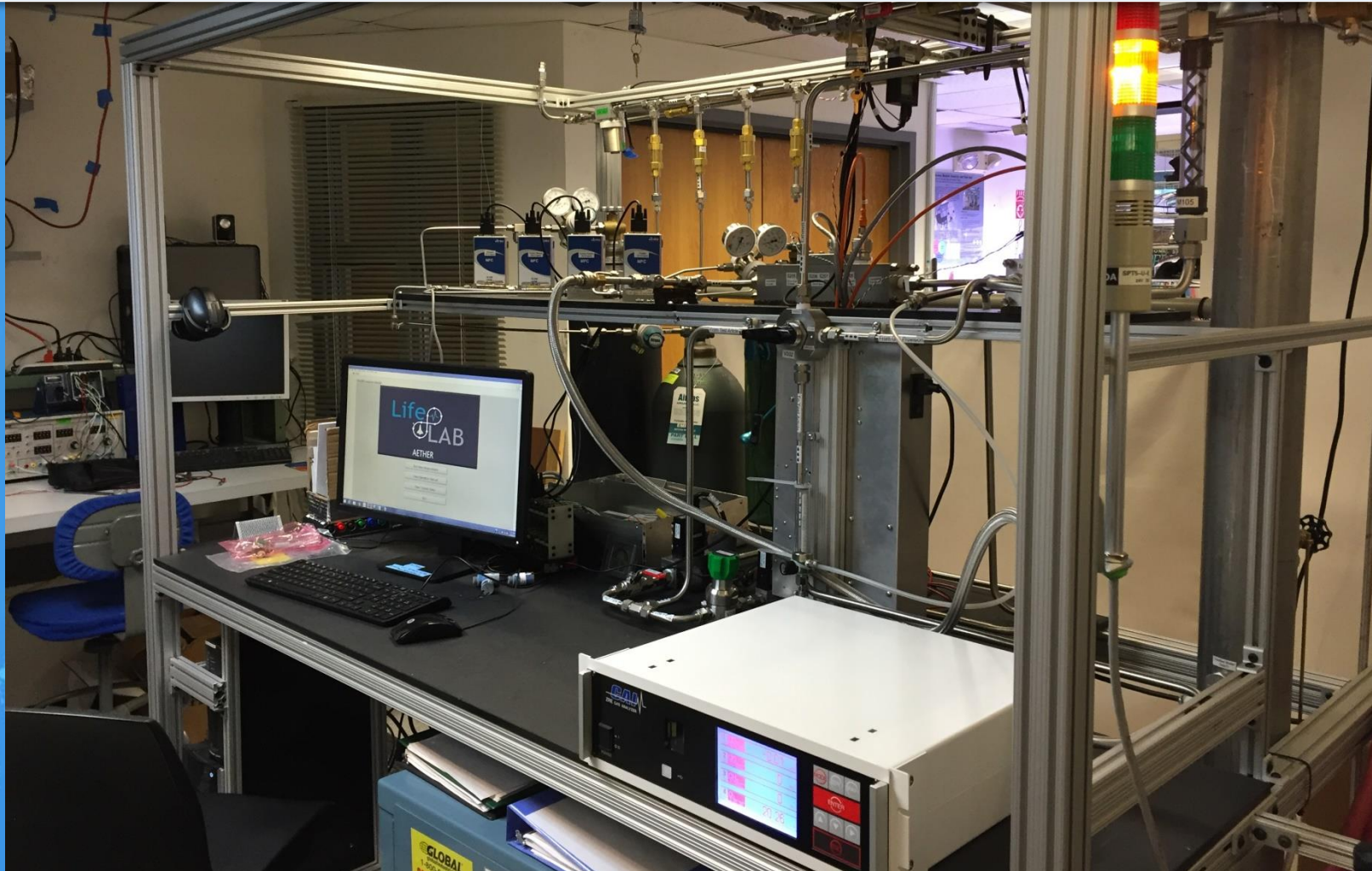
- Endcap to Fiberguide housing o-ring seal
 - O-ring for endcaps did not fit properly (nor seal properly)
 - Endcap to Fiberguide housing sealed with silicone sealant (sealed well and still allowed for easy removal of endcaps if needed)
- Fiberguide #3 to Fiberguide housing o-ring seal
 - Manufacturing tolerance on housing pipe was out of spec
 - Selected O-ring would not fit
 - Fiberguide #3 O-ring replaced with epoxy (sealed well but did not allow for disassembly if needed)



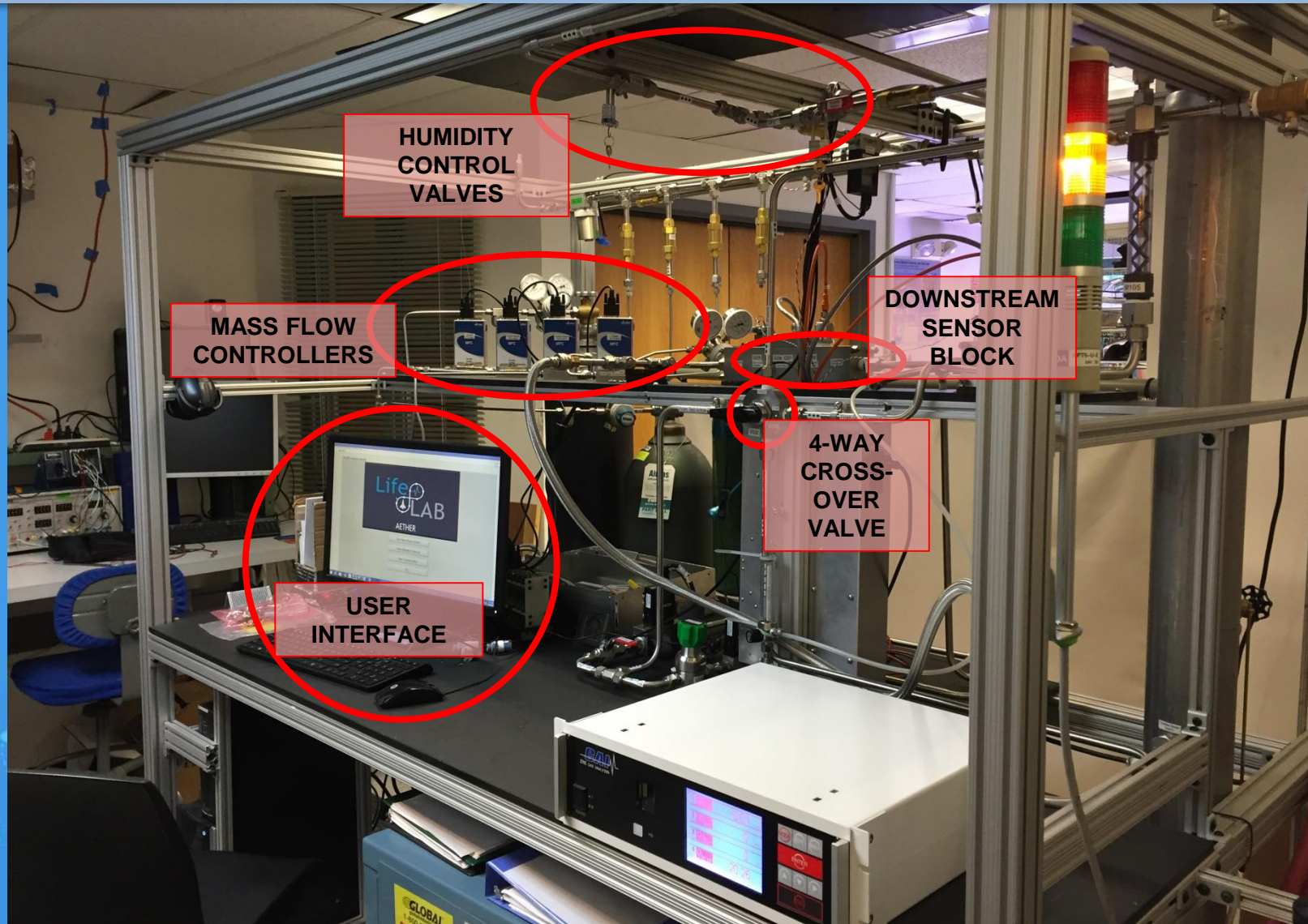
Test Facility Readiness

AETHER

Atmospheric and Environmental Test Hub for Experimentation on Revitalization



AETHER Components



AETHER Capabilities

Mode	Low Flow	Mid Flow	High Flow	Accuracy
Flow	0.2-9.5 SLPM	10-100 SLPM	100-400 SLPM	+/- 0.5, 3, 15 SLPM
Nitrogen	29-80%	76-80%	77-79%	+/- 5% rel.
Oxygen	17-23%	17-23%	20-22%	+/- 5% rel.
Carbon Dioxide	0-100%	0.03-1.3%	0.03-1.3%	+/- 5% rel.
Humidity	30-70%			+/- 3% abs.
Temperature	Ambient (18-27°C)			N/A
Pressure in Test Article	14.7 psia			+/- 0.25%
Maximum Test Duration	1 day			N/A
Control Program	LabVIEW			N/A
User Ports (Break Out Box)	58 single-ended, 19 differential analog inputs 16 bi-directional digital ports (input or output)			
Resolution	16 bits			
Sampling Rate	0.8 Hz if using AETHER VI			

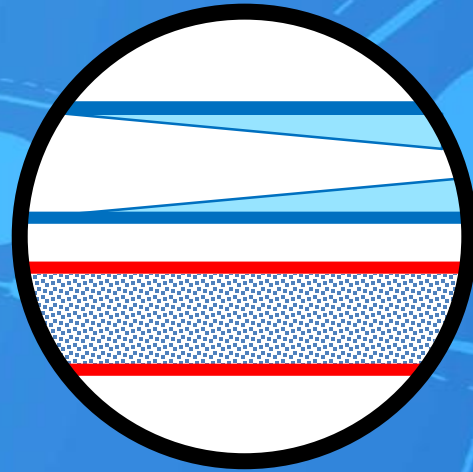


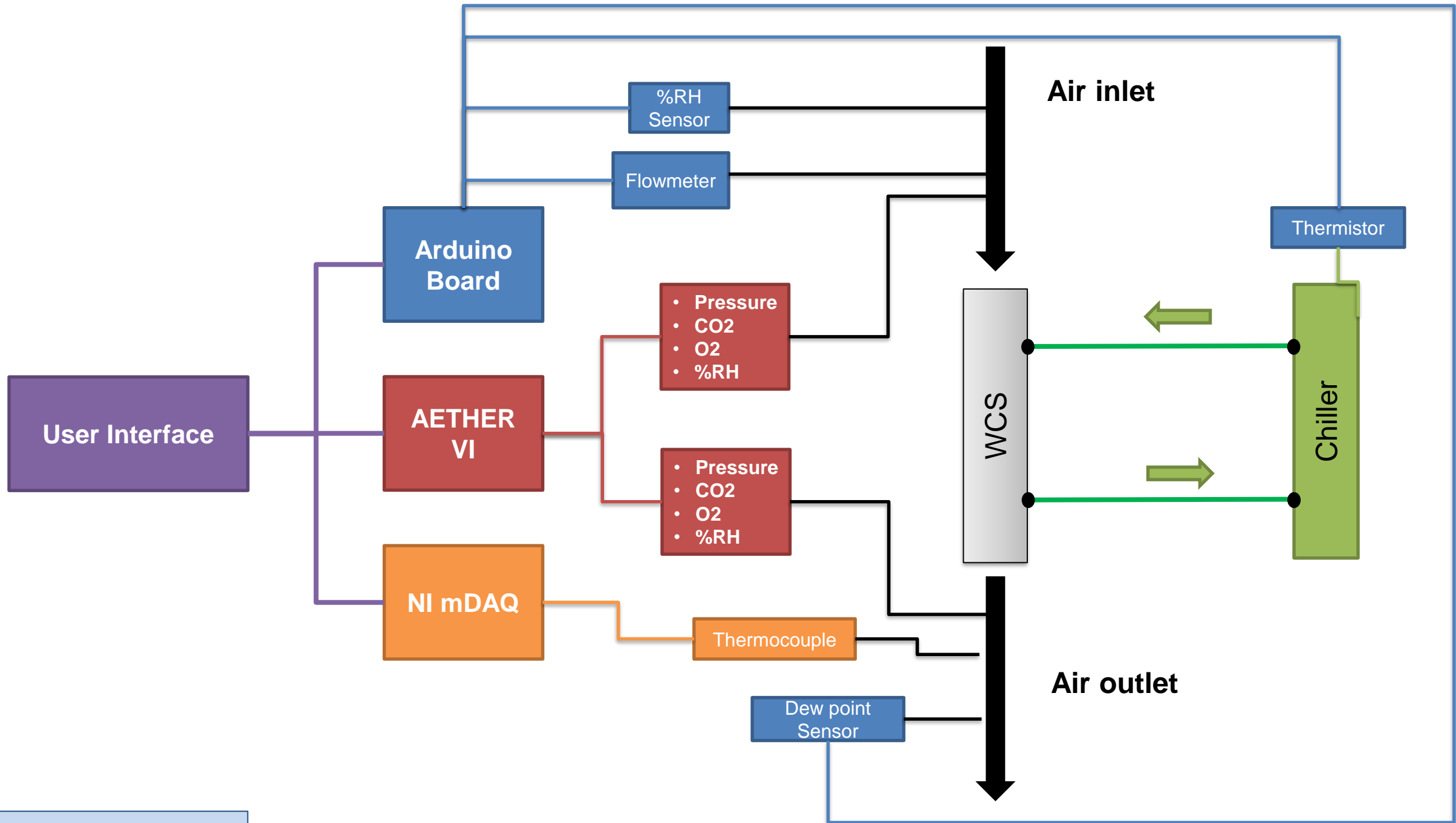
Test Article Integration

Model Validation

		Used In		Verification							
		ILS Model	WCS Model	EDC Experiment	Pump Characterization	AETHER Inputs	AETHER Sensors	%RH Sensor	Dew Point Transmitter	Thermocouple	Thermistors
Gas	Upstream Temperature	X	X				X	X			
	Upstream Pressure	X	X				X				
	Upstream Humidity	X	X			X	X	X			
	Gas Flow Rate	X	X			X	X				
IL	IL temperature	X								X	
Constants	Wall Temperature		X								X
	IL Flow Rate	X			X						
	Distribution Coefficient	X		X							
Output	Dew Point	X	X						X		
	Downstream Temperature		X				X			X	

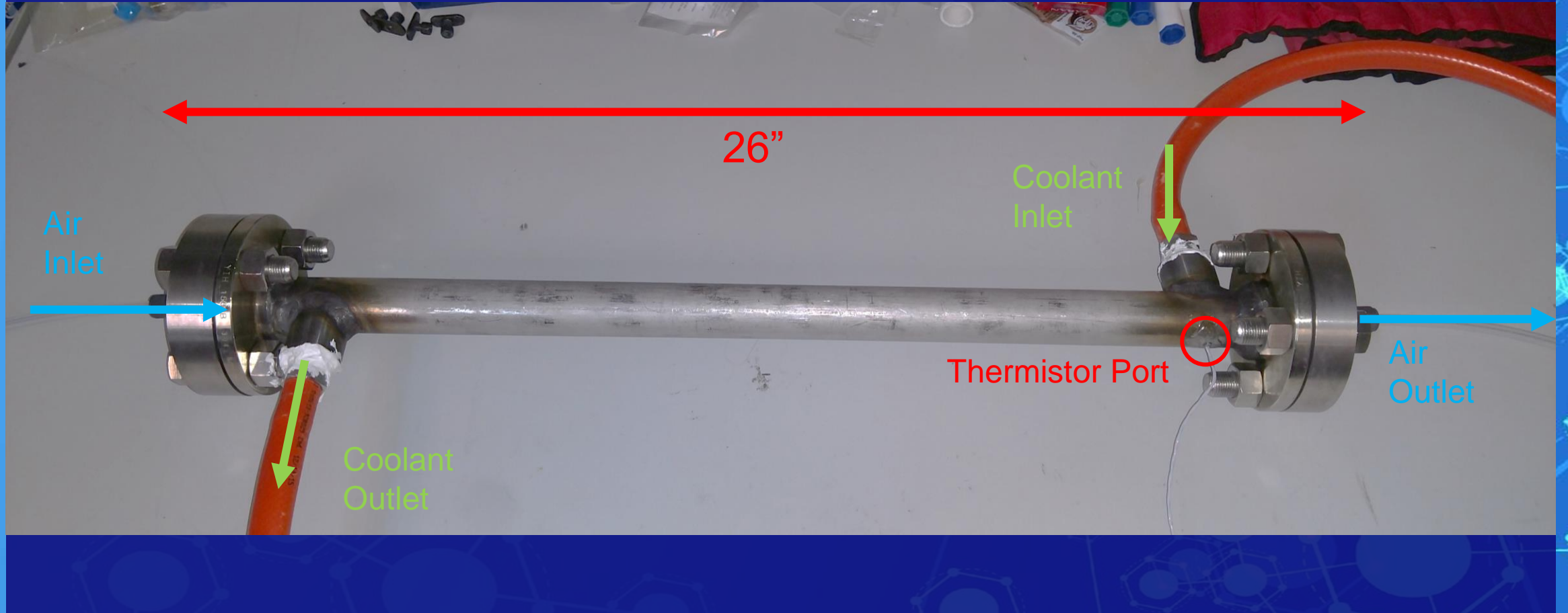
WCS Integration





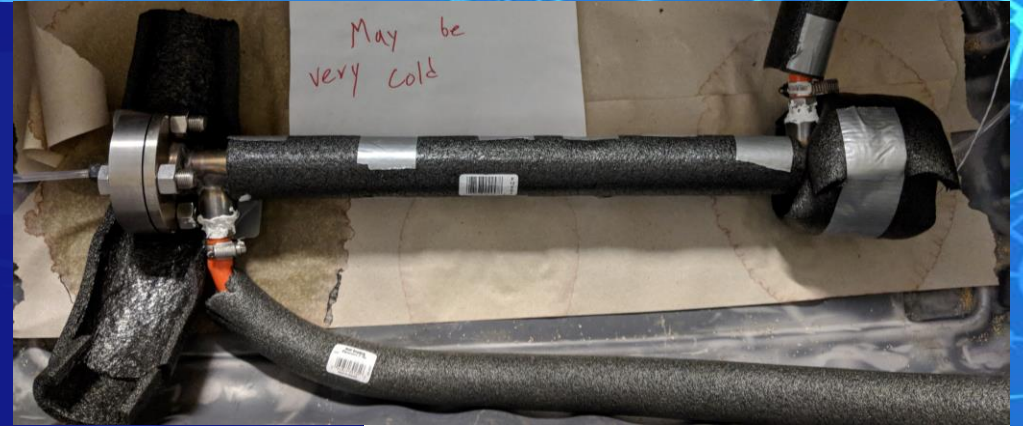
WCS DAQ DIAGRAM

Integrated WCS



WCS Article Test Preparation

- Chiller verification
 - Temperature output vs. thermistor
 - Coolant capability: -24°C
- Insulation
 - Coolant lines
 - Flanges and pipe walls
- Heat tape
 - Moved from downstream to upstream
 - Attempt to reduce inlet freezing rate



WCS Issues

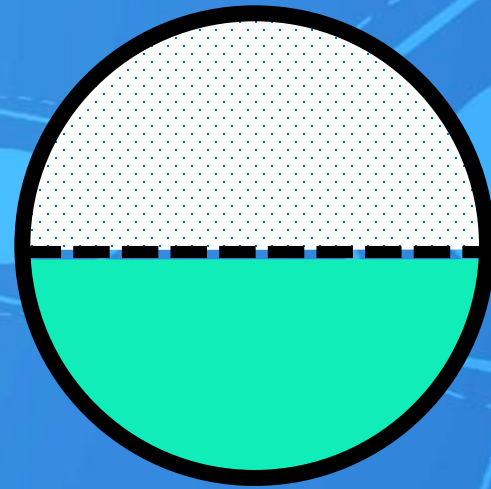
- Coolant leak
 - Issue: Coolant leaked out of WCS at the coolant hose fittings
 - Consequence: Chiller had to be refilled occasionally
- Wall temperature measurement
 - Issue: One thermistor malfunctioned, the other gave erroneous temperature readings
 - Consequence: No direct measurement of inner tube wall temperature was available.
- Downstream temperature measurement
 - Issue: Outlet air warmed to ambient temperatures between end of test article and downstream thermocouple
 - Consequence: No measurement outlet air temperature was available
- Significant leaks from airstream
 - Issue: Initial test setup had up to 20% of gas leaking
 - Consequence: Delayed testing schedule by about a week

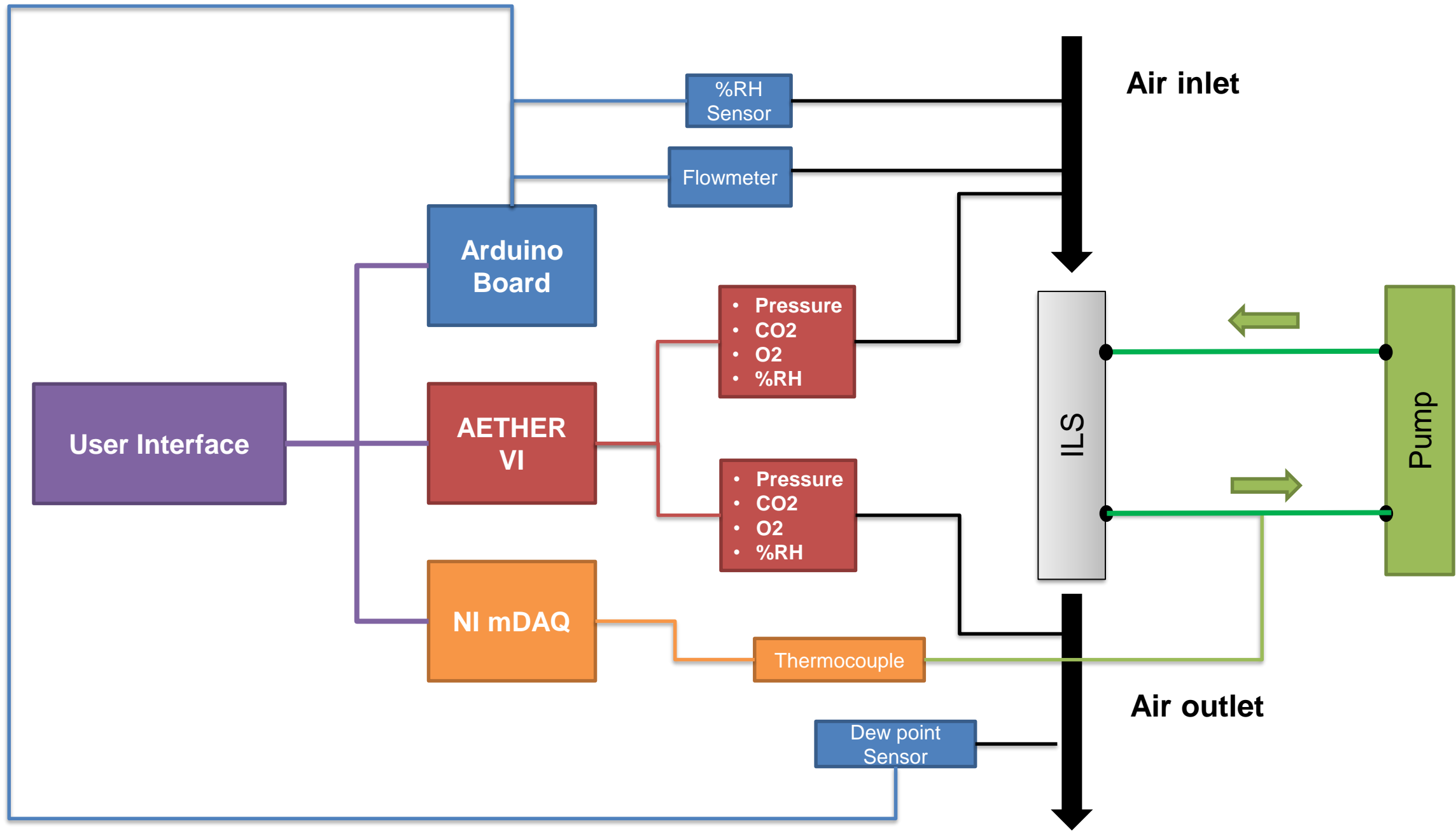
WCS Issues

- Inlet freezing
 - Issue: Air inlet froze shut well before main tube at low flowrates
 - Consequence: Needed to periodically stop testing to clear ice from inlet
 - Mitigation: Switched to a plastic fitting and heated the inlet with heat tape



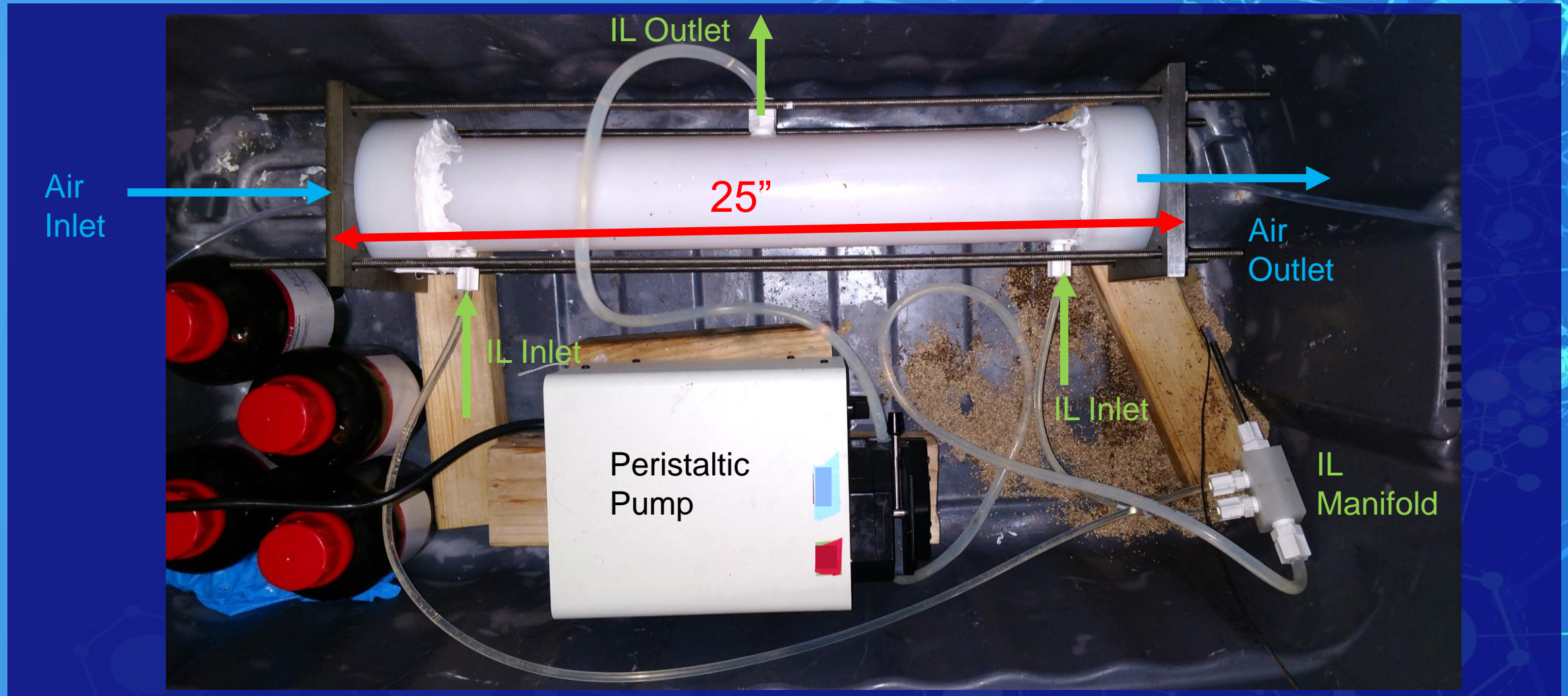
ILS Integration





ILS DAQ DIAGRAM

Integrated ILS





System Test / Model Validation

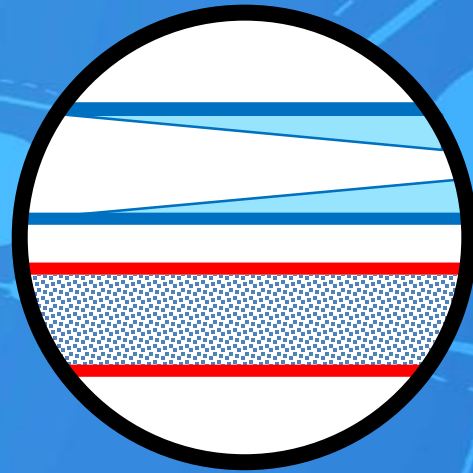
Model Validation

		Used In		Verification							
		ILS Model	WCS Model	EDC Experiment	Pump Characterization	AETHER Inputs	AETHER Sensors	%RH Sensor	Dew Point Transmitter	Thermocouple	Thermistors
Gas	Upstream Temperature	X	X				X	X			
	Upstream Pressure	X	X				X				
	Upstream Humidity	X	X			X	X	X			
	Gas Flow Rate	X	X			X	X				
IL	IL temperature	X								X	
Constants	Wall Temperature		X								X
	IL Flow Rate	X			X						
	Distribution Coefficient	X		X							
Output	Dew Point	X	X						X		
	Downstream Temperature		X				X			X	

Key

- = Worked as Expected
- = Partial functionality/Only available for some tests
- = Data not usable

Water Cryocooler System (WCS) Model

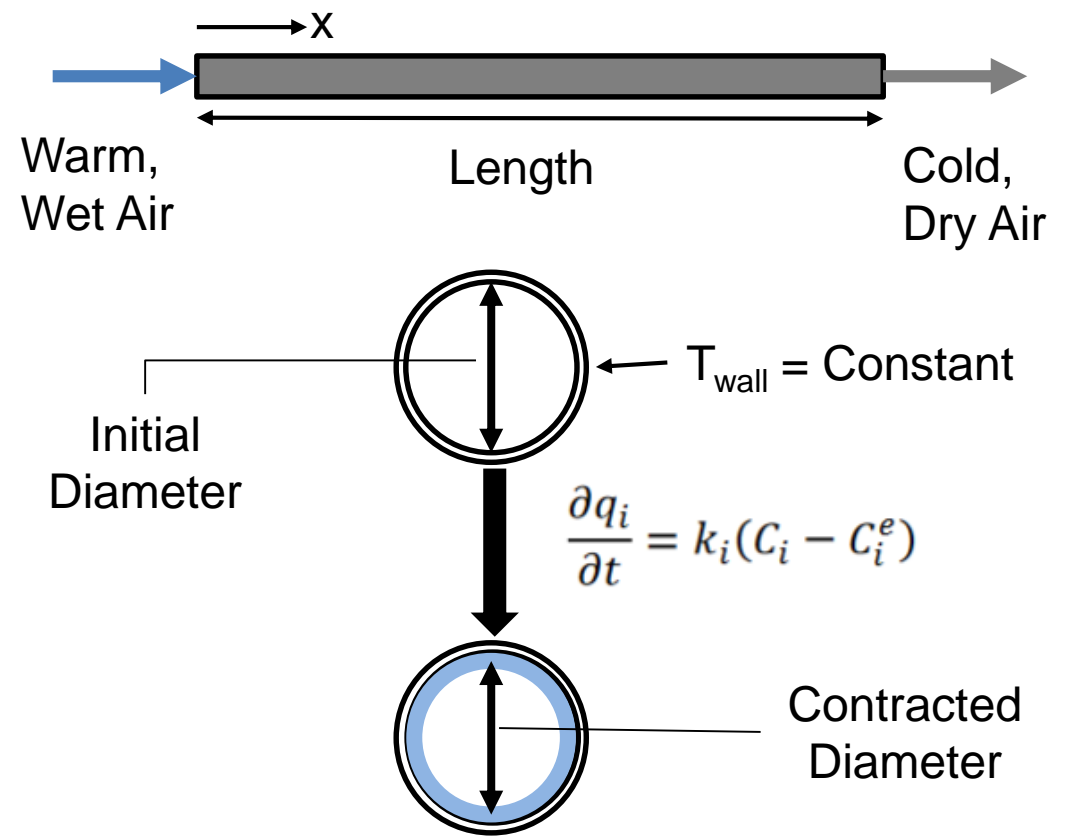


WCS Dehumidification Model Overview

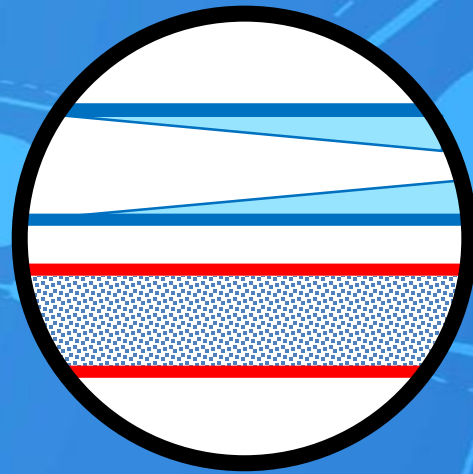
Assumptions

- Plug Flow
- 1-Dimensional
- Quasi-Steady State
- Ideal Gas
- Isothermal Wall ($\Delta T \approx 0.016 \text{ }^\circ\text{C}$)
- Neglect Liquid Phase of Water
- **Mass transfer coefficient calculated based on heat transfer analogy**

Model Geometry



WCS Test / Model Validation



WCS Test Objectives

- WCS Performance Characterization
 - Time and flow rate dependent
 - Two primary outputs: dew point and temperature

Test	Flow Rate (L/min)	Humidity (%RH)	End Criteria
1	0.2	70	Stable outlet dew point (stable within 0.1 C for 10 minutes)
2	0.2 → 3	70	Stable outlet dew point (stable within 0.1 C for 10 minutes)
3	0.2 → 9	70	Stable outlet dew point (stable within 0.1 C for 10 minutes)
4	9	70	6 hour time elapsed or outlet dew point reaches -10 °C (verify ice accumulation)

WCS Testing Procedure

- Complete dry N2 purge

10-15 minutes

- Activate chiller, allow to cool WCS to desired temperature

90 minutes

- Initialize AETHER flow rate, humidity, and gas composition settings

- Initialize system with test gas flow

- Monitor upstream humidity

- Monitor downstream dew point

- Run until test specific end condition is met

 - Outlet dew point is stable within 0.1°C for 10 minutes

90-270 minutes

- Reduce AETHER flow to zero, export all data, and begin shut down

- Deactivate chiller

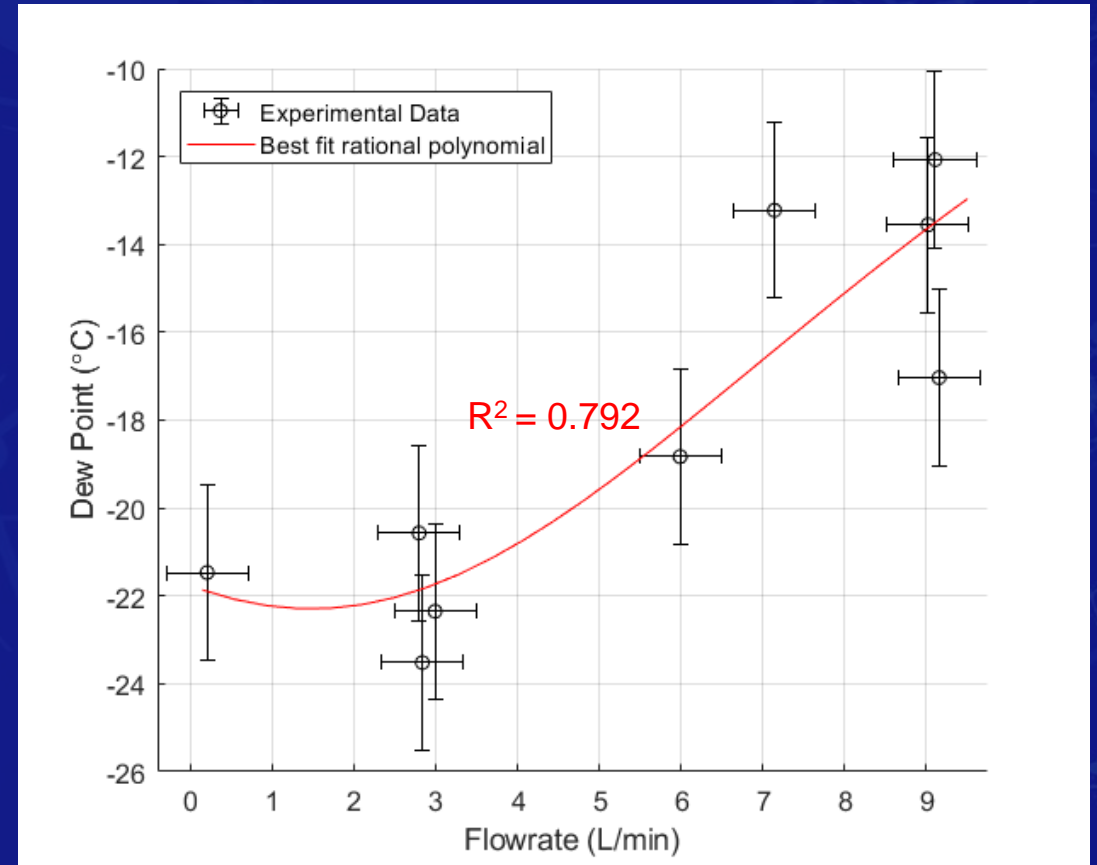
- Post-process test data

30 minutes

Flowrate Characterization Test

- Objective: Characterize output dew point dependence on air flow rate
- Inputs:
 - Flowrate: 0.2 - 9.0 L/min
 - Humidity: ~70 %RH
 - Wall Temperature: -24 to -21 °C
- Major Sources of Uncertainty:
 - Wall temperature measurement
 - Ice Buildup
 - Effective tube length

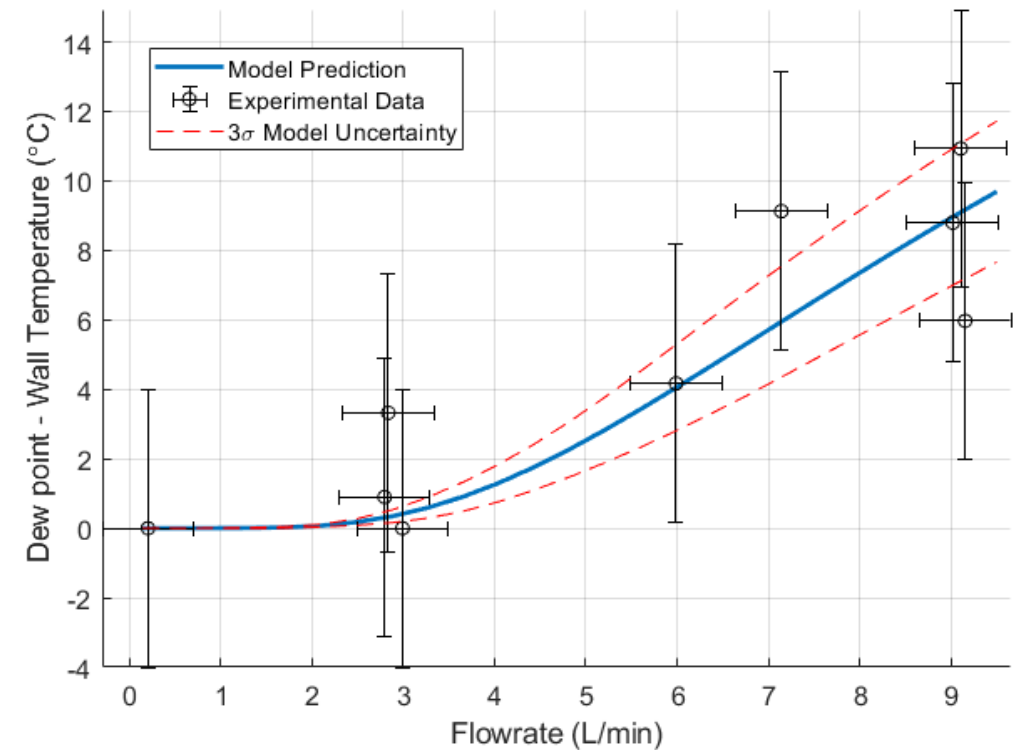
Results



Flowrate Characterization Comparison

- Experimental dew point data ranges from -24 to -12°C
- Model predicts a dew point increase with an increase in flowrate
- Experimental data agrees with model

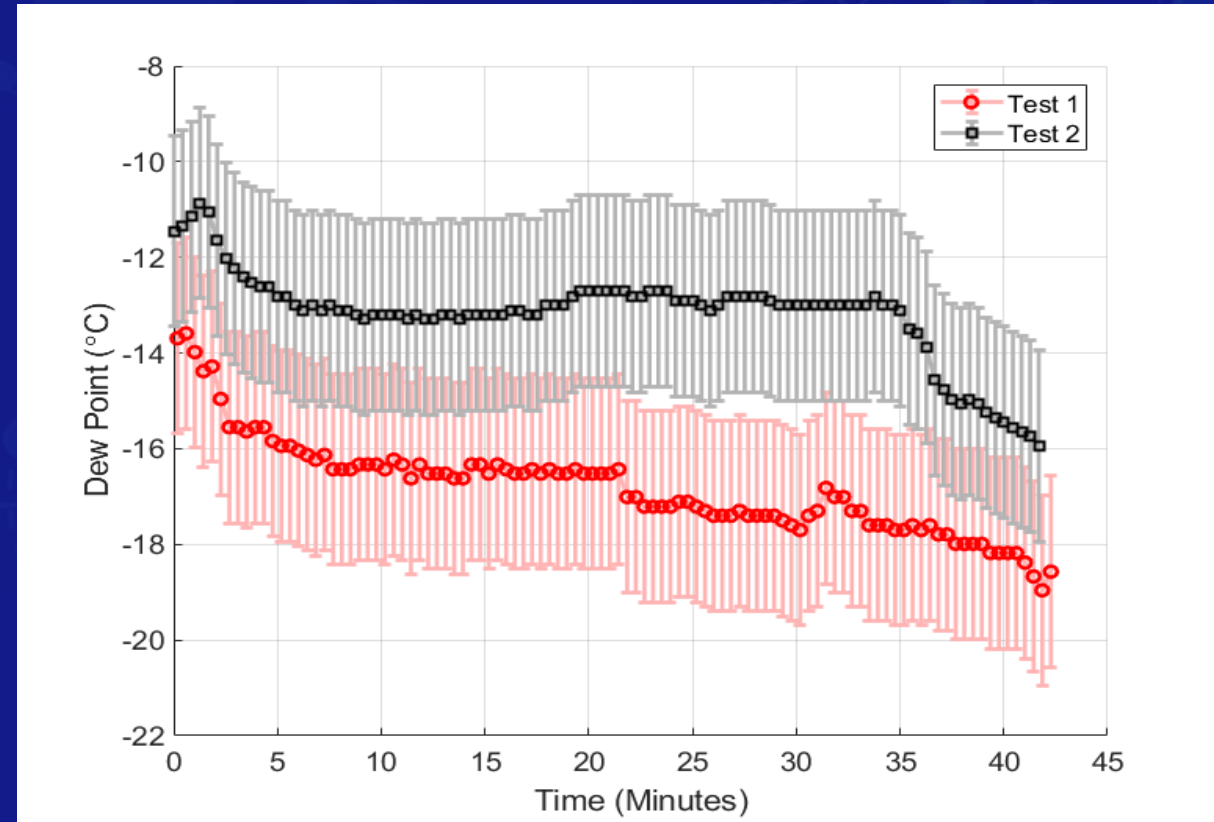
Normalized Results



Transient Behavior Test

- Objective: Collect data on output dew point of WCS over a period of 6 hours.
- Inputs:
 - Flowrate: 9.0 L/min
 - Humidity: ~70 %RH
 - Wall Temperature: -24 to -21 °C
- Major Sources of Uncertainty:
 - Wall temperature measurement
 - Ice Buildup
 - Effective tube length

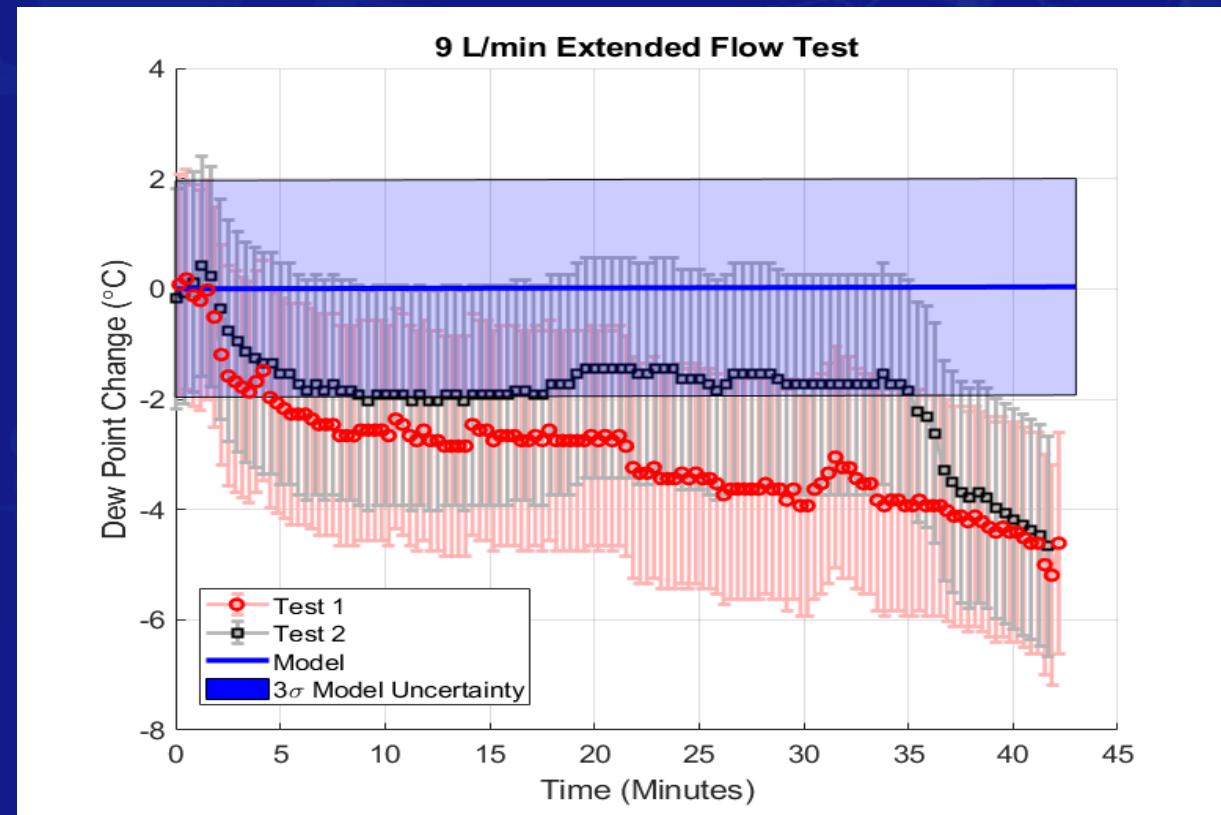
Results



Transient Behavior Comparison

- Model predicts a slow increase in dew point over time
- Test data shows the opposite trend
- Model predicts ~100 hours to ice blockage
- During testing blockage happened in less than 1 hour

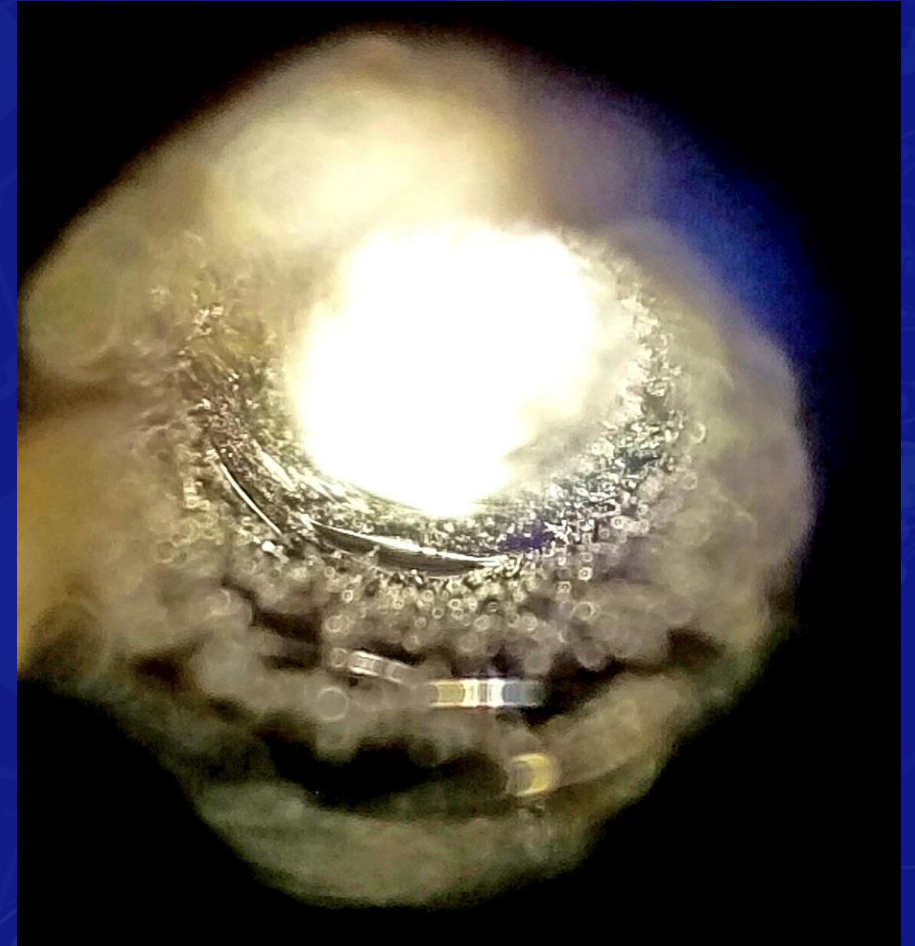
Normalized Results



Results Discussion

- Model accurately predicts initial system performance
- Transient behavior is an issue
 - Complexity of ice growth
 - Ice surface effects on mass transfer
 - Thermal conductivity of ice
 - Turbulent transition
 - Significant liquid water
- Time until blockage appears consistent

Ice accumulation after short test (inlet view)

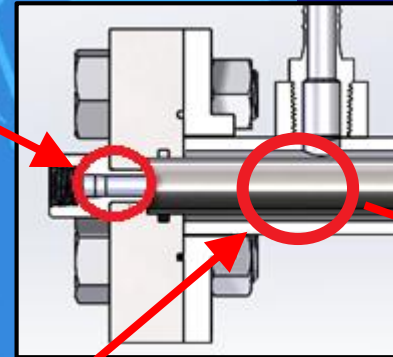


Design Insight

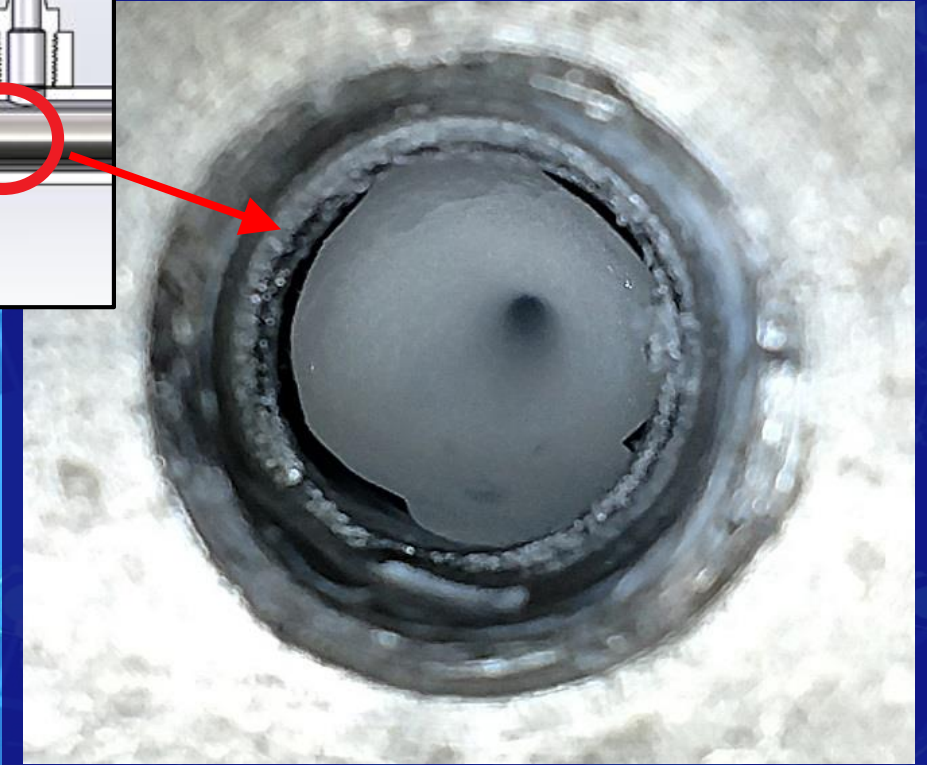
- Problem: Air inlet froze shut well before main tube at low flowrates
- Solution: Upstream air line should have a larger diameter than the main tube

- Problem: Most ice collects in one spot (inefficient use of volume, shorter cycle time)

- Solution: Gradually lower wall temperature in the direction of air flow OR gradually reduce tube diameter

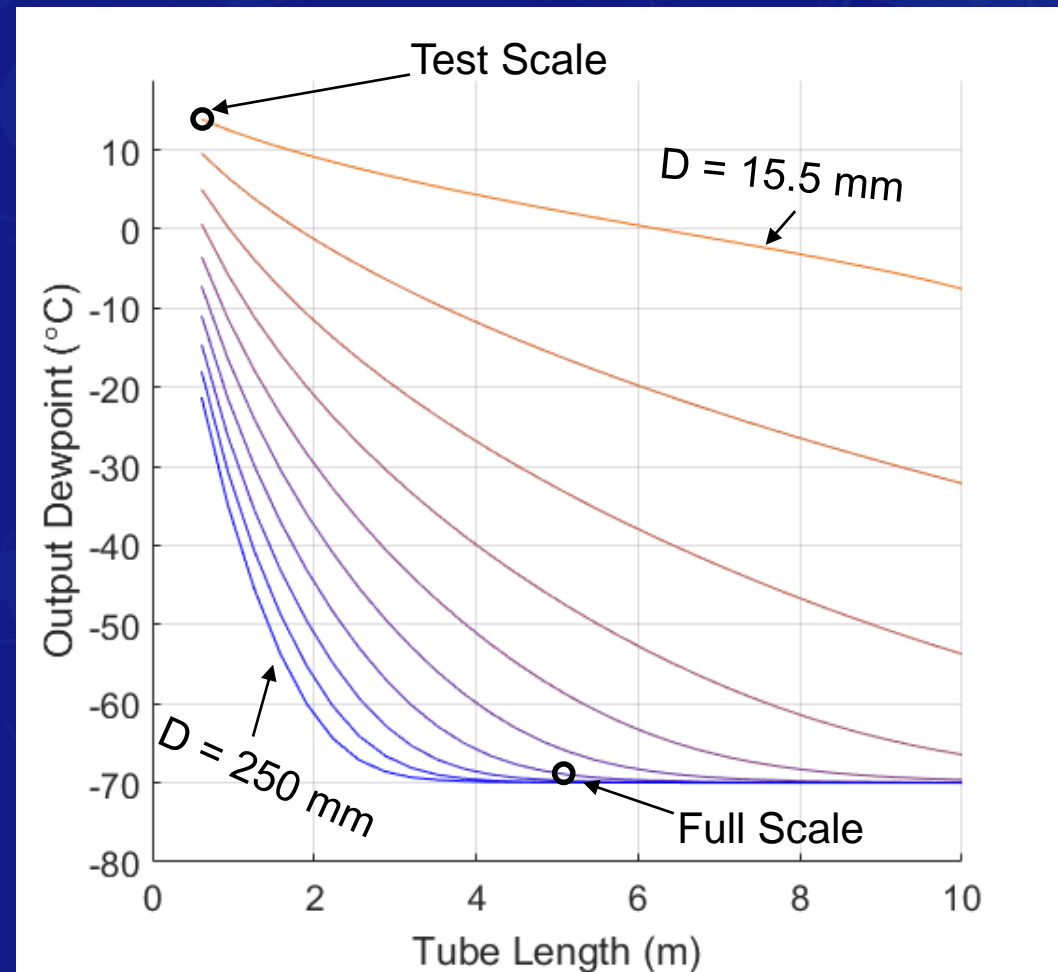


Ice blockage after long test (inlet view)

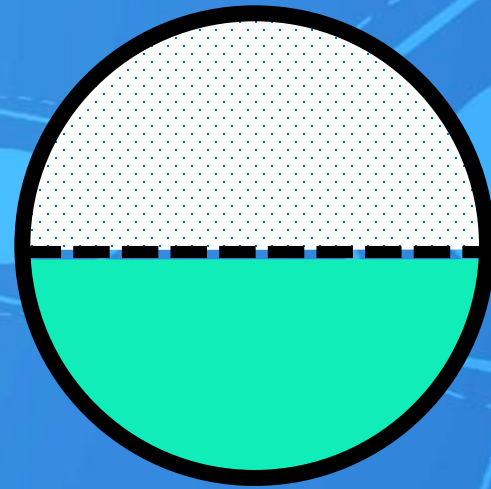


Full Scale Design (4 Crewmembers)

- Full scale flow rate: 30 scfm
- Full scale wall temperature: -70°C
- Possible design point:
 - Diameter = 88 mm
 - Length = 5.1 m
 - Volume = 0.248 m^3
 - Mass $\approx 60\text{ kg}$ (copper tube)
 - Power $\approx 30\text{ W}$
 - Output dew point = -68.9°C
- Adding fins will reduce volume required
- WCS meshes well with CO_2 cryocooler
- Water collection process is non-trivial
- **Full scale design is feasible**

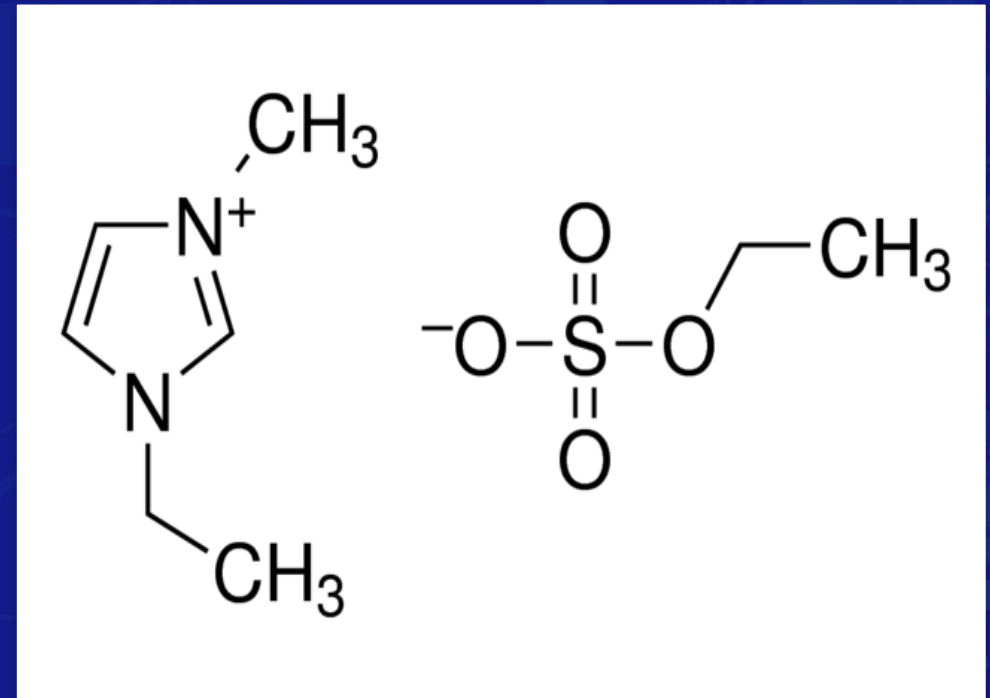


Ionic Liquid System (ILS) Modeling / Simulation



1 Ethyl-3-Methylimidazolium Ethyl Sulfate [EMIM] [ESO₄]

- Selected based on affordability, safety, and H₂O selectivity
 - Desirable hygroscopic performance
 - Both chemical and physical absorption of H₂O have been observed
 - Safety concerns are limited to:
 - Possible skin irritation
 - Possible eye irritation

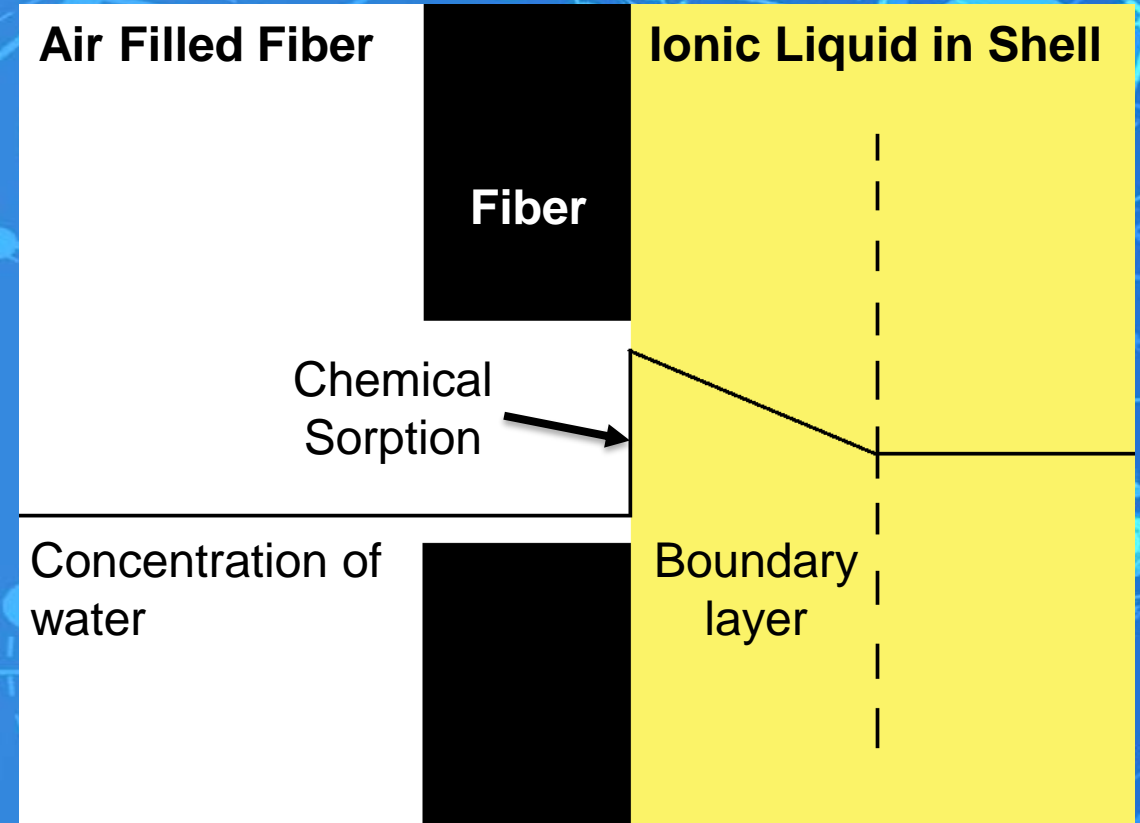


Product Name	Molar Mass	Melting Point [°C]	Viscosity at RT [mPas]	Electric Conductivity [μS/cm]	Distribution Coefficient at RT	Cost [\$/kg]
[EMIM] [ESO ₄]	236.29	< -20	122	4 - 40	11000	\$

Ionic Liquid System Model

Updates since CDR

- Heat exchanger analogy replaced to reflect mass transfer theory
- Diffusivity as a function of water concentration
- Viscosity as a function of water concentration
- Application of distribution coefficient corrected



Flow outside and perpendicular to a capillary bed

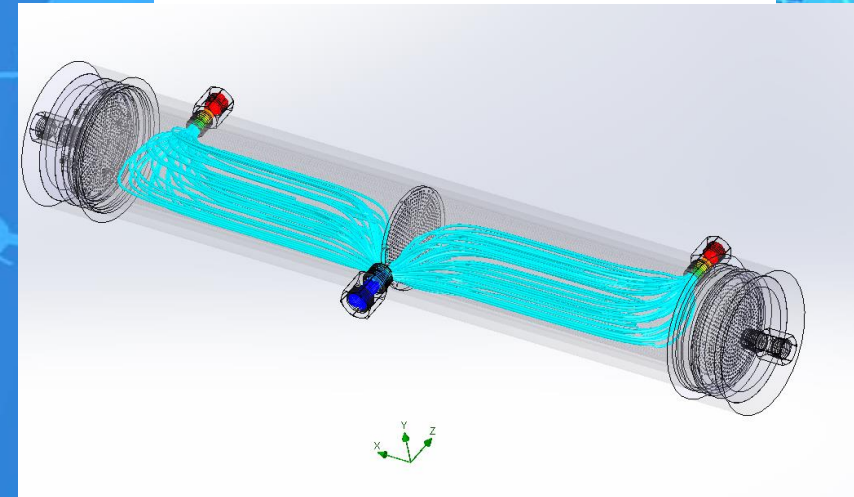
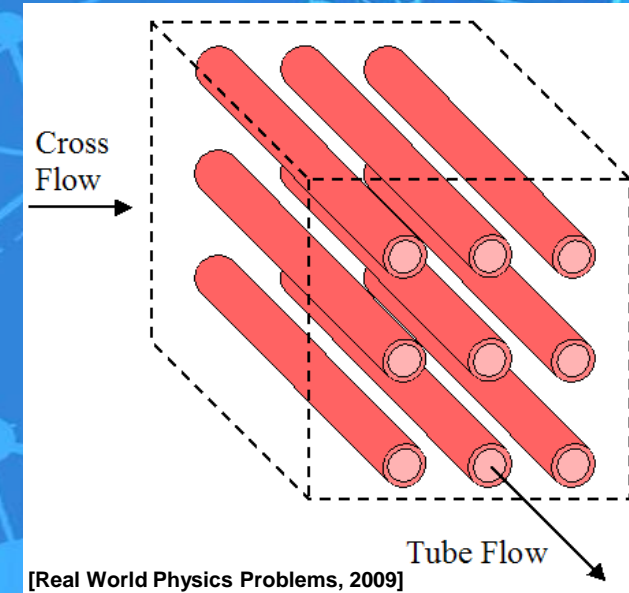
$$\frac{kd}{D} = 0.80 \left(\frac{dv^0}{v} \right)^{0.47} \left(\frac{v}{D} \right)^{1/3}$$

[Diffusion, Mass Transfer in Fluid Systems, 2009]

Ionic Liquid System Model

Simplifications

- Model still uses simplified contactor geometry
 - Rectangular prism vs cylinder
 - Distribution of fibers
- Modelled as cross flow contactor, but actual IL flow pattern is complex
- Mass transfer through air filled pores is neglected



Distribution Coefficient

- Distribution coefficient is a ratio of concentration of water in the IL to water in the air stream
- Initial test suggested 1200
 - No verification of equilibrium
 - Set lower bound on distribution coefficient
- IL desorption test did not reach equilibrium after ~24 hours
 - Indicates that initial test length was insufficient
- A distribution coefficient of 1200 would mean the IL would saturate at a molar concentration of 0.07
 - Test data indicated IL was still removing water at >0.1
- Distribution coefficient of 11000 assumed to fit with test data

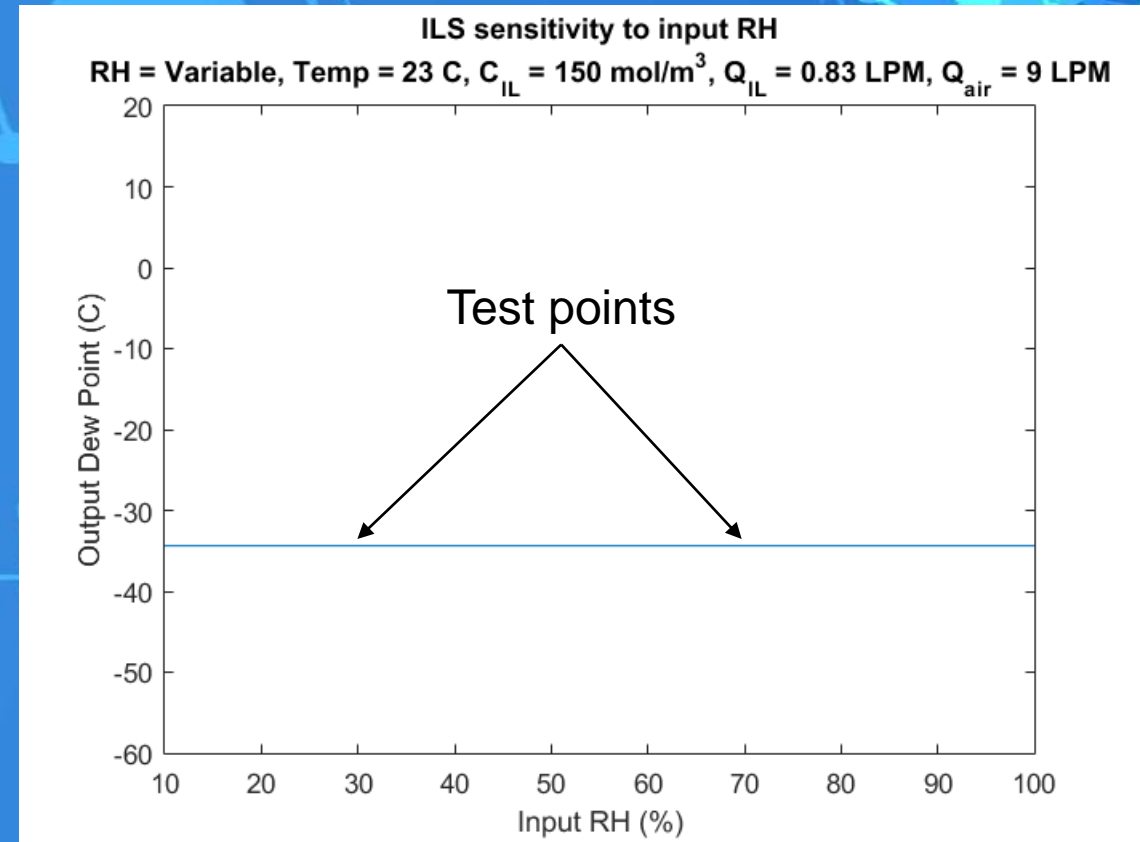
Ionic Liquid System Model Inputs

- Inlet RH
- Temperature
- Initial concentration of water in the IL
- IL flow rate
- Air flow rate
- Distribution coefficient (due to uncertainty)

- Nominal RH: 70%
- Nominal temperature: 23°C
- Nominal concentration of water in the IL: 150 mol/m³
- Nominal IL flow rate: 0.83 LPM
- Nominal air flow rate: 9 LPM
- Estimated distribution coefficient: 11000

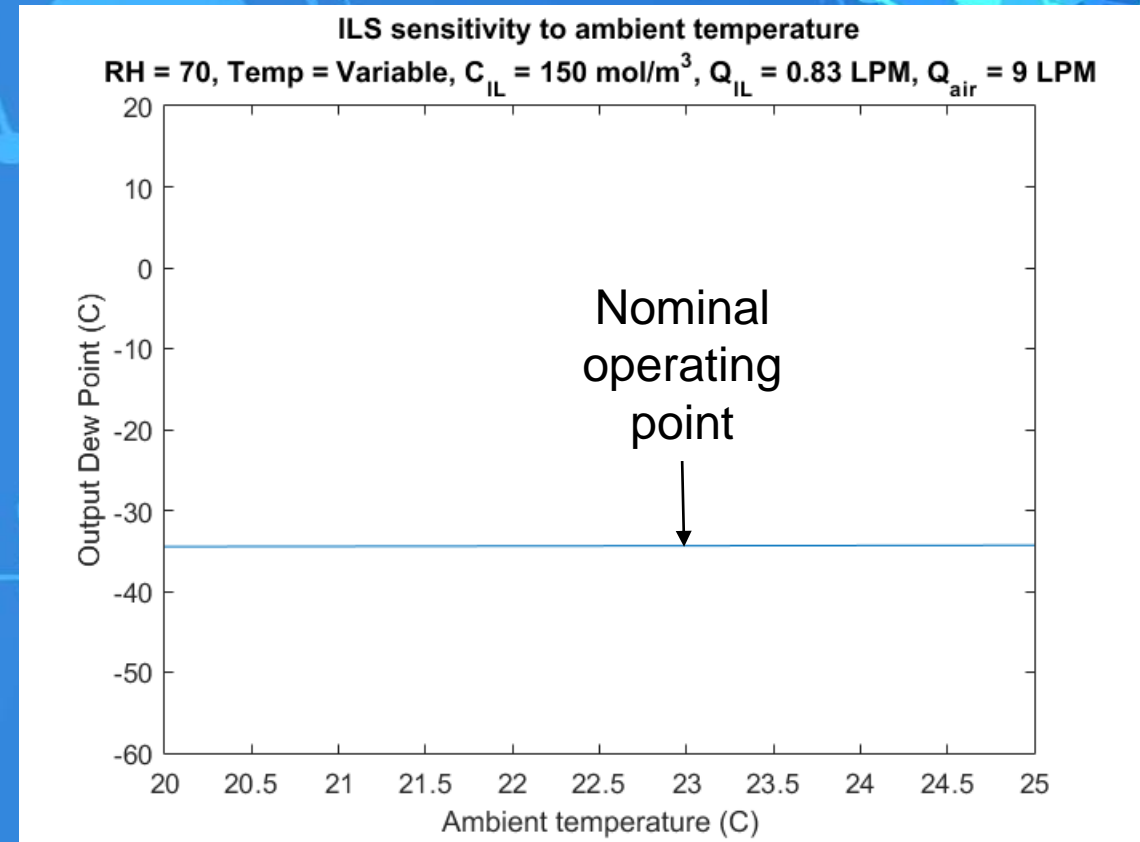
Model Sensitivity

- Inlet RH varies output by $<0.1^{\circ}\text{C}$
- Temperature
- Initial concentration of water in the IL
- IL flow rate
- Air flow rate
- Distribution coefficient (due to uncertainty)



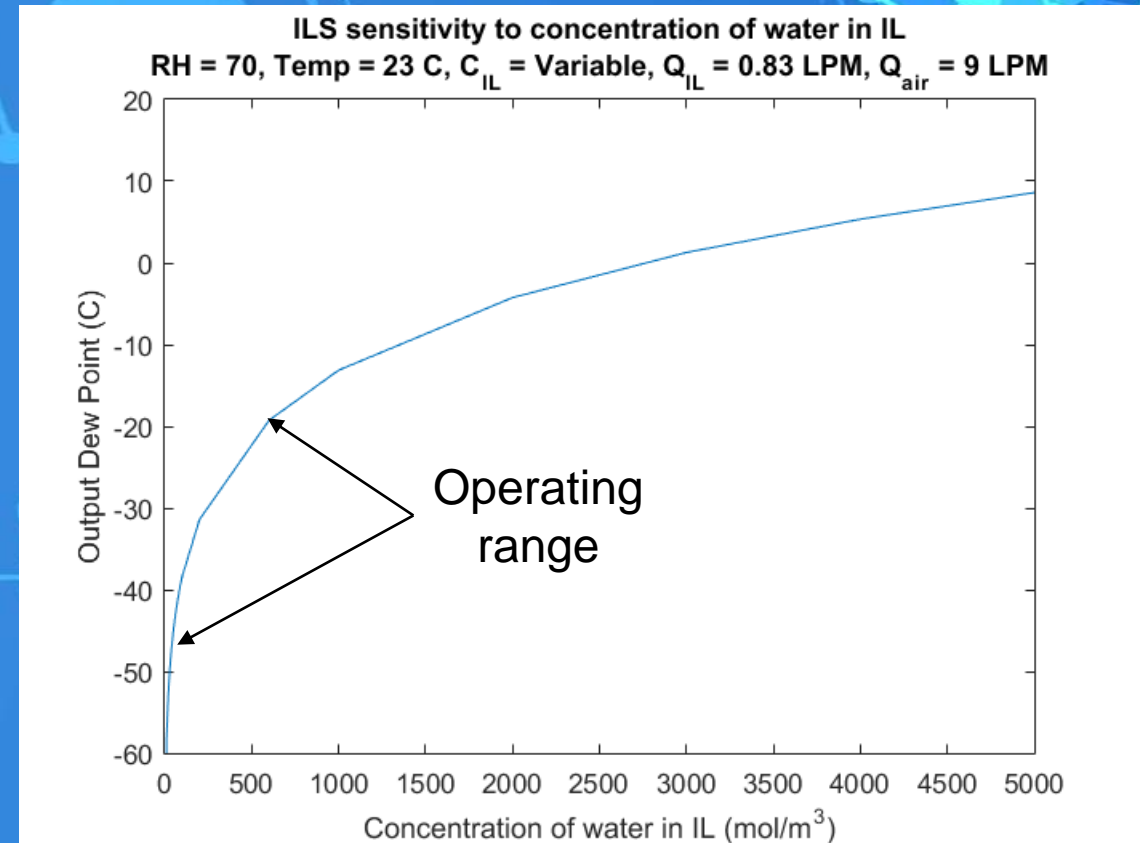
Model Sensitivity

- Inlet RH
- Temperature varies output by 0.17°C
- Initial concentration of water in the IL
- IL flow rate
- Air flow rate
- Distribution coefficient (due to uncertainty)



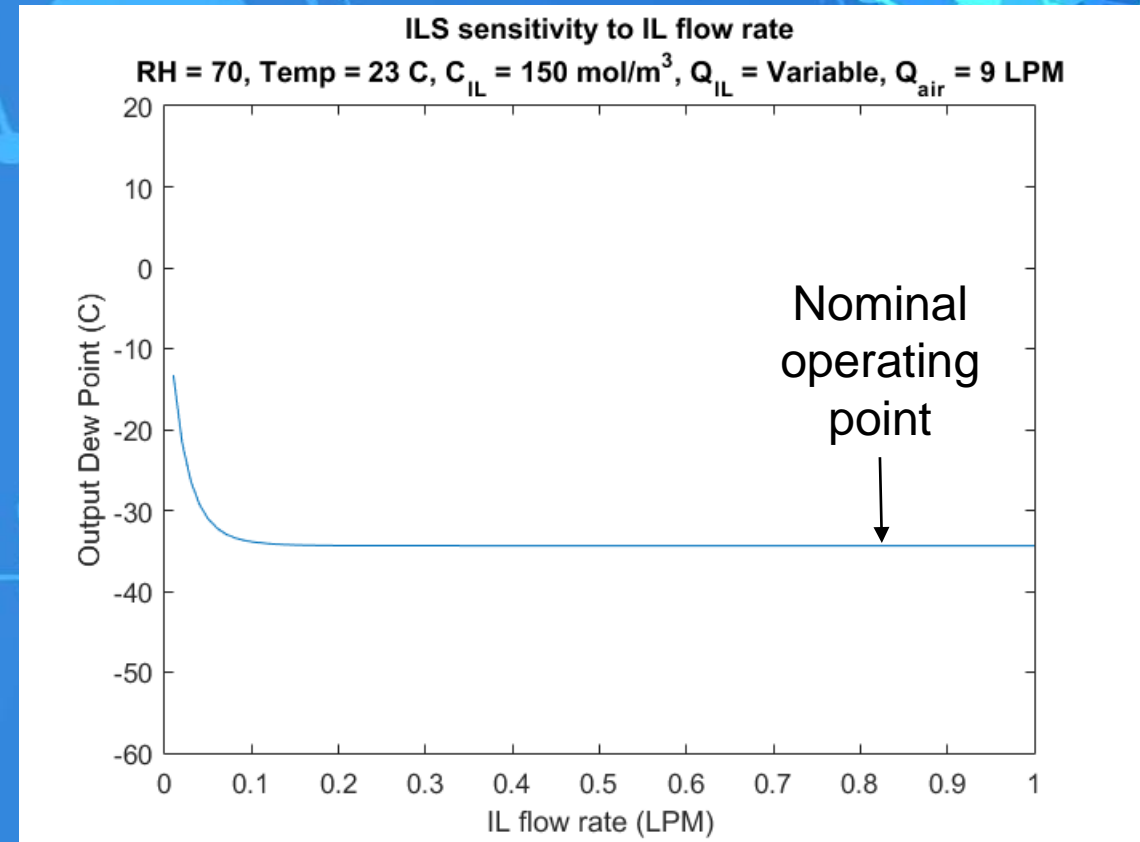
Model Sensitivity

- Inlet RH
- Temperature
- Initial concentration of water in the IL varies output from -120°C with no water to 9°C
- IL flow rate
- Air flow rate
- Distribution coefficient (due to uncertainty)



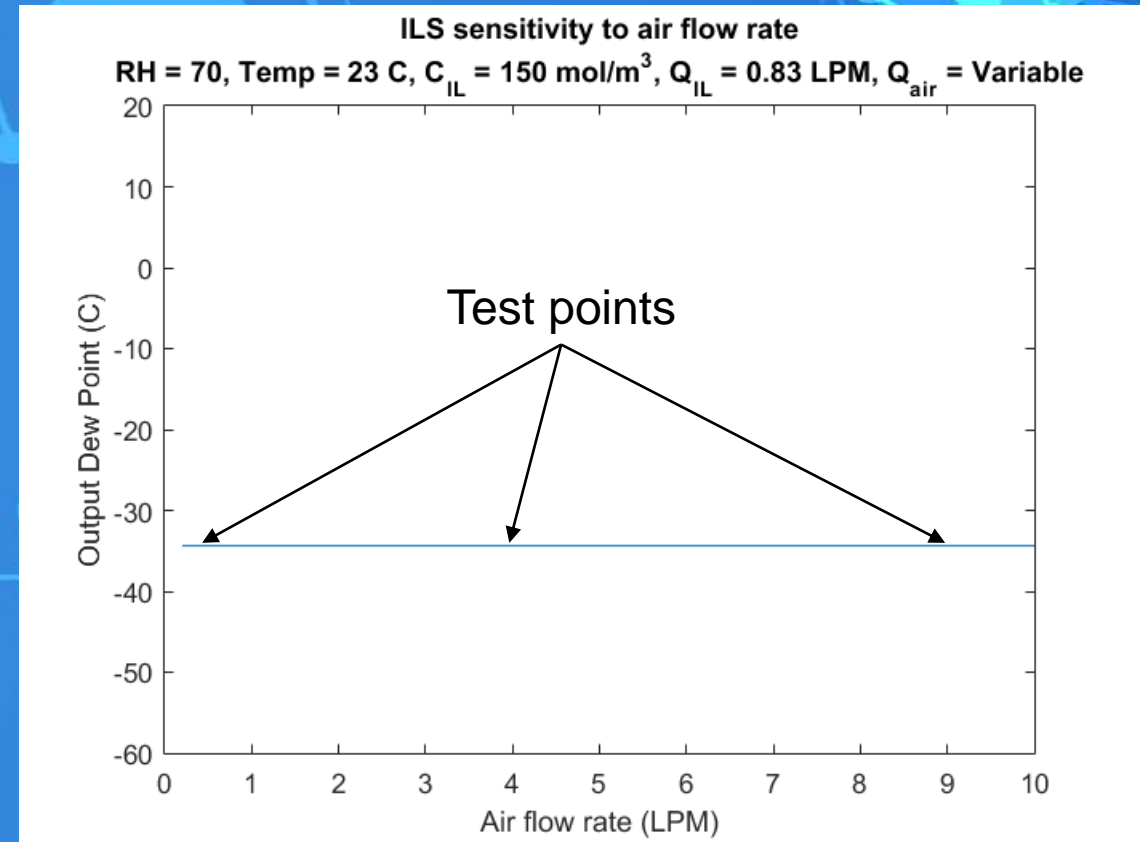
Model Sensitivity

- Inlet RH
- Temperature
- Initial concentration of water in the IL
- IL flow rate only reduces performance below 0.1 LPM
- Air flow rate
- Distribution coefficient (due to uncertainty)



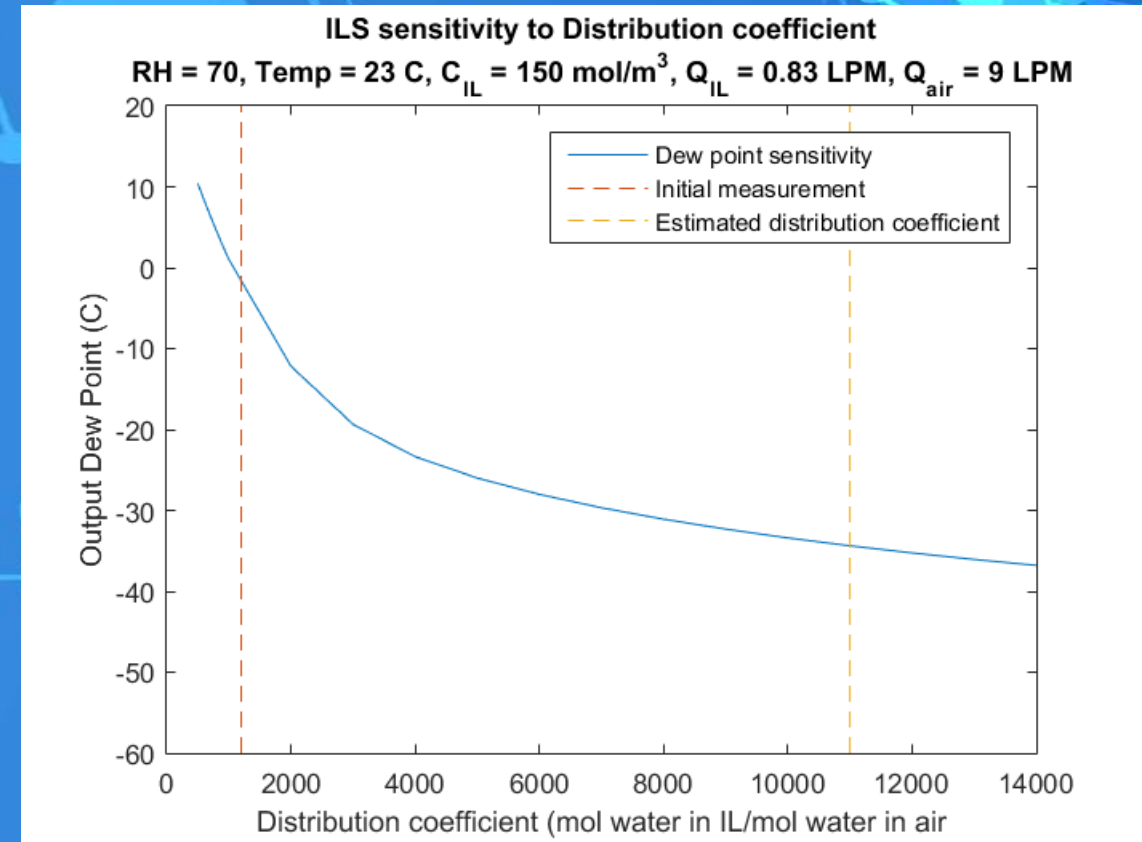
Model Sensitivity

- Inlet RH
- Temperature
- Initial concentration of water in the IL
- IL flow rate
- Air flow rate varies output by $<0.1^{\circ}\text{C}$
- Distribution coefficient (due to uncertainty)

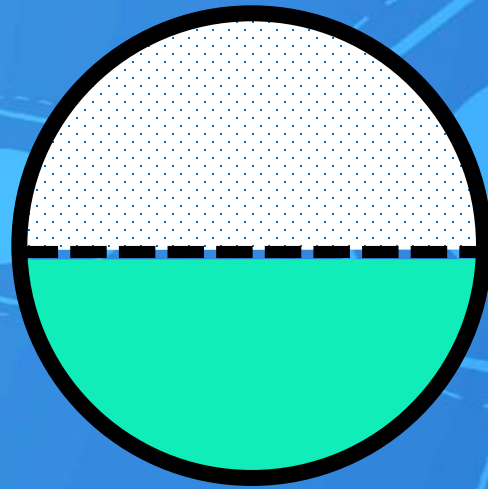


Model Sensitivity

- Inlet RH
- Temperature
- Initial concentration of water in the IL
- IL flow rate
- Air flow rate
- Distribution coefficient (due to uncertainty) varies output by 45°C



ILS Test / Model Validation



ILS Test Objectives

- ILS Performance Characterization
 - Time and flow rate dependent behavior
 - Two primary outputs: dew point and temperature

Test	Flow Rate (L/min)	Humidity (%RH)	End Criteria
1a	0.2	70	Stable outlet dewpoint (stable within 0.1 C for 10 minutes)
1b	4	70	Stable outlet dewpoint (stable within 0.1 C for 10 minutes)
1c	9	70	Stable outlet dewpoint (stable within 0.1 C for 10 minutes)
Bake out	0	0	Vacuum desorption (50 mTorr) for 24 hours
1a, trial 2	0.2	70	Stable outlet dewpoint (stable within 0.1 C for 10 minutes)
1a/b, trial 2	9,4	70	Stable outlet dewpoint (stable within 0.1 C for 10 minutes)
2a	9,4,0.2	70	30 minutes at each flow rate
2b	9,4,0.2	25-30	30 minutes at each flow rate

ILS Testing Procedure

- Refill ILS, activate pump, establish IL flow rate

15 minutes

- Complete dry N2 purge

15 minutes

- Initialize AETHER flow rate, humidity, and gas composition settings

- Initialize system with test gas flow

- Monitor upstream humidity

- Monitor downstream dew point

- Run until test specific end condition is met

 - Outlet dew point is stable within 0.1°C for 10 minutes

90-270 minutes

- Reduce AETHER flow to zero, export all data, and begin shut down

- Collect IL sample

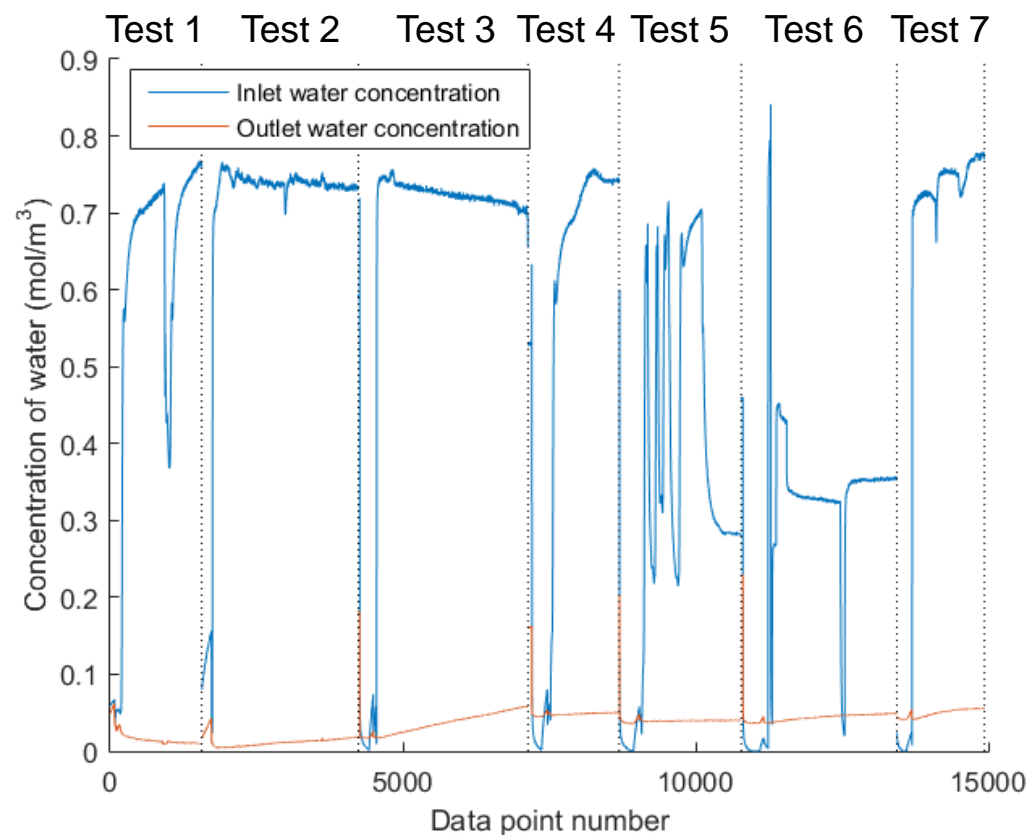
- Deactivate pump

- Post-process test data

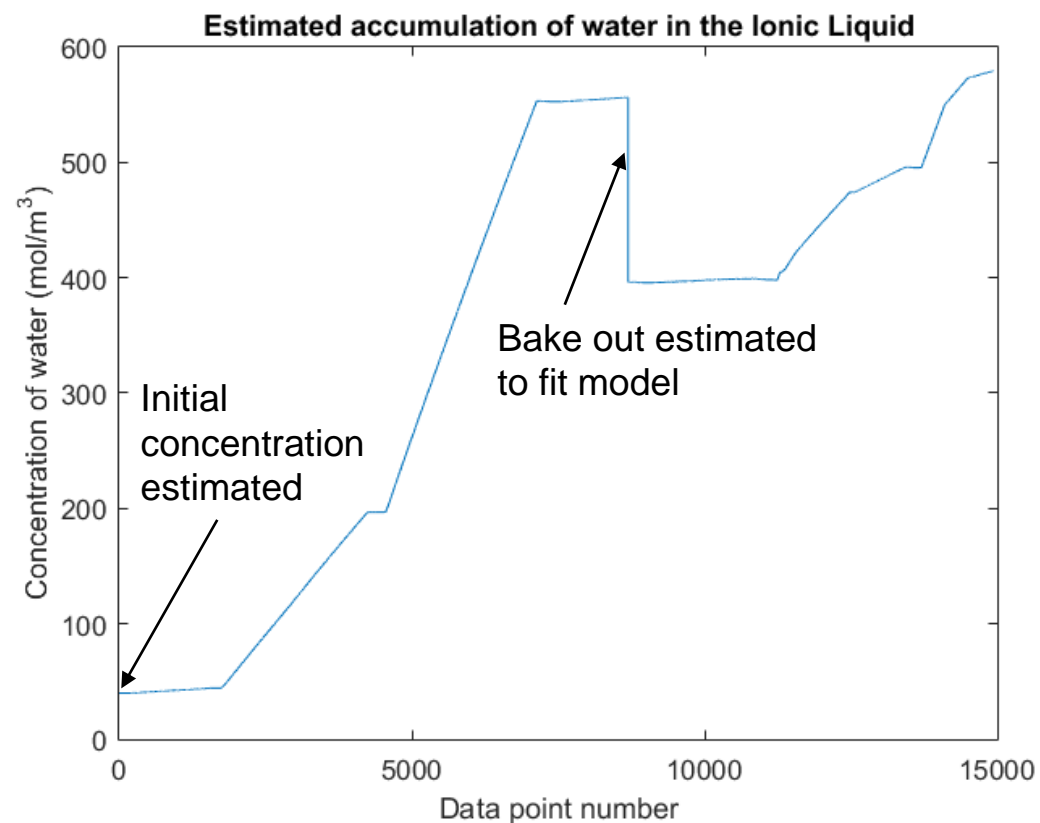
30 minutes

Tracking the Water

Concentration of Water in the Air

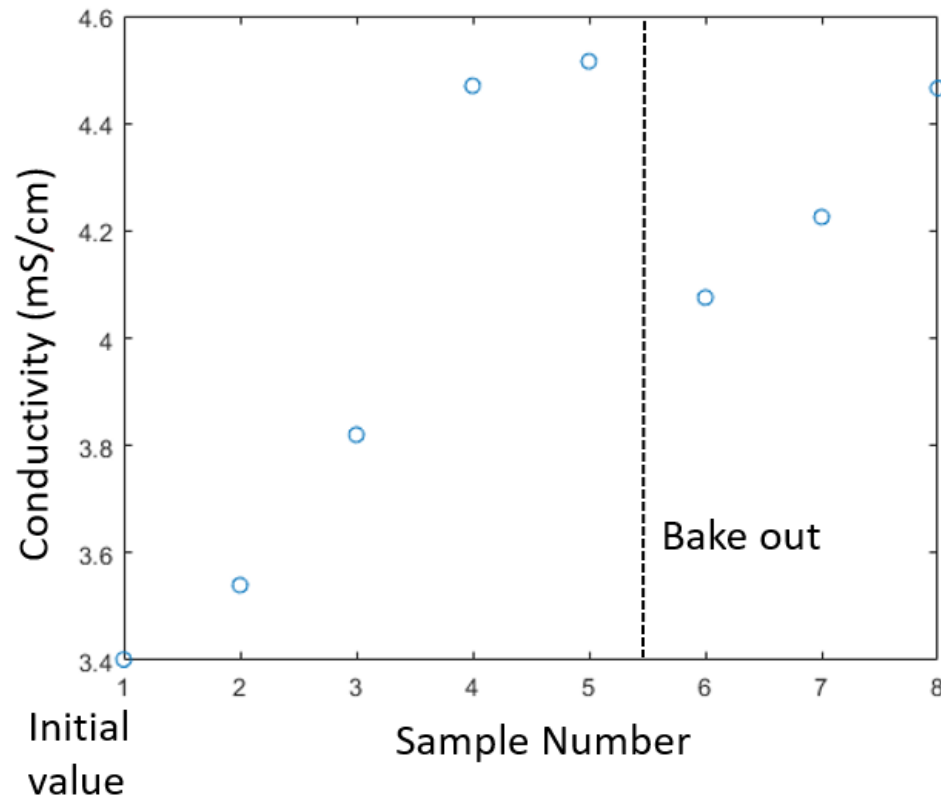


Accumulation of Water in the IL

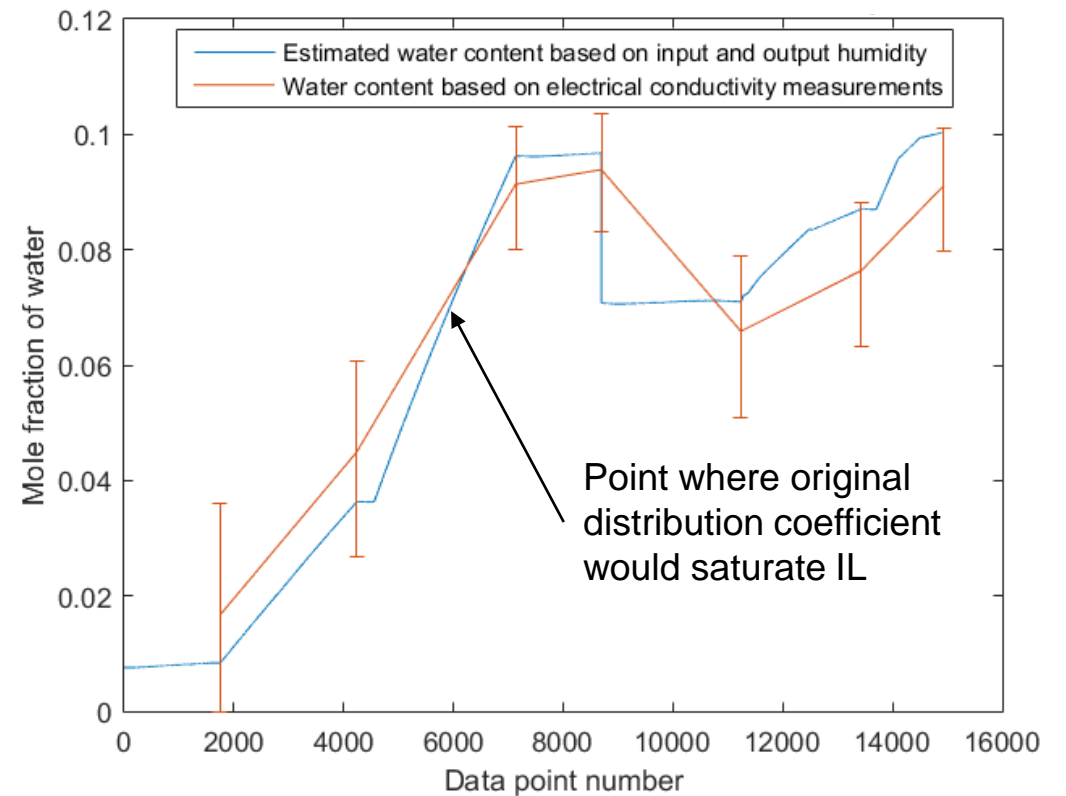


Measuring the Water

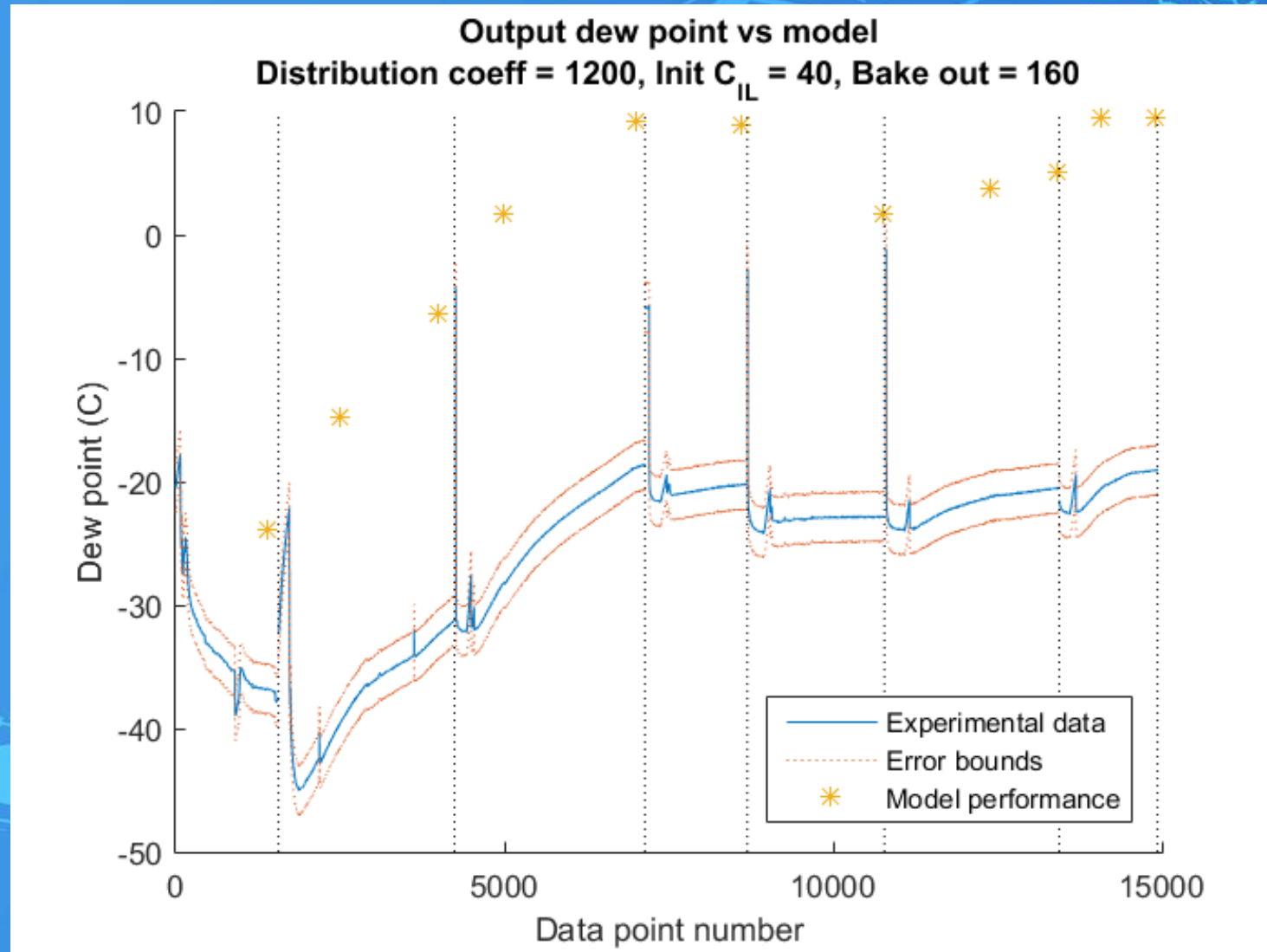
Electrical Conductivity Measurements



EC vs Accumulation Estimates



Output Dew Point



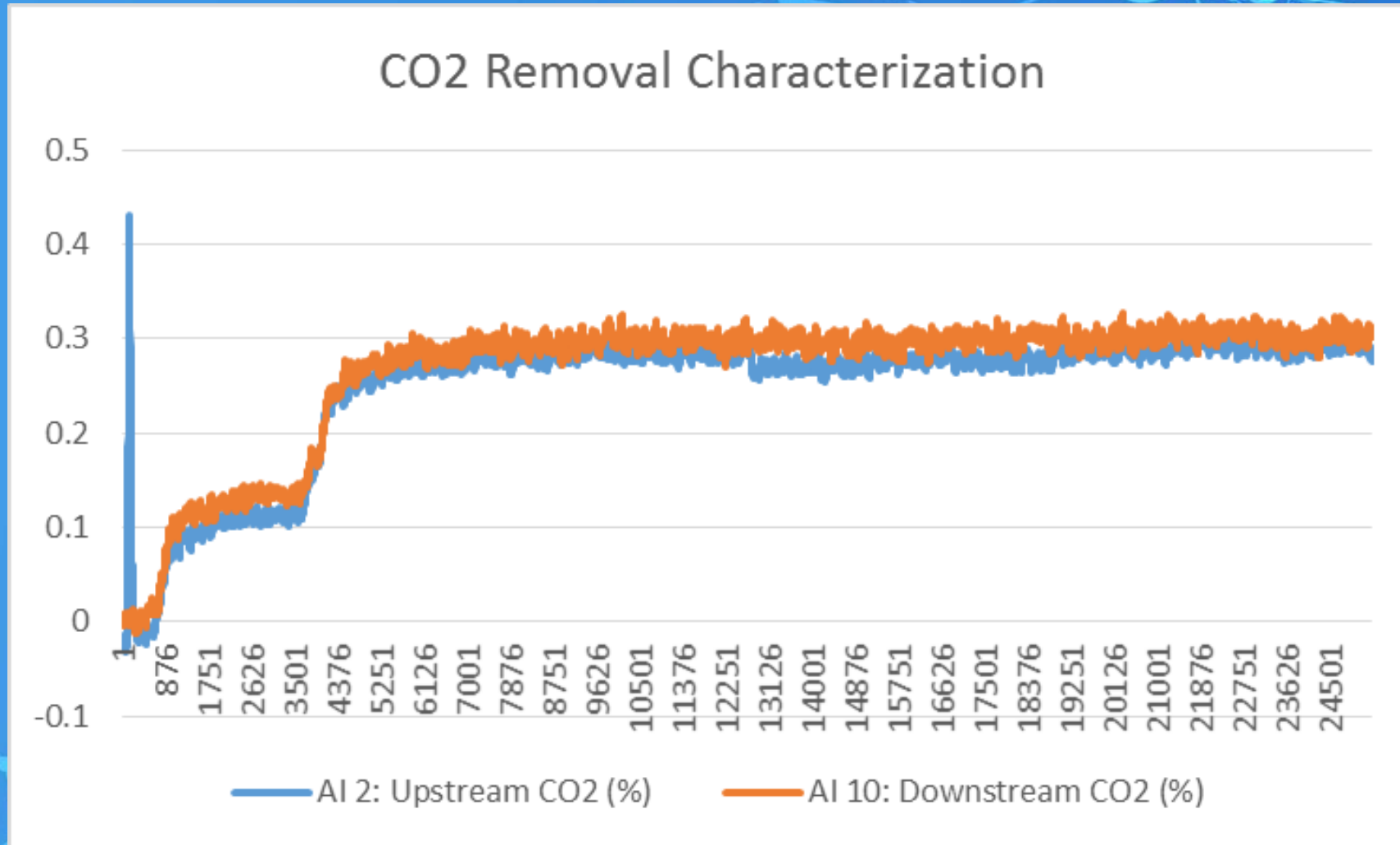
ILS Regeneration

- IL desorbed for about 24 hr
- Pressure initially leveled out at 870 mtorr and dropped to 40 mtorr over the course of the desorption process
- Lowest chamber operating pressure is 8 mtorr (2 weeks)
- Water concentration dropped from ~ 555 to 395 mol/m^3 (29%)
- Not agitated, not heated, low surface area to volume ratio



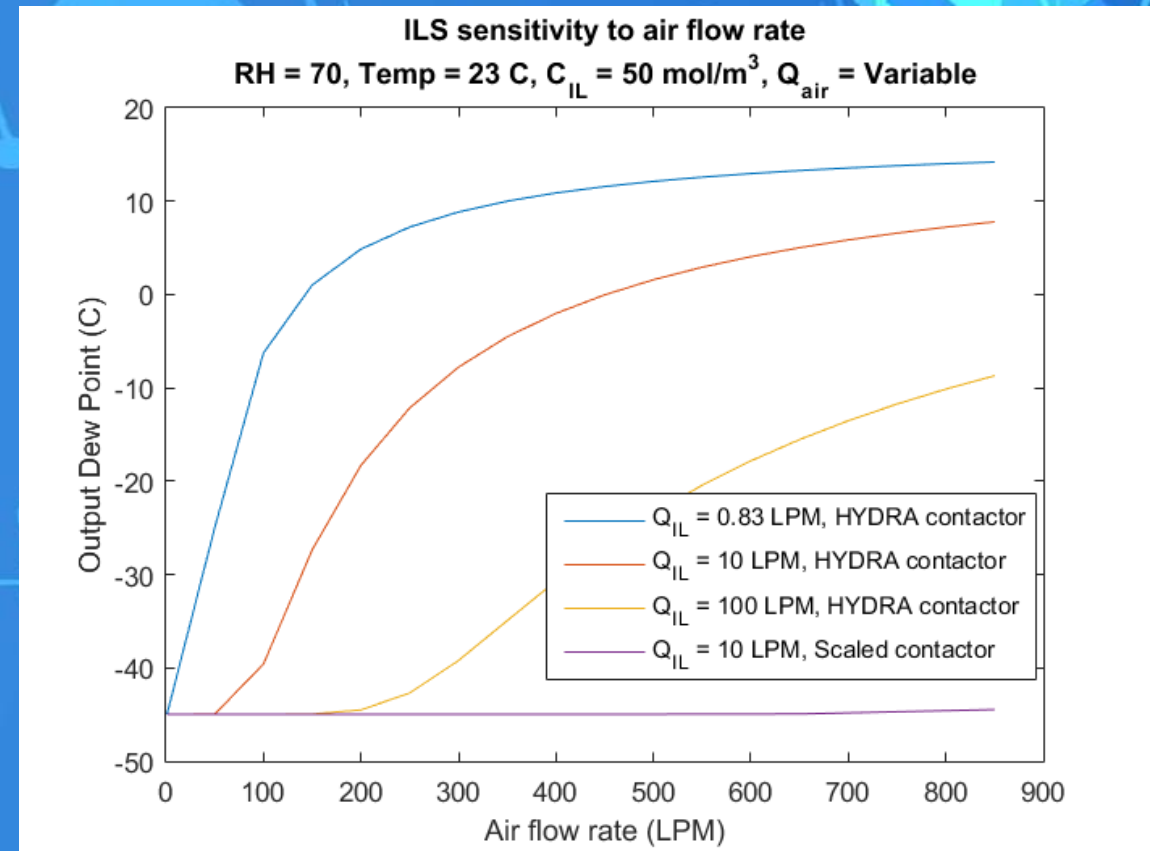
Vacuum Chamber

ILS CO2 Removal Charaterization



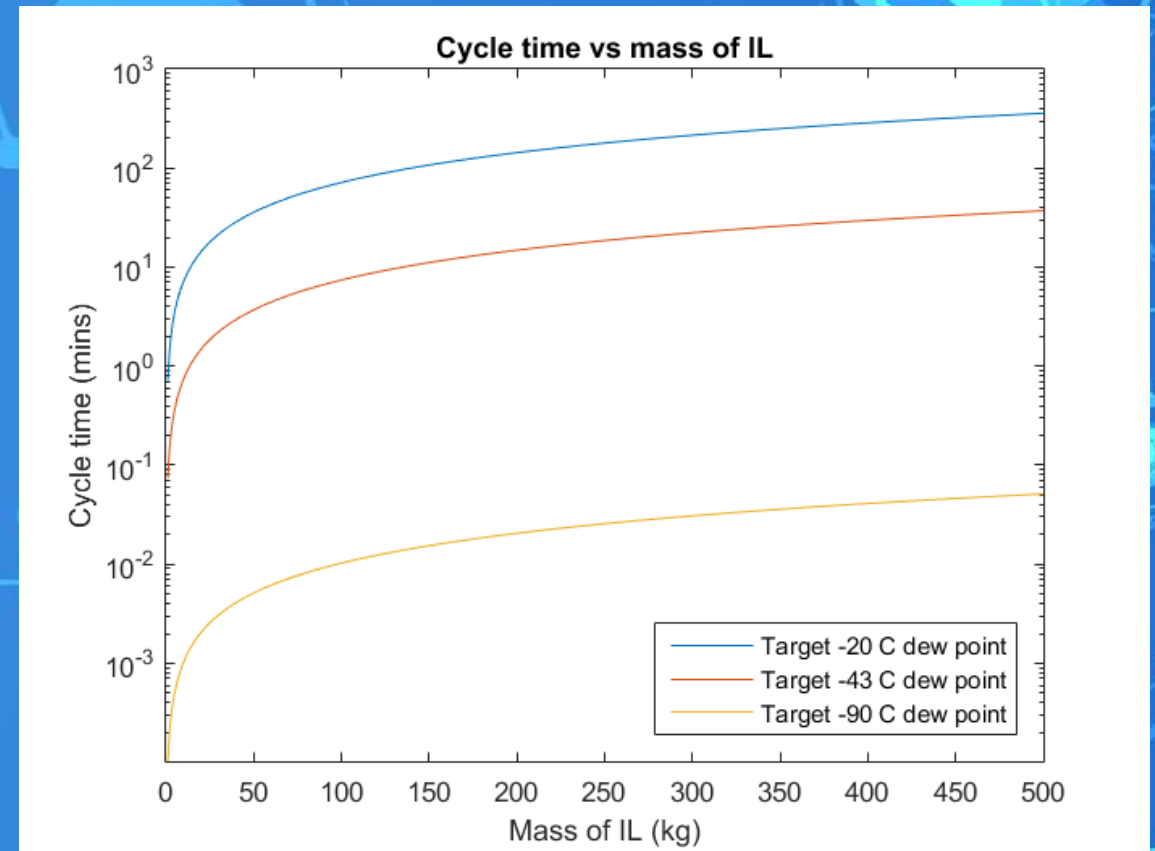
Scaling

- Target air flow rate:
 - 30 cfm (~850 LPM)
- Scaled contactor properties:
 - Length: 1m long (2x HYDRA's contactor)
 - Number of fibers: 5000 (10x HYDRA's contactor)
 - Volume: 12L (4x HYDRA's contactor)
 - IL flow rate: 10 LPM (10x HYDRA's contactor)



Scaling

- 500 kg of IL can achieve:
 - A -20°C dew point for ~ 6 hours
 - A -43°C dew point for ~ 37 minutes
 - A -90°C dew point for ~ 3 seconds
- Cycle time scales linearly with mass of IL
- **Full scale design is feasible**



Takeaways

- ILS achieves -36°C dew point
- Distribution coefficient uncertainty
 - Had to be tuned in model after acquiring data
- Mass transfer is limited by the concentration of water in IL
 - Concentration verified by two independent methods
- Contactor over spec'd in size (amount of IL in system was reasonable)
- Most of scaled up mass is from IL, not the dry mass of the system
- ILS does not sorb detectible quantity of CO_2
- ILS regeneration needs further analysis



Budget and Schedule

Path Forward

- HYDRA final presentation: May 4th
- HYDRA final report submission: May 10th
- International Conference on Environmental Systems: July 8th – 12th in Albuquerque, NM
 - Presenting a poster on the design, development, and test of the WCS and ILS
 - Submitting a conference paper on the design of the WCS



Project Takeaways

Manufacturing – Lessons Learned

- Manufacturing tolerances are imperative for sealing interfaces
- O-ring glands are not trivial
- Hollow fiber membrane contactors of this size are challenging to build
 - Consider flowing IL through larger fibers and flowing air around them to decrease the number of fibers and increase their diameters
 - The number of fibers increases complexity
 - Fibers are easily damaged



Testing – Lessons Learned - AETHER

- AETHER
 - Study the SOPs thoroughly
 - Familiarize yourself with all flow paths
 - Determine nominal leakage rates
 - Discuss past experiences with other AETHER users
 - Get very familiar with the LabView VI
 - Some versions work better for different tasks!
 - Newer version \neq best version
- DAQ
 - Have a backup plan
 - backwards compatibility
 - Shoot for the easiest solution while minimizing resolution loss
 - “nice to have” vs. “need to have”






Testing – Lessons Learned – WCS

- Identify and correct leaks early
 - Determine “good enough” criteria for testing go / no-go
 - Insulation had a major impact on wall temperature
 - Insulate coolant lines all the way back to the chiller
- N2 purge before chiller activation
 - Drain WCS after each test

Testing – Lessons Learned – ILS

- IL secondary containment critical
- Dry run pump filling procedures
- Upstream flowmeter was useful in verifying ILS air flow-rate
- Dry N2 purge before each test
- Monitor ILS closely during testing
 - Leaks are hard to isolate

Project Goal Achievement

Project Objectives	Status
PO1: Design, build and test a dehumidification system for air revitalization	
PO2: Characterize H ₂ O transport	
PO3: Report any change in flow composition including CO ₂ and contaminants	
PO4: Justify chosen flow rate to be scalable to 30 scfm	
PO5: Estimate the power required to operate the system	

Project Goal Achievement

- Levels of Success:

- Target

- Level 2: $\leq -43^{\circ}\text{C}$ Dew point (99+% of H_2O removed from the gas stream)

- Achieved

- Level 1: $\leq 0^{\circ}\text{C}$ Dew point (90+% of H_2O removed from the gas stream)

- WCS Dewpoint: -24°C

- Chiller limited

- ILS Dewpoint: -36°C

- Vacuum IL regeneration limited

Educational Outreach

- Teen Café: STEM outreach program through the University of Colorado where high school students interact with graduate students to learn about STEM research projects at CU
- Aerospace Research Symposium Poster: event through Smead Aerospace at CU boulder
- International Conference on Environmental Systems
- Try for a journal article

Educational Lessons Learned

- Learning how to be a part of a team where compartmentalized in-depth knowledge is needed and a more general overview knowledge is needed for the rest of the subsections. – **Mario**
- Gained experience in product life-cycle development and working on interdisciplinary team. – **Zach**
- I learned the importance of due diligence in manufacturing to properly account for tolerances, tooling set-ups, and production time. – **Grant**
- Being flexible during design and troubleshooting is important to the success of the project. – **Lee**
- It's sometimes better to sacrifice performance for simplicity in to validate model performance. – **Thomas**
- Don't underestimate heat transfer. – **Jon**
- Managing a team is mostly about greasing the wheels so your colleagues can be effective. – **Mitch**

The background of the slide features a complex network of blue molecular structures, including various sized circles and hexagonal rings connected by thin lines, set against a solid blue gradient. A large, semi-transparent grey rectangular box is centered horizontally and vertically, containing the text "Questions?".

Questions?



Backup Slides

Modeling Requirements

- Modeling Requirements:
 - MOD1: **Numerical model** for H₂O removal and transport shall be developed
 - MOD1.1: Model shall provide data to **inform system design** when necessary
 - MOD1.2: Model shall provide data to **predict system performance**
 - MOD2: All assumptions used in the H₂O removal and transport models shall be **documented and validated**

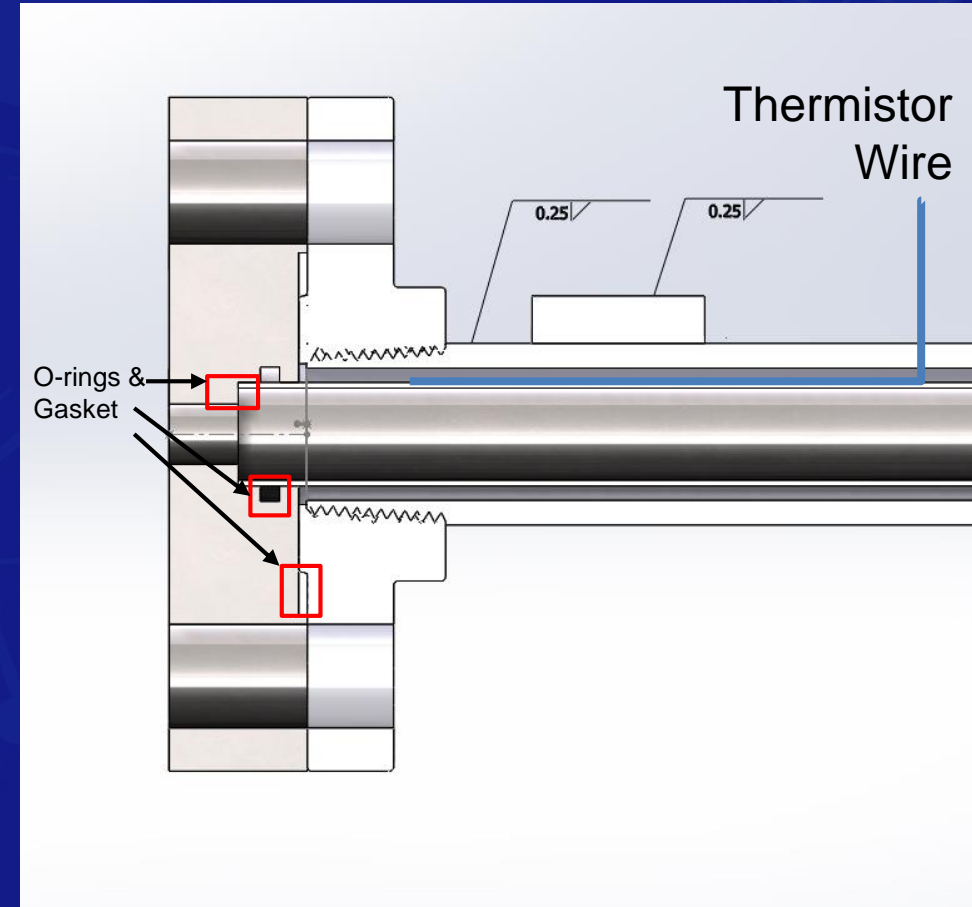
Controls Requirements

- Controls Requirements:

- CTRL1: The controls system shall **monitor** overall system health
- CTRL2: The controls system shall be capable of **halting gas flow** if testing limits are exceeded
 - CTRL2.1: The total pressure in the test article **shall not exceed 1.5 atm** during testing
 - CTRL2.2: The wall temperature in WCS **shall not be warmer than -10 °C** while gas is flowing
 - CTRL2.3: The air temperature downstream of the WCS **shall not be warmer than -10 °C** while gas is flowing
 - CTRL2.4: The pressure drop across the test article **shall not exceed 0.4 psi**
- CTRL3: The controls system shall be able to characterize the entire test setup
 - CTRL3.1: All humidity sensors shall have an accuracy of $\pm 5\%$ RH and an operating range of **5% to 80% RH**
 - CTRL3.2: All dew point sensors shall have an accuracy of $\pm 2^{\circ}\text{C}$ and operating range of **-60°C to 25°C**
 - CTRL3.3: All temperature sensors shall have an accuracy of $\pm 1^{\circ}\text{C}$ and operating range of **-60°C to 30°C**

Assembly Process

- Place Thermistors on Inner Tube and fix them with JB Weld
- Feed Wires through feedthrough holes
- Insert Inner Tube into outer tube
 - Pulling feed wires taught
- Place Intra-flange O-rings in flange grooves
- Place Gasket Seals in flanges
- Place Flanges on Inner Tube
 - Tighten to Outer Pipe/Flange
- Seal feedthrough holes with JB Weld
- Add Pipe Fittings



Assembly Process

- Attach fiberguides with support rods
- Thread Hollow Fibers through fiberguides
- Epoxy fibers in holes
- Cut Threads to appropriate length
- Place fiberguides in housing with O-rings on fiberguides 1 & 3
- Attach Spacers and End-Lock ring
- Put on Endcaps with O-rings in place
- Add Pipe fittings
- Add Compression Fittings
- Compress assembly



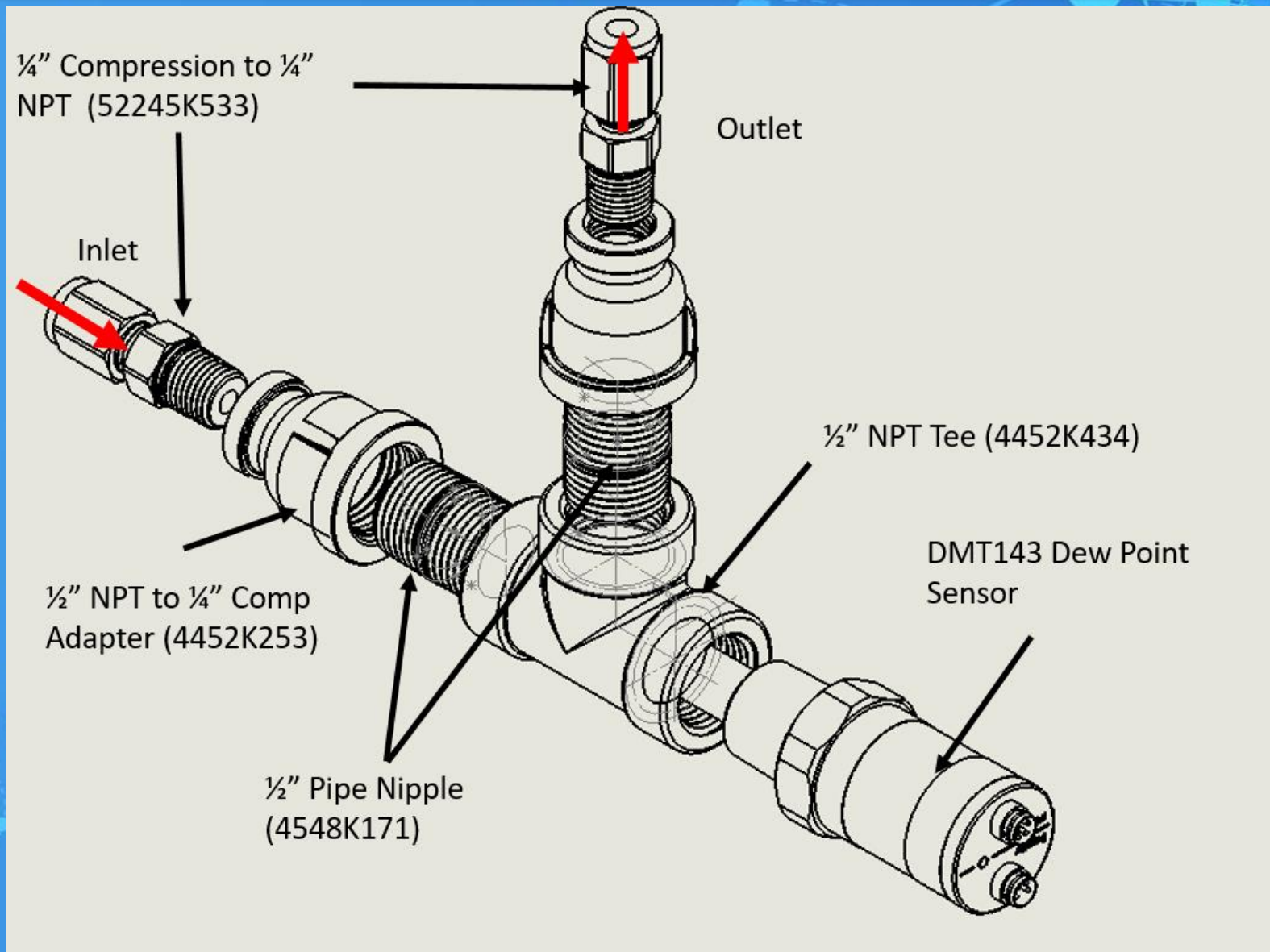
AETHER Sensors

Sensor	FS Range	Accuracy	Operational Range			Life and/or Drift Rate	Warm-Up Time	Response Time
			T (°C)	Humidity (%)	Pressure (psi)			
Temperature Sensor (HS-2000V)	-30 to 100 °C	+/- 0.40 °C	0-70	0-100	N/A	N/A	N/A	50 seconds in slow moving air
Absolute Pressure Sensors (HSCSAND030)	0 to 30 psia	+/- 0.25%	-20-80	0-95	60/120 psia	1 Million Cycles	N/A	N/A
0-3% CO2 Sensor (GMM-221)	0 to 3% CO2	+/- 450 – 1050 ppm	-20-60	0-100	18.85 psia	< +/- 5% per 2 years	Init: 30 s Full: 15 min	20 seconds
Environmental CO2 Sensor (K30)	0 to 10000 ppm	+/- 3% of Reading +/- 30ppm	0-50	0-95	145 psig	15 years	1 minute	20 seconds
O2 Sensor (Max 250)	0 to 100% O2	+/- 4.25%	5-40	5-95	22 psia	Rated at 4 years in standard atmos.	N/A	< 15 seconds

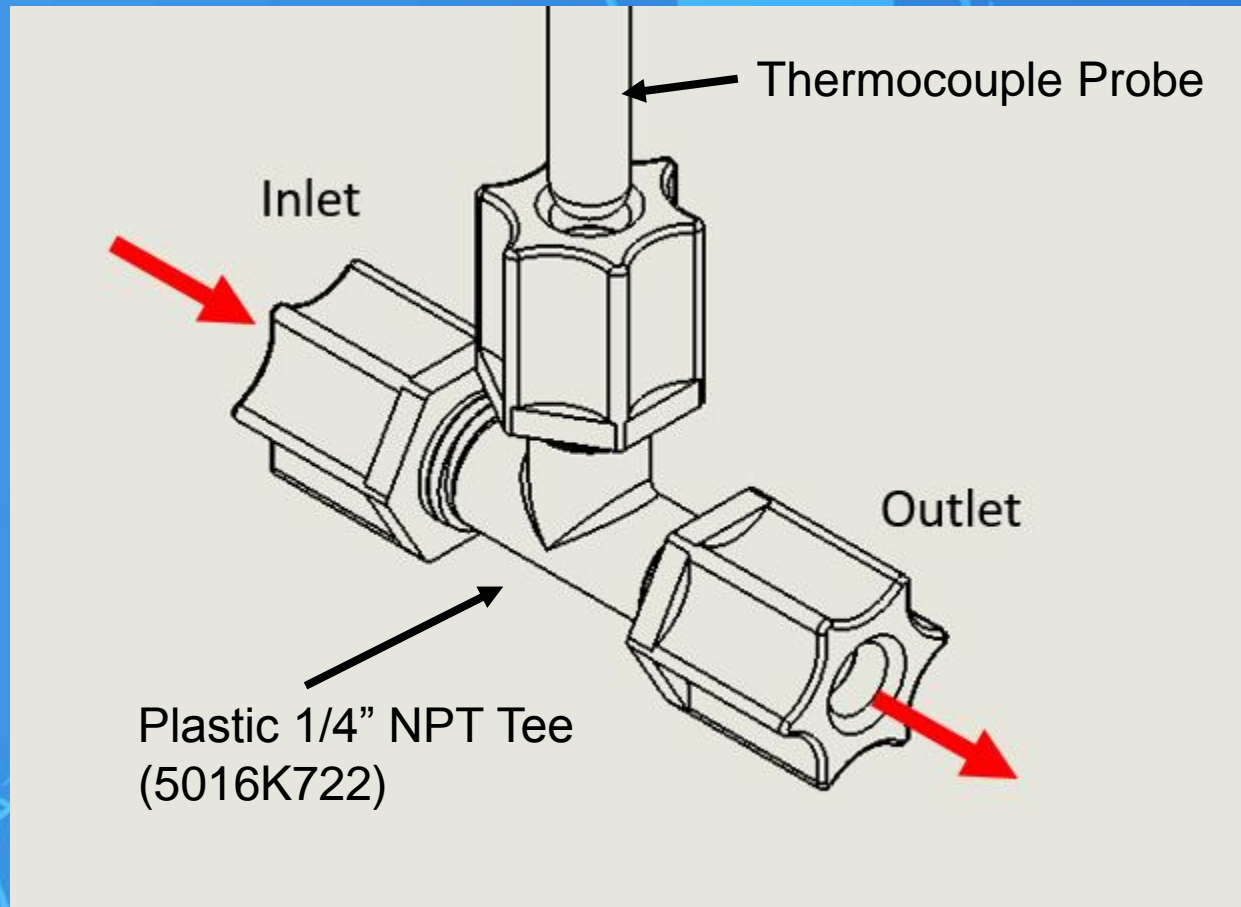
HYDRA Sensors

Sensor	FS Range	Accuracy	Operational Range			Response Time
			T (°C)	Humidity (%)	Pressure (psi)	
Dew Point Sensor (Vaisala DMT143)	-70 to 60 °C	± 2 °C	-40-60	0-100	725	10 minutes
rH Sensor (HX94BV1W)	0 to 100% rH	± 2.5%	0-100	0-100	N/A	8 seconds
Thermistors (SA1-TH-44006-40-T)	-80 to 120 °C	± 0.2 °C	-80-120	N/A	N/A	N/A
Thermocouples (McMaster 3871K77)	-200 to 375 °C	± 0.75%	-200-375	N/A	N/A	N/A

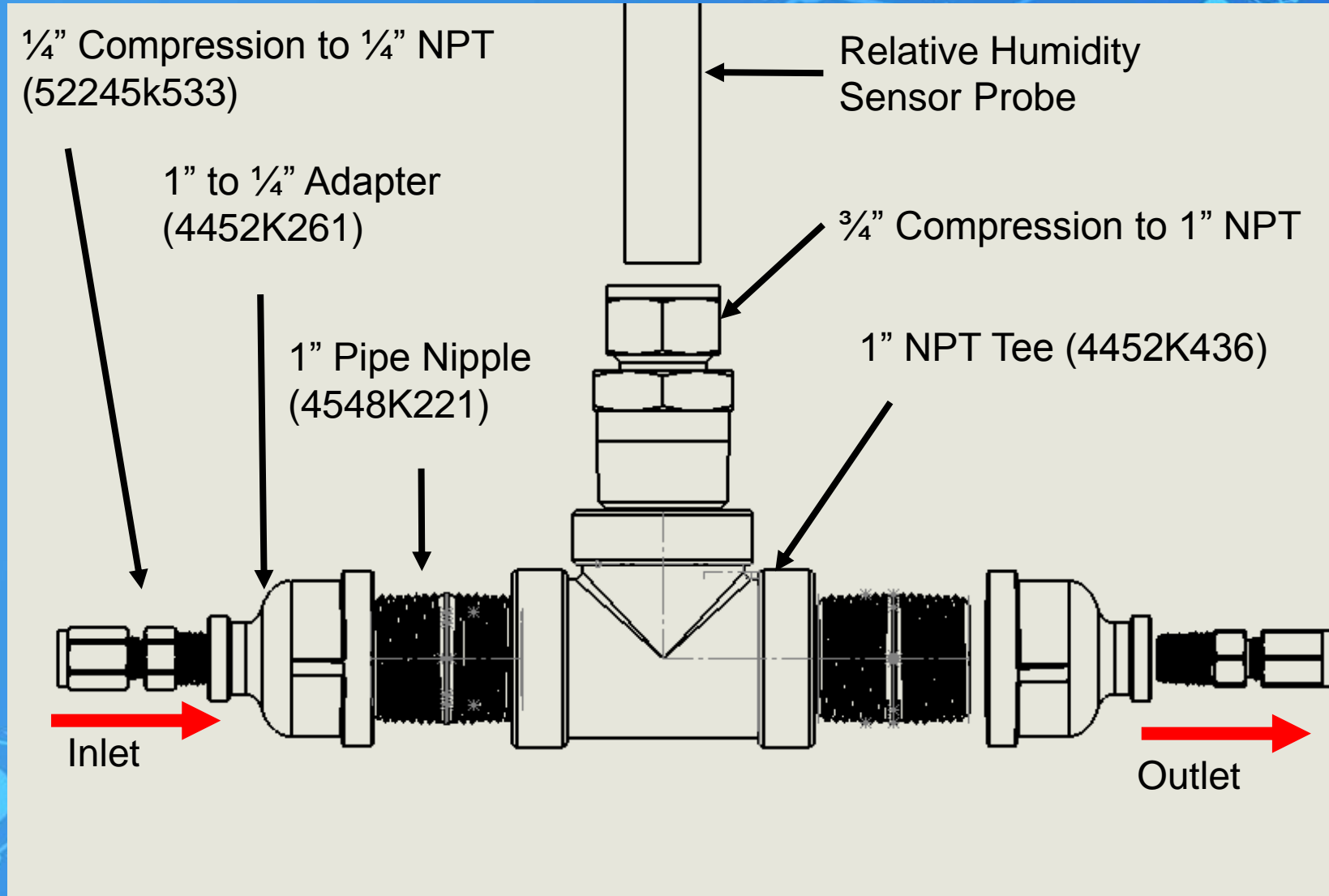
Dew Point Sensor



Inline Thermocouple



Relative Humidity Sensor



ILS Manifold

